Annual Report 2009

Institute of Safety Research

Editors:
Prof. Dr. rer. nat. Frank-Peter Weiss
Dr. Frank Schäfer

ZD Forschungszentrum
Dresden Rossendorf

Cover Picture: DENISE (Direct condensation and Entrainment Installation for Steam Experiments) experiment inside the TOPFLOW pressurized chamber. (Foto by Ronald Bonß)

CONTENTS

Preface

Selected reports

Preface

The Institute of Safety Research (ISR) is one of the six Research Institutes of Forschungszentrum Dresden-Rossendorf e.V. (FZD), which is a member institution of the Wissenschaftsgemeinschaft Gottfried Wilhelm Leibniz (Leibnizgemeinschaft). Together with the Institutes of Radiochemistry and Radiation Physics, ISR implements the research programme „Nuclear Safety Research", which is one of the three scientific programmes of FZD. The programme includes two main topics, i. e. "Safety Research for Radioactive Waste Disposal" and "Safety Research for Nuclear Reactors".

The scientific work of ISR aims at the analysis of the safety of current and future reactors, the development of advanced simulation tools including their validation against experimental data, and the development of sophisticated measuring techniques for multi-phase flows and liquid metals.
The different research subtopics we are dealing with, as well as our large scale thermal hydraulic test facility TOPFLOW (**T**ransient Tw**o-P**hase **Flow** Test Facility) are listed in Table 1 together with the assignment to FZDs scientific programmes.

The subtopic of "Materials and Components Safety" is focussed on the experimental investigation and modelling of the irradiation induced ageing of reactor construction materials. This ageing phenomenon decisively affects the maximum operational lifetime of power reactors and the design of components of future reactors. Monte-Carlo transport calculations are used to characterize the neutron irradiation in terms of flux and dose. Authentic irradiated specimens from decommissioned reactor pressure vessels and irradiated model alloys are subjected to fracture mechanical tests in dedicated hot cells. The irradiated reactor pressure vessel steels are investigated by advanced techniques as e.g. by SANS, REM/TEM, and PAS in order to detect and characterize the neutron induced defects on the nano and sub-nano meter scale. On the one hand, these experimental data along with the mechanical test results are used to gain basic understanding of the ageing mechanisms, like for instance the influence of alloying elements and impurities upon the neutron induced embrittlement, and to develop in close international collaboration evaluation methods for the degradation of reactor steels over their operational lifetimes. On the other hand, these data constitute the reference for the multi-scale modelling of the ageing effects ranging from molecular dynamics and rate theory up to fracture mechanical calculations on the behaviour of the aged steels under the loads connected with hypothetical accidents. This subtopic relies on close collaboration with the Institute of Ion Beam Physics and Materials Research inside the FZD regarding the modelling efforts, as well as on the collaboration with other Research Centres to get access to advanced methods for micro-structural analysis. The research work is embedded in EURATOM projects on the ageing of reactor materials like NULIFE, PERFORM60, and LONGLIFE. The latter one will be started beginning of 2010 and will be coordinated by FZD.

The subtopics "Thermal Fluid Dynamics of Multi-Phase Flows" and "Magneto-Hydrodynamics" deal with the thermal hydraulics of LWRs and liquid metal flows. The current thermal hydraulics system codes represent 1D tools based on steady state flow map correlations valid for fully developed flows, only. These correlations were derived from dedicated experiments. However, they are not scalable and do not apply to transient flows. Therefore, the subtopic aims at the development of a new generation of thermal hydraulic simulation tools, so called CFD (Computational Fluid Dynamics) codes that are capable of describing transient spatial multi-phase flows relying on models which consider the local flow

characteristics. Though much more physics based, these tools have to be validated against CFD-grade experimental data of sufficient resolution in space and time to allow for appropriate comparison with the calculations. For that reason, the transient two-phase flow test facility TOPFLOW is an essential element of FZDs reactor safety research programme. Due to its industry relevant scale, its sophisticated experimental techniques, as e.g. the pressurised chamber, and above all because of the advanced instrumentation, TOPFLOW represents a unique facility, worldwide. The development of measuring techniques for multi-phase flows, up to fast tomographic imaging, is constitutional part of our reactor safety research. This field of research will decisively be strengthened by the AREVA endowed professorship on imaging techniques for energy and process engineering. The new professor will commonly be appointed by the Dresden Technical University and FZD.

Generation IV fast nuclear reactors use liquid metal coolants like sodium or lead. Adequate instrumentation for such liquid metal flows, providing reliable information on the flow fields and on the status of the components covered by the liquid metal, is decisive for the basic safety concept of these reactors. The same applies to the availability of early detection techniques for gas bubbles in the liquid metal and to the design of heat exchangers, which exclude energetic interactions of primary and secondary coolants, like sodium-water interaction. The new multi-purpose sodium platform DRESDYN, of which the design has just started, will offer the unique chance for the development of the above mentioned technologies. The results obtained at DRESDYN will also be used to develop and validate adequate simulation tools for liquid metal flows.

DRESDYN will also be designed to astrophysical laboratory experiments, related for instance to the self-excitation of cosmic magnetic fields and to the role of magnetic fields in destabilising cosmic flows. The platform offers the unique chance to combine both types of experiments in one and the same experimental environment.

Both, the activities on LWR thermal hydraulics and on liquid metals are integrated into key European projects like NURISP or CP ESFR.

Beyond that, our "Magneto-Hydrodynamics" research is partly engaged in the "Advanced Materials" programme of FZD. There, it is devoted to the improvement of materials manufacturing technologies by optimising the involved flow processes of electrically conducting fluids through the application of external magnetic fields. The research on "Magneto-Hydrodynamics" is implemented in close collaboration with partners from TU Dresden, TU Bergakademie Freiberg, and IFW Dresden in frame of the Collaborative Research Centre SFB 609 funded by DFG.

The subtopic "Accident Analysis of Nuclear Reactors" makes use of the results generated by the materials and thermal hydraulics research of the reactor safety programme in order to create new quality simulation tools for current and future reactors and to analyse the safety of these reactors. In the centre of this subtopic, our in house 3 dimensional reactor dynamics code DYN3D is continuously developed with regard to the

- implementation of neutron transport options into the diffusion based code,
- the availability of multi-scale options in neutronics calculations,
- the integration into a multi-physics environment,
- the link to sensitivity and uncertainty analysis tools, and
- code versions for GEN-IV reactors.

These efforts are embedded into the European initiative NURESIM (Nuclear Reactor Simulation) on the creation of a uniform simulation platform for nuclear reactors which is currently pursued in the NURISP project. DYN3D is one of the reference codes for neutronics calculations within this platform.

DYN3D can refer to a growing user community in and outside NURESIM. The support of these users, in particular of the Eastern European users applying DYN3D to the safety analysis of VVER reactors, is part of the subtopic. There is a clearly growing interest of the industry in getting access to DYN3D.

Moreover, the subtopic addresses experimental and theoretical mixing studies in the context of LWR boron dilution and cold water scenarios as well as experiments and simulations on the possible clogging of LWR sump screens and of the fuel assembly spacer grids by insulation material released in a loss of coolant accident.

The activities in accident analysis are parts of large international (EU, OECD, AER, etc.) and national research projects. There is a clear tendency to shift the emphasis in the subtopic from LWRs to HTRs and GEN-IV reactors.

By participating in the development and operation of the pulsed photo-neutron source at the radiation source ELBE (**E**lectron **l**inear accelerator for **b**eams of high brilliance and low **e**mittance), as well as in the interpretation of the measurements of neutron reaction cross sections for candidate materials for future nuclear reactors and with radioactive waste isotopes, we also contribute to the "Transmutation" subtopic coordinated by the Institute of Radiation Physics.

Programme	Subtopic / User Facility
Nuclear Safety Research	Materials and Components Safety
	Thermal Fluid Dynamics of Multi-Phase Flows
	Magneto-Hydrodynamics
	Accident Analysis of Nuclear Reactors
	Transmutation
	Transient Two-Phase Flow Test Facility TOPFLOW
Advanced Materials	Magneto-Hydrodynamics

Table 1. Research subtopics and user facility of the Institute of Safety Research, 2009

Our work is financed through the basic funding of FZD, as well as by external funds from public research grants and from contracts with the industry. In 2009, 42 % (3.136 k€) of our total expenditure were covered by such external funds with 19 % from research grants of the Federal Government, 8 % originated from Deutsche Forschungsgemeinschaft, 7 % from the EU, and 8 % from research contracts mainly with the industry (see Fig. 1). The deployment of the total budget on the different projects and the user facility TOPFLOW (see Table 1) is illustrated in Fig. 2.

Together with the Dresden Technical University, the Zittau University of Applied Sciences, and VKTA (Verein für Kernverfahrenstechnik und Analytik) Rossendorf, the ISR represents the East German Centre of Competence in Nuclear Technology (Kompetenzzentrum Ost für Kerntechnik) which in turn is a member of the German Alliance for Competence in Nuclear Technology (Kompetenzverbund Kerntechnik). As such, the ISR also takes care to keep and promote the expertise in nuclear engineering. For that end, a strategic partnership exists between FZD on the one side and AREVA and the nuclear power plant operators on the other side.

Beyond this, ISR cares for the next generation of young scientists by supervising PhD, Master, and Diploma students, for example.

The quality of the education at ISR is underlined by the prizes awarded to our PhD students. Christian Cierpka received one of FZDs PhD prizes 2009 for his dissertation on "Time Resolved PIV Investigations on Flow Control by Means of Periodical Electromagnetic Forces in Electrically Weakly Conducting Fluids". Marco da Silva was awarded the "Messtechnikpreis 2009" of the Arbeitsgemeinschaft der Hochschullehrer in der Messtechnik for the development of "Impedance Sensors for Multi-phase Flow Measurement and Imaging". The Dresden Barkhausen Poster Prize 2009 of the Dresden Technical University was awarded to Martina Bieberle for the presentation of the results of her dissertation on "Image reconstruction for Ultra-fast Limited Angle X-Ray Computed Tomography for Two-Phase Flows".

During the reporting period, the ISR organised important meetings and workshops with international participation, such as the international workshop on "Multi-Phase Flow: Simulation, Experiment and Application", which was jointly hosted by ISR and ANSYS Germany GmbH, and which continues the series of meetings on that topic in Dresden-Rossendorf. Moreover, we organised and hosted the 6th International Conference on Electromagnetic Processing of Materials, which was attended by almost 300 participants.
Meetings such as these underline the national and international scientific reputation of the Institute of Safety Research.

I would like to thank all staff members of the institute for their high quality work and for making the year 2009 another successful one for ISR.

F.-P. Weiß   Rossendorf, 15 April 2010

Fig. 1: Funding sources 2009

basic budget
58%

research orders
(industry, public orders)
8%

research grants from EU
7%

research grants
from DFG
8%

public research grants
from BMBF, BMWi, DAAD, ...
19%
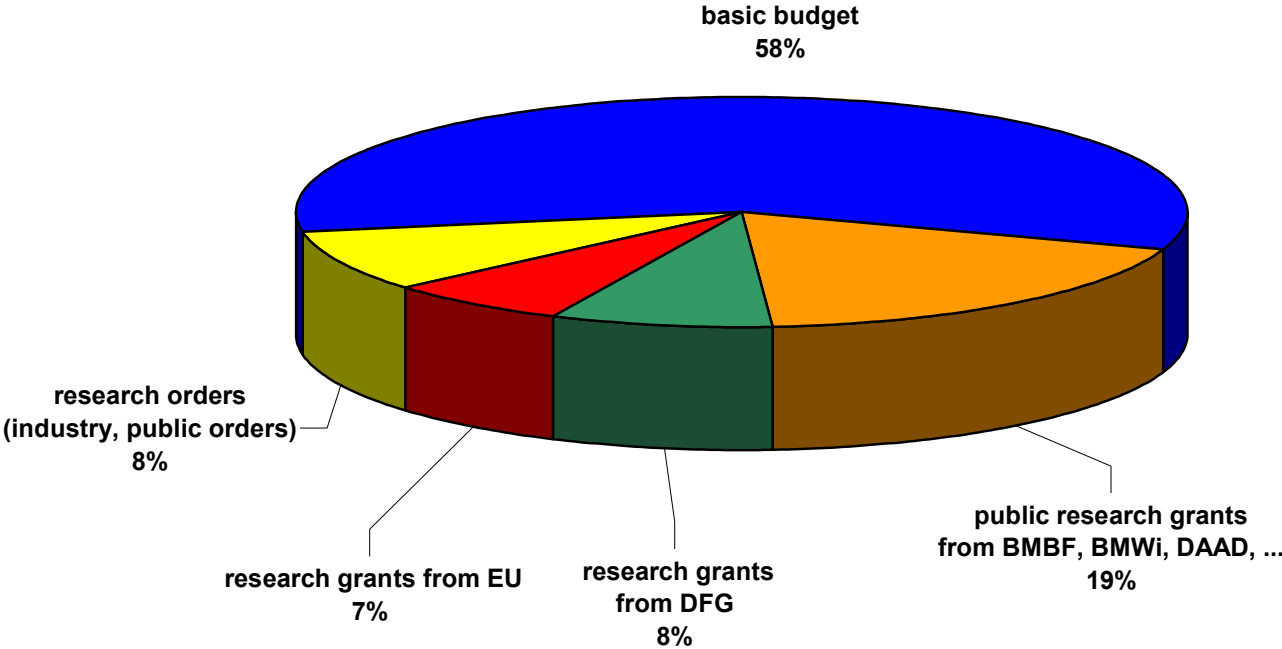
Fig. 2: Deployment of funding on the projects and user facilities 2009

Liquid metal
magnetohydrodynamics
28%

Material and components
safety
21%

Thermal fluid dynamics of
multi-phase systems
24%

Accident analysis of
nuclear reactor
20%

TOPFLOW
7%
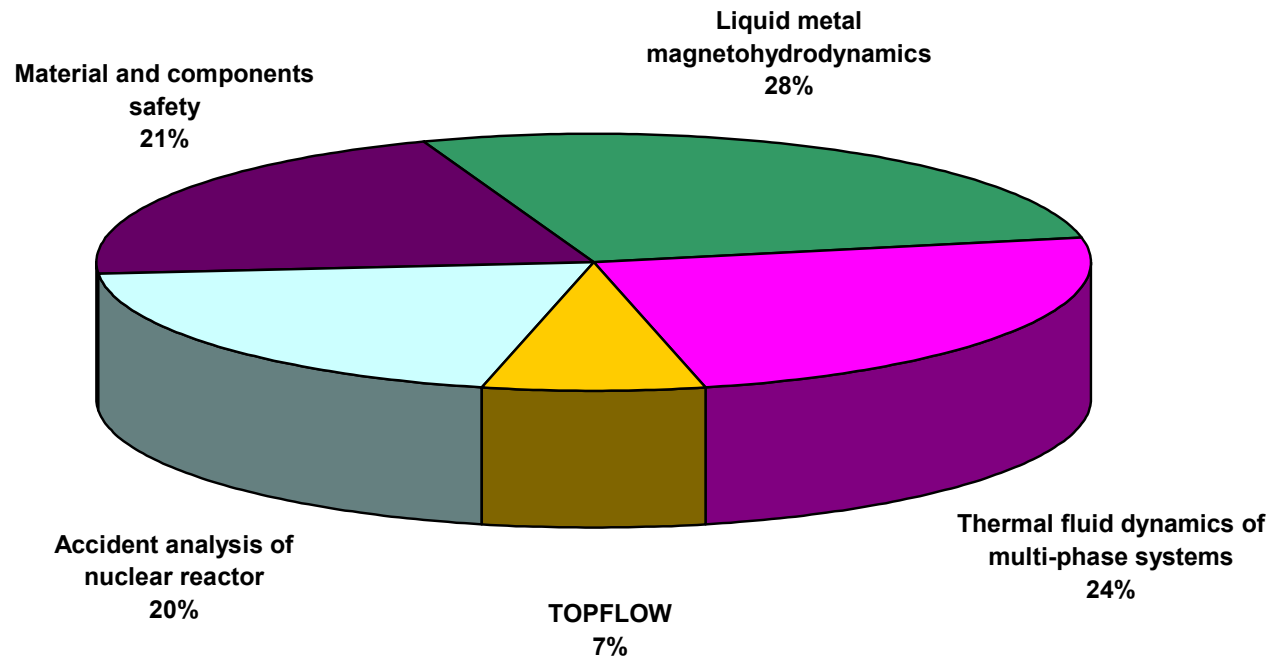
Selected reports

ULTRAFAST X-RAY TOMOGRAPHY TWO-PHASE FLOW STUDIES OF GAS-LIQUID AND GAS-SOLID TWO-PHASE FLOWS

Martina Bieberle, Eckhard Schleicher, Frank Fischer, Dieter Koch[1], Hans-Jürgen Menz[1], Hans-Georg Mayer[1], and Uwe Hampel

1.   Introduction

In order to ensure the safety and to improve the efficiency of industrial processes considerable effort is being spent in the understanding and modelling of multiphase flows. The development of computational fluid dynamics (CFD) codes in this field is furthermore fostered by the increasing computational power available today. Hence, there is a great interest in multiphase flow measurement technologies, which can provide detailed and accurate validation data for CFD codes. Although many imaging modalities, such as optical and acoustic methods, are well developed for single phase flow, there are only few which are applicable to multiphase flows. Problems here are refracting phase boundaries or opaque media. Many tomographic techniques have been proposed as an alternative. However, they in turn encountered the difficulty of reaching high spatial and temporal resolution at the same time.

Computed tomography (CT) methods based on either ionising radiation or magnetic resonance have long been considered as incapable to capture fast flows. However, in recent years some attempts have been made to adapt such techniques to the needs of flow measurement. For example, a fast gamma ray modality was introduced by Johansen et al. (1996), who built a scanner with five stationary Am-241 sources, which achieves frame rates of up to 100 Hz. Misawa et al. (2003) and Hori et al. (2000) built fast multi-tube X-ray scanners and claimed to achieve frame rates of up to 2 kHz. An alternative is electron beam tomography, which was first introduced by Boyd and Lipton (1983) for cardiac imaging. An electron beam scanner does not employ the classical CT principle of a rotating source-detector setup but rather uses an inertia-free electron beam, which is focused onto a tungsten target and swept across this target very rapidly by means of an electromagnetic deflection system. At the position of beam impingement, X-ray radiation is produced within the focal spot. While medical devices are limited to frame rates of about 20 Hz, which is sufficient to image the beating heart, the principle can also be adapted for flow imaging. This has successfully been demonstrated by our group who built an ultrafast electron beam X-ray CT system which was then applied to different two-phase flow experiments (Hampel et al. 2005, Bieberle et al. 2007, Bieberle et al. 2009, Bieberle et al. 2010).

2.   Electron beam X-ray CT

2.1.   Setup

The principle of the electron beam X-ray CT is illustrated in Fig. 1. The electron beam is generated by an electron gun, typically at an acceleration voltage of 150 kV and a beam current between 5 and 10 mA. The gun is followed by an electromagnetic lens system for beam centring, focussing and deflection. The electron beam is focussed on a tungsten target to a focal spot with an effective diameter of 300 µm. The scan is performed linearly on the target with a deflection width of 160 mm and a frequency of 2.5 kHz, giving 5000 sweeps and thus

---

[1] Institute of Nuclear Energy Technology and Energy Systems, Stuttgart University

images per second. Opposite to the target a semicircular X-ray detector is mounted with the detector pixels at the same height as the path of the focal spot. The detector consists of 256 cadmium-zinc-telluride (CZT) semiconductor detector elements, which are operated in current mode. The detector is sampled at 1 MHz, which gives 200 detector readings per electron beam sweep across the target.

The whole assembly is arranged in a commercial electron beam processing box, which provides a flexible setup, but requires components capable for operation in vacuum and vacuum-tight experiments. Another limitation is the maximum available height in the box which is about 50 cm and does not enable the study of larger vertical objects, such as pipes.

The idea to perform a linear scan rather than a circular scan originated from the intention to prevent an axial offset between focal spot path and detector. This offset arises from the angular overlap of a static massive target and a static detector when trying to fully sample the Radon space of an object, which in turn is necessary for accurate image reconstruction. However, with focal spot path and detector lying in one plane, radiographic projection cannot be acquired from all angles, which leads to the so called limited-angle-problem. Nevertheless, adequate image reconstruction algorithms adapted from the algebraic reconstruction technique (ART) (Gordon et al. 1970) provide an acceptable image quality for recovering the phase distribution of two-phase flow experiments.
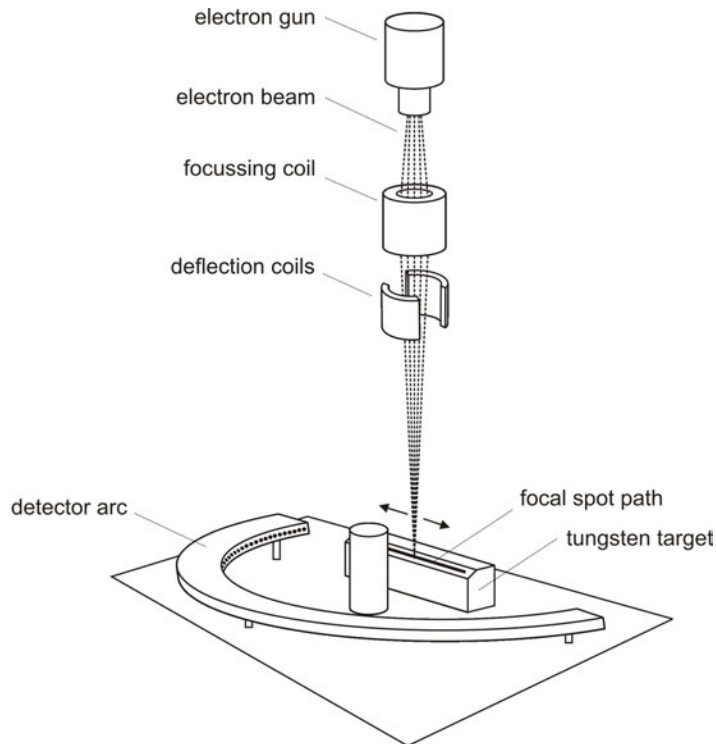
Fig. 1: Principle of ultrafast electron beam X-ray CT

2.2.   Data processing

During the measurement of each of the 5000 frames per second, the focal spot passes once across the target. On its continuous path from one turning point to the other, N_s data samples are taken synchronously at $N_d = 256$ detector elements. The number of temporal samples per sweep depends on the scanning frequency and was $N_s = 200$ in this study. Beside the X-ray intensities $\mathbf{I}^{(\mathrm{TP})} = \left\{ I_{s,d}^{(\mathrm{TP})} \right\}$ for the two-phase flow of interest, a so-called dark scan $\mathbf{I}^{(\mathrm{dark})}$ and a

reference scan $\mathbf{I}^{(\text{ref})}$ are acquired. The dark scan data represents the detector readings without X-ray exposure, that is the baseline detector output. The reference scan data is taken from the flow channel completely filled with one phase[2] as a reference state. This way, for each sweep a projection data set $\mathbf{p} = \{p_{s,d}\}$ is generated according to

$$p_{s,d} = -\ln \frac{I_{s,d}^{(\text{TP})} - I_{s,d}^{(\text{dark})}}{I_{s,d}^{(\text{ref})} - I_{s,d}^{(\text{dark})}} \,, \tag{1}$$

which represents the integral attenuation values of all possible X-ray paths from a source to a detector position. The forward problem of the limited-angle electron beam tomography is given by the equation system

$$p_{s,d} = \sum_{m=1}^{N} \sum_{n=1}^{N} \mu_{m,n} \cdot a_{s,d,m,n} \,, \tag{2}$$

wherein $N \times N$ is the number of pixels, $\mu_{m,n}$ is the average X-ray attenuation coefficient for pixel (m, n) and $a_{s,d,m,n}$ is the so called pixel weight, i.e. the share of pixel (m, n) with the area of ray (s, d).

The problem of image reconstruction is solved using the ART algorithm, which is defined as an iterative updating scheme according to

$$\mu_{m,n}^{(\tau+1)} = \mu_{m,n}^{(\tau)} + \lambda \cdot \frac{p_{s,d} - \sum_{m=1}^{N} \sum_{n=1}^{N} a_{s,d,m,n} \mu_{m,n}^{(\tau)}}{\sum_{m=1}^{N} \sum_{n=1}^{N} a_{s,d,m,n}^{2}} a_{s,d,m,n} \,, \tag{3}$$

wherein λ is a relaxation factor that regulates the speed of convergence. In our case it has been set to 0.1 at 10 iterations per reconstruction, which was determined as an optimum value for this problem. As a convergence stabilizer, the positivity constraint was applied, i.e. only physically plausible positive attenuation coefficient values $\mu_{m,n}$ were allowed during reconstruction. Image reconstruction was followed by extraction of the phase distribution including a Gaussian filter operation and the binarization using a threshold value at half of the attenuation coefficient of the liquid or solid phase, respectively.

3.   Experiments

3.1.   Water-air two-phase flow

The performance of the ultrafast limited-angle electron-beam X-ray CT has been demonstrated with an experimental water-air two-phase flow loop. Fig. 2 illustrates the experimental setup with the specially designed flow loop which has to cope with the spatial restrictions inside the vacuum box. Water is continuously pumped at a defined flow rate through a short vertical test section of a 38 mm diameter pipe.

---

[2] If the denser phase is used as a reference, the sign changes in equ. (1).
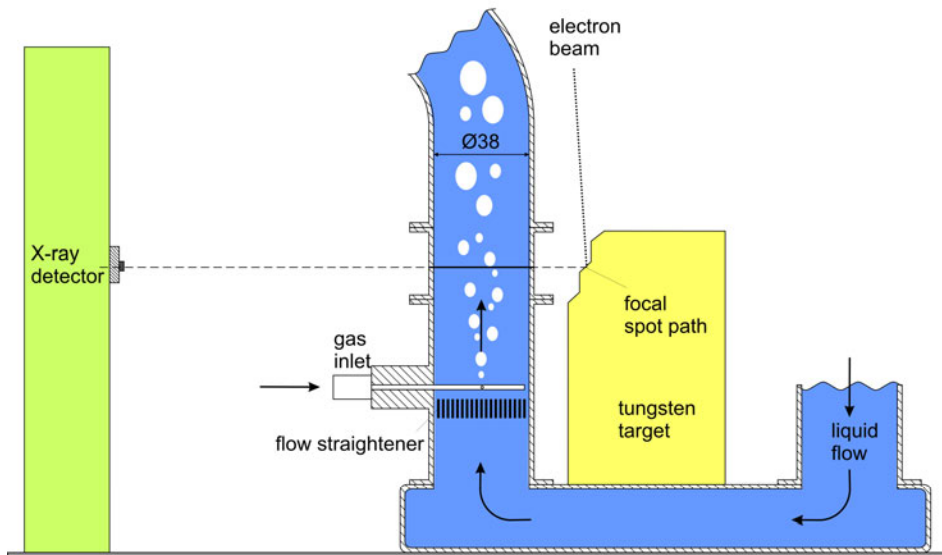
Fig. 2: Experimental two-phase flow loop setup

After passage of a flow straightener gas is injected via a single-hole cannula. After 22 mm this two-phase flow passes the X-ray plane and goes off the vacuum box into a separator. Due to the small distance between the gas inlet and the tomography plane, the two-phase flow is not fully developed in the imaged cross-section. Different flow regimes were generated by varying the liquid and the gas flow rate. For electron beam X-ray CT a beam current of 6 mA was used and sequences of 0.4 s were acquired for each of the parameter combinations. Selected axial cuts of the observed flow patterns with constant liquid flow rate on one hand and constant gas flow rate on the other hand are given in Fig. 3. The results show, that the ultrafast X-ray CT is able to image different structures of gas-liquid two-phase flows with high temporal and spatial resolution and without significant motion or limited-angle artefacts.
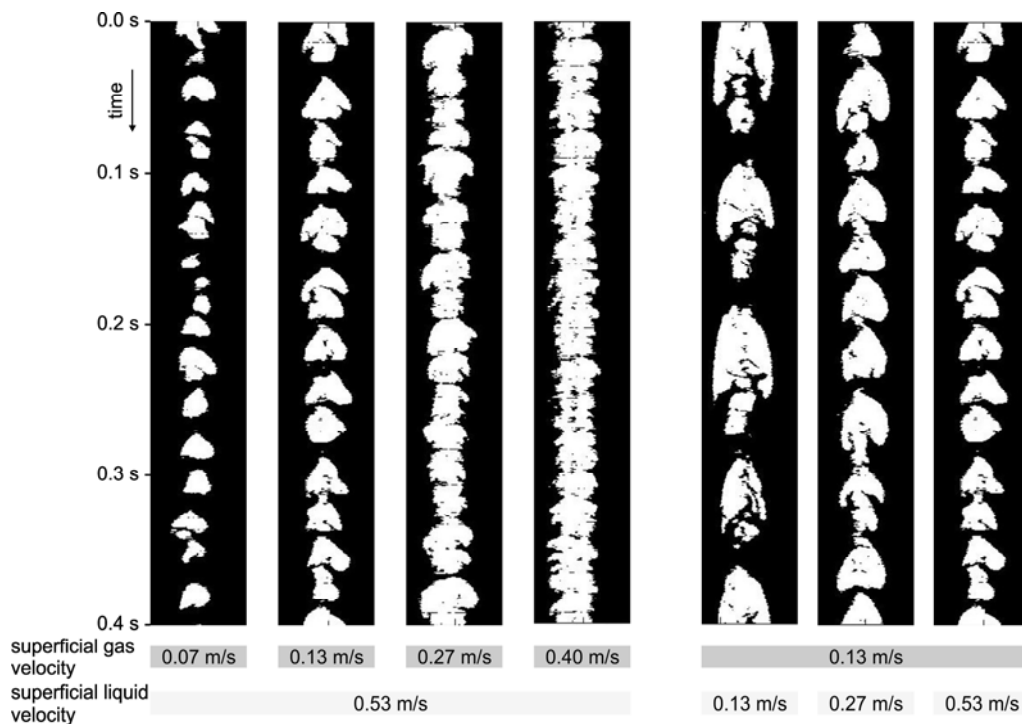
Fig. 3: Axial cuts of the reconstructed phase distributions at different gas and liquid flow rates

3.2. Fluidized bed

As an example for gas-solid two-phase flow an experimental fluidized bed with tube diameter 40 mm was investigated. The particle bed consisted of monodisperse glass beads of diameter 0.9 mm, 1.7 mm and 3.0 mm, respectively. As shown in Fig. 4 , the particle bed was fluidized through feeding gas in from the bottom of the bed. The volumetric gas flow rate was varied between 250 l/min and 2000 l/min. Electron beam X-ray CT scanning was performed at a beam current of 8 mA. In the scanning time of one second, projection data for 5000 cross-sectional images were gathered for each configuration.
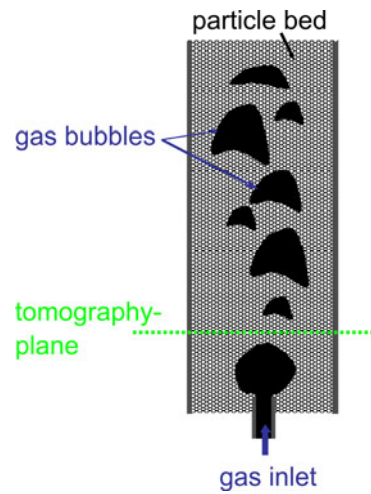
Fig. 4: Schematic of fluidized bed setup

In Fig. 5a selected cross-sectional phase distributions for different particle sizes are shown. Evidently, even the smallest particles are resolved by the ultrafast electron beam X-ray CT at full flow dynamics when they are loosely distributed.
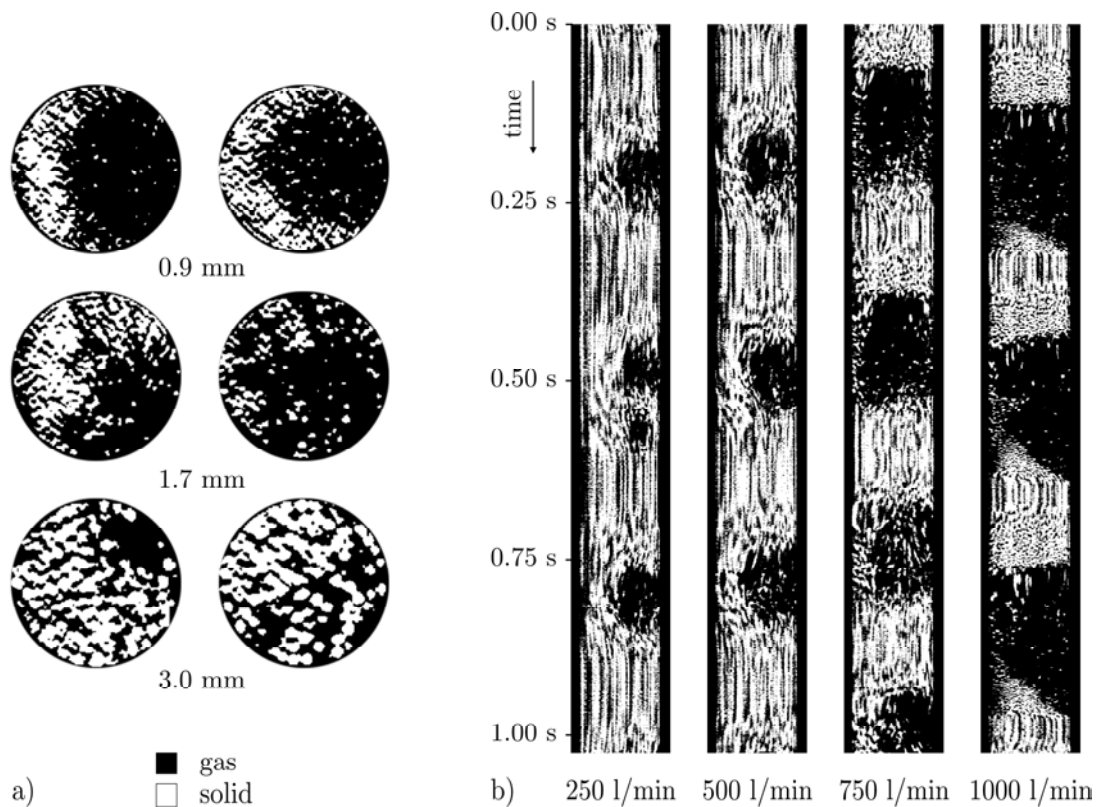
Fig. 5: Reconstructed phase distributions of the gas-solid two-phase flow in a fluidized bed: a) cross-sectional images for different particle sizes, b) axial cuts through the sequences with 1.7 mm spheres at different gas flow rates

This manifests the expected spatial resolution of the system of about 1 mm. It gives the chance to study the particle dynamics in detail which is to our knowledge unprecedented. Fig. 5b illustrates the progress of the phase distribution along the diameter line through the

fluidized bed perpendicular to the target for the 1.7 mm particles at different gas flow rates. Ultrafast electron beam CT clearly reveals periods of quasi static distributions inside the imaging plane from periods of higher particle dynamics before bubble or slug formation, which cannot be seen with imaging techniques of lower temporal or spatial resolution. It can also be observed, that the size of bubbles increases with higher gas flow rate whereas the bubble frequency remains nearly constant.

4.   Conclusions

It has been shown in a series of experiments that ultrafast electron beam X-ray CT is a suitable measurement technique for imaging gas-liquid and gas-solid two-phase flows with high temporal and high spatial resolution. The frame rate of 5000 images per second in combination with the spatial resolution of about 1 mm enables detailed studies of phase structures and flow dynamics. Especially in the example of a fluidized bed, a so far unprecedented insight into the particle dynamics of an opaque particle bed has been achieved, which opens up new possibilities for studying and understanding gas-solid flows.

References

[1]   G. A. Johansen, T. Frøystein, B. T. Hjertaker, Ø. Olsen (1996), A dual sensor flow imaging tomographic system, Meas Sci Technol 7, 297–307

[2]   M. Misawa, I. Tiseanu, H.-M. Prasser, N. Ichikawa, M. Akai (2003) Ultra-fast X-ray tomography for multi-phase flow interface dynamic studies, Kerntechnik 68, 85–90

[3]   K. Hori, T. Fujimoto, K. Kawanashi, H. Nishikawa H (2000), Development of an ultra fast X-ray computed tomography scanner system: application for measurement of instantaneous void distribution of gas–liquid two-phase flow, Heat Trans Asian Res 29(3),155-165

[4]   D. P. Boyd, M. J. Lipton (1983), Cardiac computed tomography, Proc IEEE 71, 298-307

[5]   U. Hampel, M. Speck, D. Koch, H.-J. Menz, H.-G. Mayer, J. Fietz, D. Hoppe, E. Schleicher, C. Zippe, H.-M. Prasser (2005), Ultrafast X-ray computed tomography with a linearly scanned electron beam source, Flow Meas Instrum 16, 65–72

[6]   M. Bieberle, F. Fischer, E. Schleicher, D. Koch, K. S. do Couto Aktay, H.-J. Menz, H.-G. Mayer, U. Hampel (2007), Ultra fast limited-angle type X-ray tomography, Appl Phys Lett 91, 123516

[7]   M. Bieberle, F. Fischer, E. Schleicher, D. Koch, H.-J. Menz, H.-G. Mayer, U. Hampel (2009), Experimental two-phase flow measurement using ultra fast limited-angle-type electron beam X-ray computed tomography, Exp. Fluids 47(3), 369-78

[8]   M. Bieberle, F. Fischer, E. Schleicher, H.-J. Menz, H.-G. Mayer, U. Hampel (2010), Ultrafast cross-sectional imaging of gas-particle flow in a fluidized bed, AIChE Journal 56(8), 2221-2225

[9]   R. Gordon, R. Bender, G. T. Herman (1970), Algebraic reconstruction techniques (ART) for three-dimensional electron microscopy and X-ray photography, J Theor Biol 29, 471-481

LIQUID PHASE DYNAMICS IN PACKED BED CONTACTORS

Markus Schubert, Marco Jose da Silva, and Holger Kryk

1. Introduction

Packed bed contactors, particularly trickle bed reactors, are widely applied chemical and process engineering, as they are most flexible with respect to varying throughput demands. Packed bed reactors consist of random packing elements such as of catalyst particles or rings, saddles etc., making the scale-up and the prediction of the performance very complex. Due to the random packing structure, local liquid phase dynamics can differ significantly and affect transfer and reaction rates. The full hydrodynamic characterization of the fluid field requires local phase fractions and local velocity parameters. While measurement of spatially resolved gas and liquid holdups in trickle beds was made possible with the transfer of tomographic methods mainly from medical into chemical engineering applications, velocity measurement techniques are still quite rare with a degree of success in their application to packings.

In this study, a capacitance wire-mesh sensor (WMS) setup is applied for determination of local liquid velocities and liquid saturation in the cross-section of a packed bed contactor with co-current gas-liquid downflow. The axial velocity distribution is measured by the spatial tracer pulse time-of-flight between corresponding sensing points of the two WMSs installed at a small distance. Eventually, both parameters are considered to validate the system using a segmented liquid collector [1].

2. Experimental setup and processing

2.1. Packed bed contactor setup

The experimental setup is shown in Fig. 1a. A transparent column (D = 100 mm) was packed up to a height of 135.5 cm with a commercial γ-alumina catalyst packing of spherical particles (2.5 mm diameter, internal porosity of 0.79 and packing porosity of 0.34).

1 liquid reservoir
2 liquid pump
3 Coriolis flow meter
4 gas flow controller
5 gas/liquid distributor
6 packed bed contactor
7 pressure transducer
8 flow meter
9 liquid collector
10 wire-mesh sensors
11 sensor electronics
12 tracer injection port
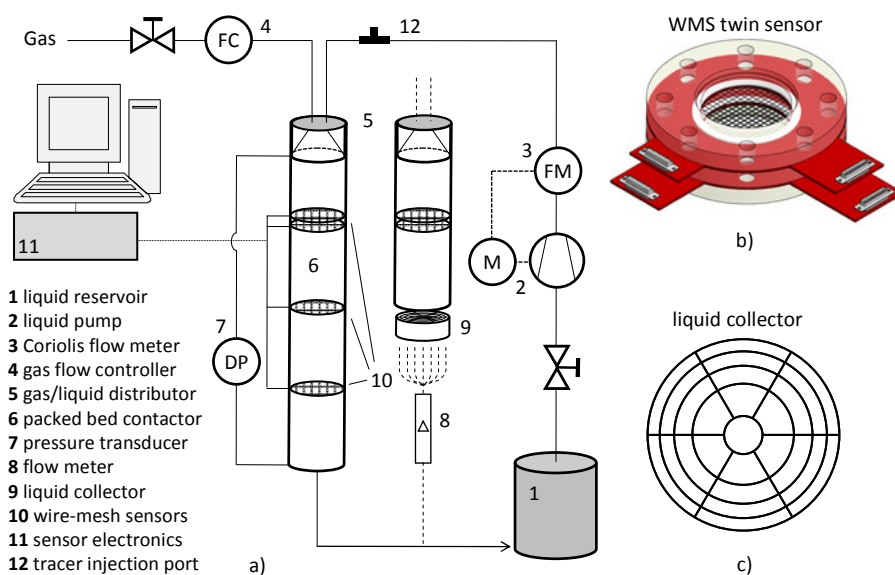
Fig. 1: Experimental contactor setup with WMS twin sensor and liquid collector

Water and air were used as liquid and gas phase, respectively. The experiments were performed in the liquid recycle-mode at room temperature and atmospheric pressure conditions. A uniform initial distribution of the liquid phase was realized by a full cone spray nozzle. A syringe tracer injection port is installed upstream the liquid inlet. Sodium sulfate solution (0.005 mol/L) was used as tracer. Due to low concentration, the effect of tracer on the liquid properties can be neglected. The packed bed consists of segments of different length to flange-mount the WMS at individual heights of the column. Four WMSs were installed in the column at heights 20.4 cm (S1), 22.1 cm (S2), 62.5 cm (S3) and 103.0 cm (S4) downstream the upper end of the packing. For measurement of local liquid velocities, two sensors (twin-sensor: S1 and S2) were installed separated by a spacer segment of 17 mm (Fig. 1b). Optional, a 25-compartment liquid collector was installed below the twin-sensor (Fig. 1c).

2.2. Wire-mesh sensor

The WMSs are composed of two planes with 16 stainless steel wires of 0.2 mm diameter and 6.0 mm separation in-between them. The distance between planes is 1.5 mm and the wires from different planes run at right angles to one another. This arrangement gives 256 sensing points, thereof 208 inside the circular cross-section of the column. Since the wires run through the bed, care was taken not to disturb the bed structure.

The WMSs use an AC based method for capacitance measurement, where a logarithmic detector scheme is employed for the demodulation of the AC signal. The associated electronics measure the capacitance between the gaps of all sensing points. Since liquids and gases have different electrical permittivity values and thus produce different capacitances in the sensing points of a WMS, images of liquid distributions can be generated from the measurements of the capacitance.

3. Data processing

3.1. Determination of dynamic liquid saturation

Dynamic liquid saturation, $\beta_{L,dyn}$, is the liquid volume divided by the extra-granular volume. However, at first WMS measurements in every crossing point x provide permittivity that requires high and low reference measurements ($K_{x,H}$, $K_{x,L}$) to calculate the dynamic liquid fraction. In our case, the "high" reference represents the permittivity of the fully saturated packing, $K_{x,H}(\beta_{L,dyn} = 1)$. Subsequently, the measurement after draining represents the permittivity of the "low" reference, $K_{x,L}(\beta_{L,dyn} = 0)$. The parallel model was applied to relate the permittivity to the liquid saturation according to equ. (1).

$$\beta_{L,x} = \frac{K_x - K_{x,H}}{K_{x,H} - K_{x,L}} \tag{1}$$

3.2. Determination of liquid velocity

Although the circuit of the capacitance WMS was conceived and implemented to measure only the capacitance, the introduction of conducting fluids (such as saline water) will produce changes in the measured voltage, V_{log}.

$$V_{\log,x} \sim \log(\sigma_{L,x}) \tag{2}$$

10

For $\sigma_{L,x}$>500 µS/cm, the WMS response signal becomes logarithmic dependent on the conductivity (equ. (2)).

$$\nu_{L,x} = \frac{\Delta s}{\Delta \tau_x}$$

(3)

Utilizing this behavior, conductivity tracers can be applied to measure the velocity based on the tracer pulse time-of-flight between the planes of two stacked WMSs (equ. (3)). It should be mentioned that axial dispersion and tortuous liquid pathways cannot be detected. However, due to low distance between both WMSs, these effects were neglected.

Fig. 2 shows the tracer pulses at both sensors S1 and S2. Shifting the normalized tracer signal of sensor S2 by $\Delta\tau_x$ to the left side demonstrates the consistent shape of the response curve, which indicates a negligible dispersion within the short distance.
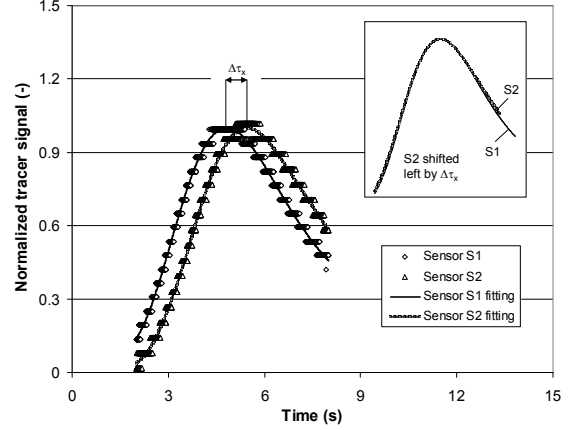
Fig. 2: Tracer signals S1 and S2 (u_L = 0.49 cm/s, u_G = 2.12 cm/s, pixel position {07;11})

4.   Results and discussion

4.1.   Liquid saturation measurement

In Fig. 3, the distribution of the dynamic liquid saturation in the cross-section is depicted for sensor S4 at 103.0 cm downstream the upper end of the packing. The cross-sectional images in Fig. 3 confirm the low effect of the gas flow rate on the cross-sectional averages dynamic liquid saturation. It becomes more obvious, considering the frequency distribution of the local data for the dynamic liquid saturation.
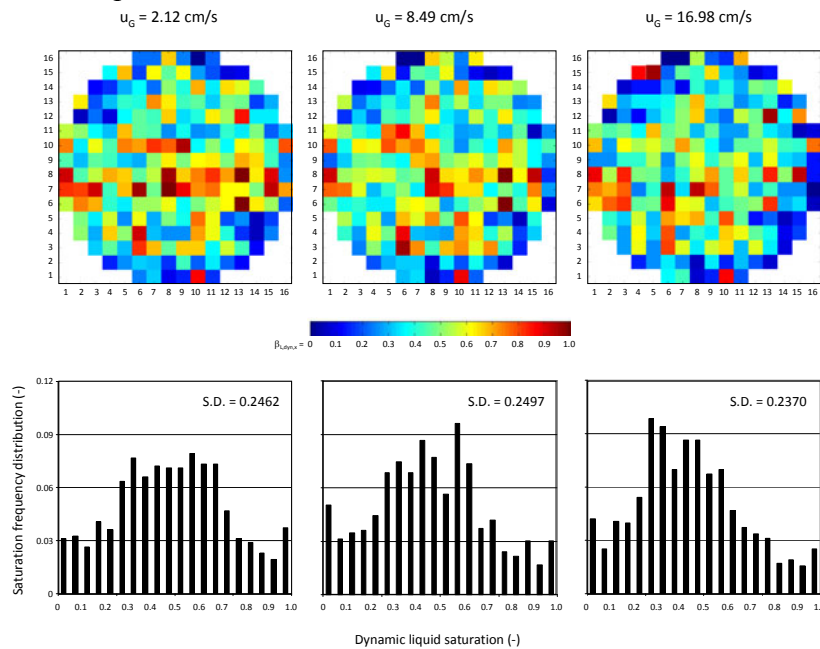
Fig. 3: Effect of superficial gas velocity on dynamic liquid saturation and corresponding frequency distribution of the local dynamic liquid saturation (u_L = 0.53 cm/s)

11

The mode of the distribution is not affected by the increasing gas flow rate. However, the peak plateau of the distribution at the lowest gas flow rate acuminates slightly with higher values. The gas phase hardly has an effect on the mean value of the dynamic liquid saturation, as channel flow is reduced towards higher gas flow rates (see pixels in rows 7 and 8 in Fig. 3).

Contrary, increasing superficial liquid velocity results in transition from right-skewed to left-skewed frequency distributions. Furthermore, the standard deviation increases monotonically.

4.2. Liquid velocity measurement

Fig. 4 shows the liquid velocity distributions in the cross-section and the corresponding frequency distributions. It is obvious that the velocities at many local positions increase with increasing gas flow rate even if the velocity at some pixels positions remains constant. The packing structure was not modified from experiment to experiment.
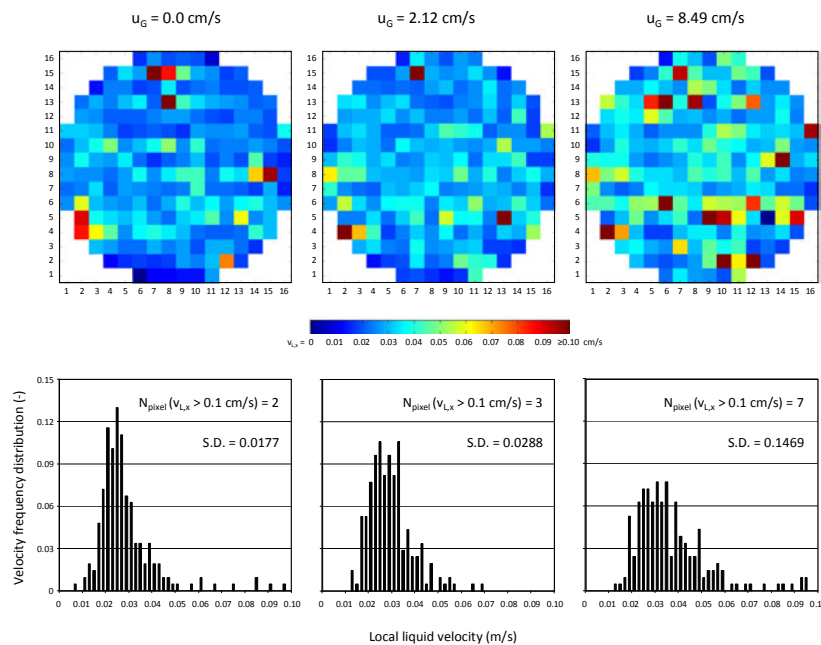
Fig. 4: Effect of superficial gas velocity on liquid velocity distribution and corresponding frequency distribution of the local liquid velocities (u_L = 0.71 cm/s)

The liquid distribution and flow in the voidage is stable in the trickling flow regime. The preferred flow paths persist even if the gas velocity increases (see pixels {15;7} and {4;2} in Fig. 4). Such pixels can also be an indication for higher local void fractions (in-homogeneities) as higher porosity directly results in higher flow rates. The mode values of the corresponding frequency distributions increase with increasing gas flow rate from approximately 0.025 cm/s for liquid only flow to approximately 0.035 cm/s for a gas superficial velocity of 8.49 cm/s.

Furthermore, the distributions become clearly wider for higher gas flow rates. Pixels with velocities higher then 0.1 cm/s are not considered in the frequency distribution for ease of comparison. The number of such pixels, $N_{pixel}(v_{L,x} > 0.1$ cm/s), increases with augmentations in the gas flow rate, indicating a higher number of flow channels. On the other hand, increasing the superficial liquid velocity shifts the frequency distribution to higher values.

5.   Conclusion

A new capacitance-based WMS system was successfully applied to a porous particle packing that enables access to the liquid phase dynamics in the whole cross-section of a packed bed contactor. Experiments that studied the influence of different superficial gas and liquid velocities on local dynamic liquid saturations and velocities were performed.

In order to validate the WMS measuring approach, local flow rates based on WMS measurements were calculated and compared to data from local flow rate measurements using a 25-compartment liquid collector mounted below the twin-WMS. Thus, saturation and velocity obtained from WMS measurements were applied to equ. (4) together with the area-weighting factor of every sensing point ($f_x \cdot A_{pixel,x}$) contributing to compartment j of the collector.

$$\dot{V}_{L,j} = \sum_x \beta_{L,dyn,x} \cdot v_{L,x} \cdot f_x \cdot A_{pixel,x} \qquad (4)$$

Fig. 5 shows an excellent agreement and demonstrates the applicability of the combined velocity/saturation measurement to analyze spatial distributed flow rates.
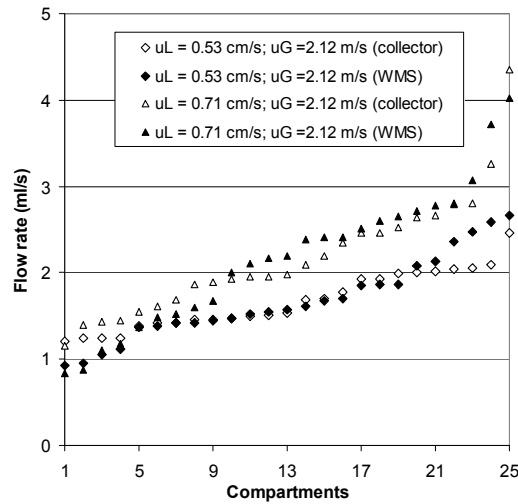
Fig. 5: Comparison of compartments flow rates from collector and wire-mesh sensor(sorted by increasing flow rate)

References

[1]   M. Schubert, A. Khetan, M.J. da Silva, H. Kryk (2010) Spatially Resolved Inline Measurement of Liquid Velocity in Trickle Bed Reactors, Chem. Eng. J., DOI:10.1016/j.cej.2010.02.009

INVESTIGATION OF CORROSION PROCESSES AT LOCA CONDITIONS

Wolfgang Hoffmann, Holger Kryk, and Frank-Peter Weiss

1. Introduction

In case of a loss-of-coolant accident (LOCA) in light water reactors, cooling water spilling out of the leak in the primary cooling circuit is collected in the reactor sump and recirculated to the reactor core by emergency cooling pumps as part of the emergency-core-cooling-system (ECCS). To retain any debris, sump strainers are mounted at the inlet of the ECCS.

Due to an incident in the Barsebäck-2 nuclear power plant in Sweden in 1992, concerns have been raised that fibrous insulation material could form a mat on the strainers and obstruct the flow. Beside insulation material, other forms of debris may also influence the sump strainer clogging behavior as well as the cooling water chemistry [1-3]. Especially the long-term contact of the leaked water-jet with grating treads consisting of hot-dip galvanized (zinc coated) steel grids may cause the formation of soluble as well particulate corrosion products. A typical LOCA scenario is depicted in Fig. 1.
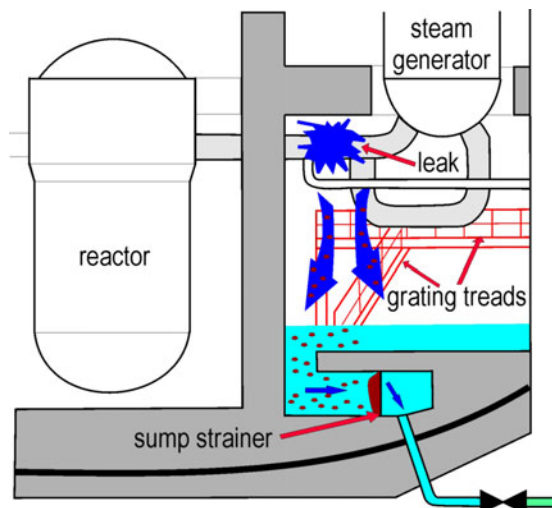
Fig. 1: Scheme of a LOCA scenario

As part of a common research project of the FZD and the HS Zittau/Görlitz[1], the influence of such corrosion processes on the chemical composition of the cooling water as well as on the strainer clogging behavior is currently being investigated. The aim is to provide a base for an integrated numerical flow simulation of LOCAs including long-term chemical effects.

2. Experimental setup

Due to the complex nature of electrochemical corrosion mechanisms, the decision was made to carry out the corrosion experiments in the following steps:

- batch experiments for clarification of basic electrochemical corrosion mechanisms and for investigation of chemical influences on the corrosion process,
- long-term corrosion experiments for quantification of the corrosion mechanisms at process conditions and estimation of the obstruction behavior.

2.1. Batch experiments

The batch corrosion studies were carried out under isothermal conditions in a double jacket 1.8-liter chemical stirred tank reactor for a week per run. As corrosion material samples,

partially submerged baffle-shaped hot-dip galvanized steel coupons were mounted on the reactor lid. Fig. 2 shows schematically the experimental set-up. A micrograph showing the depth profile of a hot-dip galvanized steel sample is presented in Fig. 3.
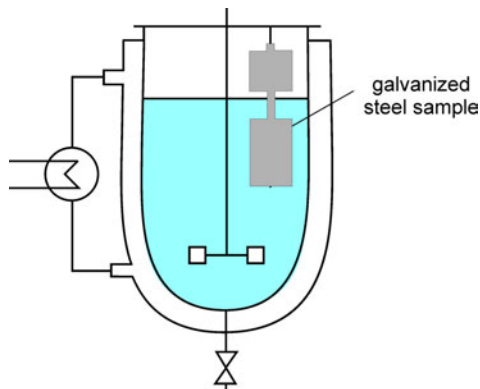
Fig. 2: Experimental set-up for batch studies
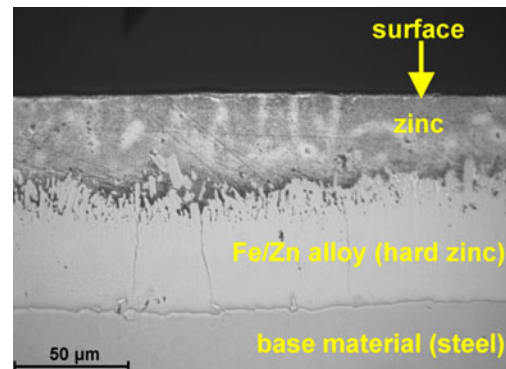
Fig. 3: Depth profile of a sample

According to the water chemistry of operating conditions in LWRs, deionized water, boric acid solutions (13 g/l) and boric acid with 15 ppm Li added as lithium hydroxide were used as liquid phases. The experiments were executed at 45, 70 and 90°C. Based on the results of the batch experiments, the test conditions for the long-term experiments were specified.

2.2. Corrosion test facility KorrVA

The long-term corrosion experiments are carried out for 13 days per run in a modular test facility (KorrVA) shown in Fig. 4.
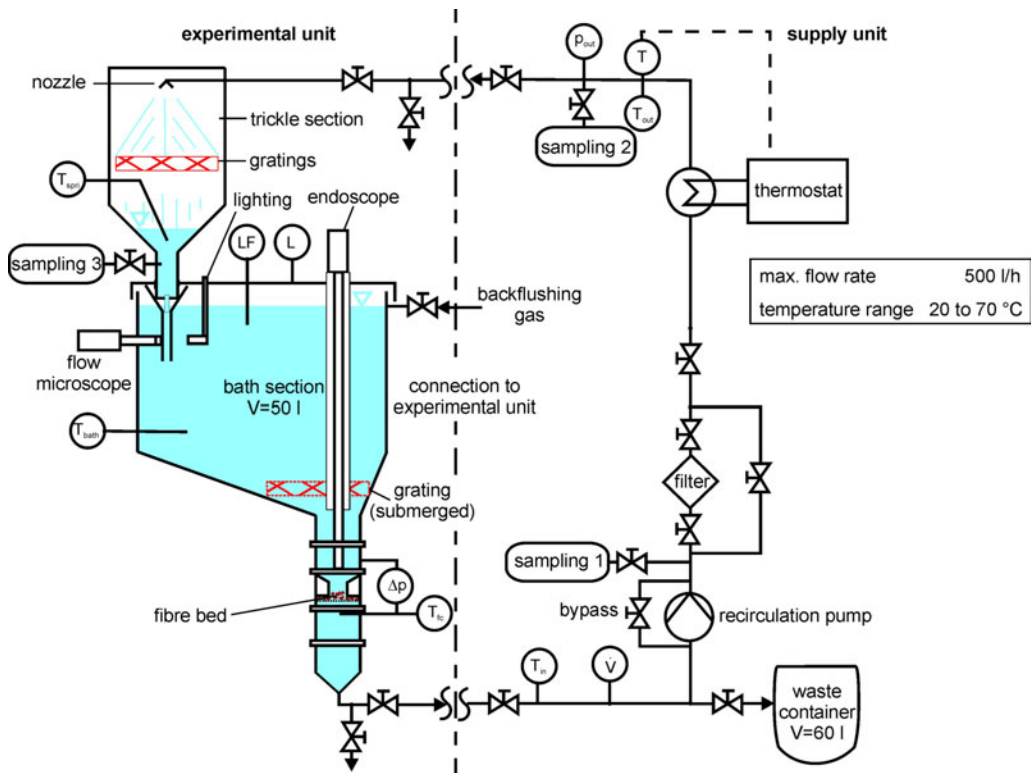
Fig. 4: Experimental set-up for long-term corrosion experiments

The design of the corrosion facility is based on a scale-down of ECCS and the sump geometries of typical PWRs. Thus, it represents the ECCS operation during a LOCA in a simplified manner. The supply unit provides the experimental unit with the liquid media with the desired process parameters. The experimental unit consists of a trickle section including a spray nozzle (representing the leakage) and a bath section (representing the sump) with a liquid volume of about 50 liters. The bath includes a strainer unit with appropriate applied insulation fiber samples that represents the clogged sump strainer. Since the investigations are focused on the study of chemical long-term effects, it is assumed that the transport and sedimentation of the insulation fibers is completed before the corrosion begins. At the outlet of the trickle-section, a flow microscope is placed in order to detect corrosion particles. In the bath, sensors for temperature and conductivity are installed and the differential pressure over the strainer is measured. The deposition of solids on the insulation material can be observed by a flexible endoscope. The construction of the KorrVA enables corrosion investigations of sprinkled as well as of submerged hot-dip galvanized steel gratings.

3.   Experimental results and conclusions

3.1.   Results of the batch experiments

The analytical results of solutions of the batch experiments, obtained using atom absorptions spectroscopy (AAS), show different trends depending on temperature. However, the greatest changes occur during the first day. Fig. 5 shows the significant increase of the concentration of Zn-ions up to 90 mg/l in solutions containing boric acid, caused by soluble corrosion products. The lower concentrations of Zn in the solutions result from the experiments starting with deionized water (green curves, right axis).
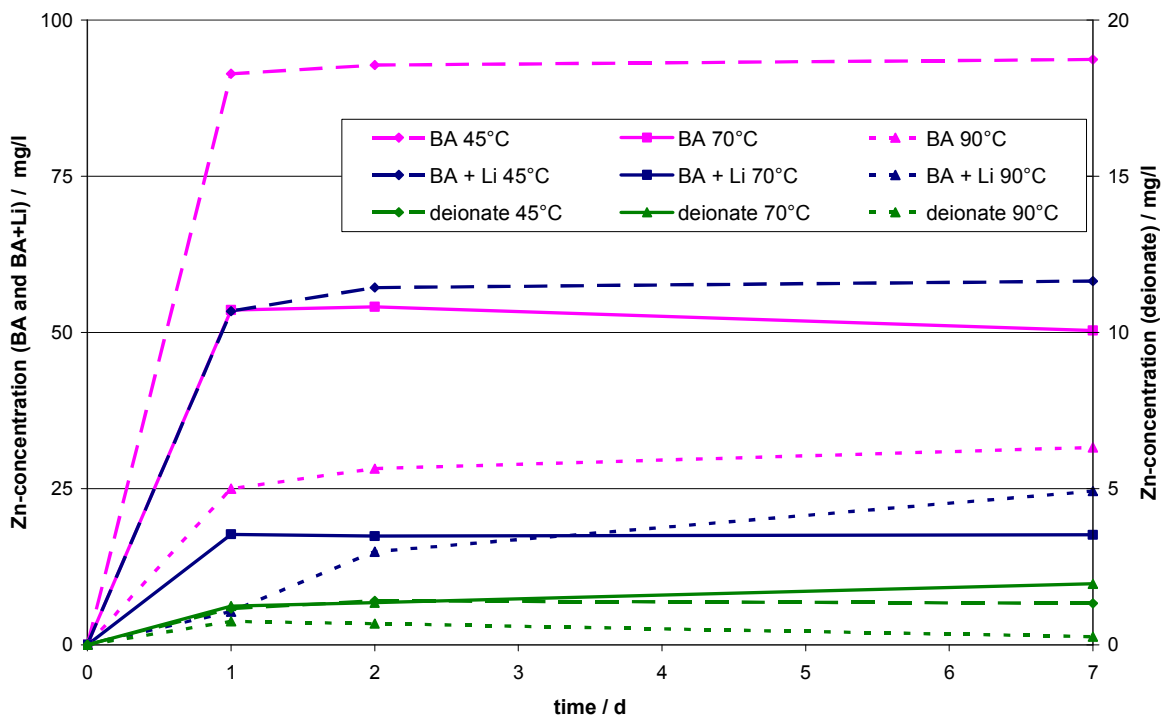
Fig. 5: Zn-concentration in solutions with deionized water (deionate), boric acid 13 g/l (BA) and boric acid 13 g/l with 15 ppm Li (BA + Li) depending on reaction time and temperature

The decrease of Zn-concentration with increasing temperature seems to contradict the normal increase of solubility of most salts with temperature. Such behavior can be explained by the

formation of zinc borate found at the surface of the samples by Raman microscopy (see below). Similar concentration changes were observed for Pb, but only of the order of about 0.1% of Zn-concentration since up to 1% Pb is added to the hot-dip galvanizing Zn melt as an alloy component for technical reasons. Fe-concentrations above the detection limit of 10 μg/l were not observed. Experiments with deionized water led to much lower zinc-concentrations. This agrees with the low corrosion rate under these conditions known from literature [4]. As main products, $Zn(OH)_2$ (at low temperatures) and ZnO (at higher temperature) were reported, which cause the corrosion resistance of zinc. In the presence of CO_2 from air, the basic carbonate $Zn_5(CO_3)_2(OH)_6$ can be formed, which is known to cause the very good stability of galvanized steel in the atmosphere.

The surfaces of the galvanized steel samples at the end of the batch experiments show clearly the corrosion effects (see Fig. 6).

new	45°C	70°C	90°C	
				deionized water
				boric acid 13 g/l + 15 ppm Li
				boric acid 13 g/l
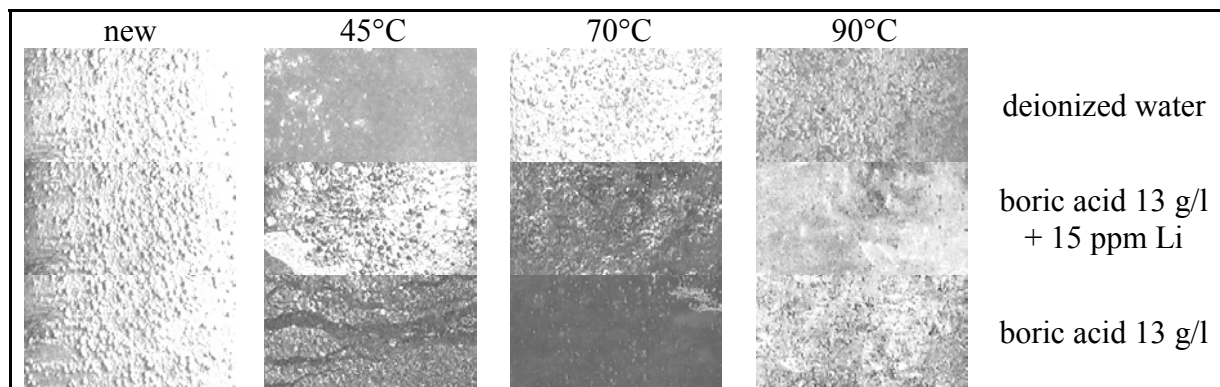
Fig. 6: Photos of sample surfaces after 7 days of treatment

Parts of the typical silver shining surface of a new untreated sample were observed on both samples treated with boric acid at 45°C and on the samples treated with deionized water at 70 and 90°C. Black layers were formed in boric acid and boric acid + 15 ppm Li, which were slightly transparent in the samples obtained at 45°C. Additional white particles were formed at 90°C on the samples surfaces as well as in the corresponding solutions. It is assumed that
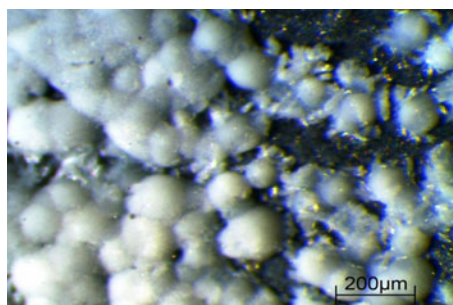
Fig. 7: Zinc borate on a sample

the black layer consists of Zn/Fe-particles inside of the Zn coating, which remained by selective dissolution during corrosion since an alloy phase containing Fe is formed during hot-dip galvanizing. By partial dissolution of zinc from a new sample with hydrochloric acid, a similar black thick layer was formed consisting of 90% Zn and 10% Fe.

White spherical particles up to 100 μm diameter found on samples treated with boric acid at 90°C were identified by laser Raman microscopy as zinc borate (see Fig. 7). For comparison, this substance was synthesized from a zinc salt solution with an excess of boric acid by addition of sodium hydroxide solution containing also excessive boric acid. The zinc borate, formulated as $2ZnO*3B_2O_3*3.5H_2O$, is a sparingly soluble salt. An unusual decrease of its solubility with increasing temperature was noticed. This effect can explain the reduction of zinc-concentration with increasing temperature in solutions containing boric acid shown in Fig. 5.

3.2.   Results of the long-term experiments

Experiments in the test facility KorrVA with galvanized gratings over a period of 13 days show the influence of medium and temperature on the corrosion of zinc. The corrosion rate in deionized water is much lower than in boric acid (BA) solutions (pH 4.6) and is also reduced by addition of LiOH (partial neutralization, pH 6.6). However, in all cases, the corrosion is decreased at higher temperatures. The mass losses of the grating samples during the KorrVA experiments and the resulting decrease of the zinc layer thickness (assuming a uniform surface abrasion) are summarized in Tab. 1. Most of the zinc coat remains on the gratings compared to the original coat thickness of about 100 µm (see Fig.3).

Table 1: Mass loss and decrease of Zn layer thickness depending on medium and temperature

Medium	Temperature [°C]	Mass loss [g]	Loss of thickness [µm]
deionate	45	0.29	0.5
deionate	70	0.04	0.1
BA (13 g/l) + Li (15 ppm)	45	4.09	6.9
BA (13 g/l) + Li (15 ppm)	70	1.50	2.5
BA (13 g/l)	45	6.65	11.3
BA (13 g/l)	70	3.38	5.7

3.3.   Conclusions

Regarding the maximum concentration of dissolved corrosion products, the results of chemical solution analyses of the long-term experiments are in good agreement with the batch experiments. Depending on reaction conditions, the zinc-concentration increases more slowly in the corrosion test facility. Thus, it can be concluded that the results of batch experiments are transferable to the target process regarding the chemical corrosion mechanisms and the formation of soluble corrosion products. During the experiments, the zinc concentration in the solution increases within the first few days significantly and seems to reach a steady state. Corrosion scars were observed especially in the region of direct solution shower. Only the outer layer of pure zinc is damaged. The inner layer containing iron seems to be more stable against corrosion and no scars reaching the base material were found. It is remarkable that no significant amount of corrosion products of the basic material (Fe) were determined on galvanized samples, in the solutions and on the fibres. The Zn-coating prevented the corrosion of steel in the used media. The absence of impurities such as chloride seems to be a precondition for this behavior. Problems regarding the clogging are expected due to the formation of sparingly soluble zinc borate in boric acid solutions at elevated temperatures.

References

[1]   D. Chen, K.J. Howe, J. Dallman, B.C. Letellier, M. Klasky, J. Leavitt and B. Jain (2007), Experimental analysis of the aqueous chemical environment following a loss-of-coolant accident, Nucl. Eng. Des. 237, 2126–2136

[2]   D. Chen, K.J. Howe, J. Dallman and B.C. Letellier (2008), Corrosion of aluminium in the aqueous chemical environment of a loss-of-coolant accident at a nuclear power plant, Corros. Sci., 50, 1046-1057

[3]   Integrated Chemical Effects Test Project, Consolidated Data Report, NUREG/CR-6914, LA-UR-06-3673

[4]   X.G. Zhang (1996), Corrosion and Electrochemistry of Zinc, Plenum Press, New York 157-176

CFD SIMULATION OF FIBRE MATERIAL TRANSPORT IN A PWR CORE UNDER LOSS OF COOLANT CONDITIONS

Thomas Höhne, Alexander Grahn, Sören Kliem, and Frank-Peter Weiss

1.   Introduction

In the event of a loss-of-coolant accident inside the containment, energetic pressure waves and fluid jets would impinge upon materials in the vicinity of the break such as thermal

Fig. 1: RPV with ECC injection

insulation, coatings, concrete, corrosion products and dust [1]. Through transport mechanisms such as entrainment in steam/water discharge from the break and wash down due to condensate flow in the containment, a fraction of the generated debris and other material in the containment would be transported to the containment sump. Subsequently, if the ECCS pumps are operating in sump recirculation flow, the debris suspended in the containment sump would begin to accumulate on the sump strainers or be transported through the ECC system and the primary coolant system to the core. The accumulation of this suspended debris on the sump strainers can create an almost uniform covering on the strainer, which would tend to increase head loss across the strainer.

On account of this phenomenon, modifications of the insulation, the strainer size and the mesh size at the strainers were carried out in most of the German NPPs to improve the design for emergency core cooling during sump recirculation mode. Moreover, back flushing procedures to remove the mineral wool from the strainers and differential pressure measurement were implemented to assure the performance of emergency core cooling during the containment sump recirculation mode.

Nevertheless, it cannot be completely ruled out, that small fractions of the insulation material are transported into the RPV. During hot leg ECC injection, the fibres enter the upper plenum and can accumulate at the fuel element spacer grids, preferably at the uppermost grid level. This effect might cause a reduction of the ECC flow into the core and degradation of core cooling. Fig. 1 shows the process of the accumulation of insulation material at the uppermost grid spacers of the fuel elements which might be transported through the ECC system of the hot legs. In this figure the numbers mark the following components: (1) upper support plate, (2) control rod guide tubes, (3) fuel element, (4) RPV, (5) core wall, (6) lower support plate, (7) perforated drum, (8) hot leg ECC injection of colder fluid. To analyse the flow behaviour in the core at LOCA condition and ECC injection from the hot legs, experiments at the Upper Plenum Test Facility (UPTF) were carried out [5]. It was shown, that coolant from the ECC injection in the hot legs, where liquid is carried from the reactor sump into the core, is distributed in break-trough channels that correspond with falling water regions, while hotter and therefore lighter coolant rises in the centre of the core (Fig. 1). In general, numerical and

19

experimental studies have been performed in the past to assess the transport behaviour of insulation debris in the containment [2]. In addition, transport of the insulation material through the containment sump via sedimentation and resuspension is an area of interest in quantifying the effect that insulation materials have on ECCS performance. However, the possible transport of insulation material from the ECC injection in the hot legs into the upper plenum and then into the core has not yet been analysed in detail. Therefore, the aim of the numerical simulations by Computational Fluid Dynamics (CFD) presented in this study is to determine where these break-trough channels are situated and how the mineral wool fibres are deposited across the grid spacers of the fuel elements of a German PWR. All fibres which reach the upper-most spacer grid are completely retained giving rise to the formation of a compressible cake of high porosity. Thus, the spacers act like a strainer and the pressure drop over the accumulated fibres can be computed in terms of local deposited fibre mass and flow velocity. The strainer model which was presented in [2] was modified for spacer grids.

2. DYN3D calculation of decay heat

A one-phase CFD calculation was carried out to determine the initial flow conditions on starting of the hot-leg ECC injection in the sump cooling mode. The temperature distribution
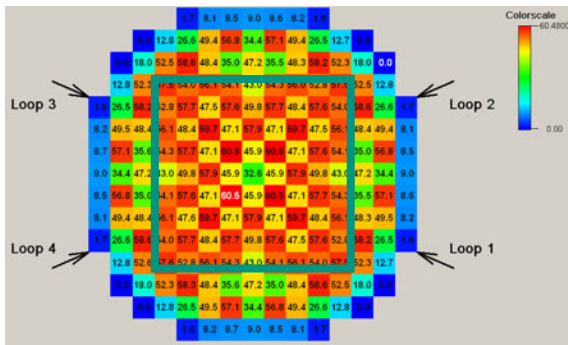
Fig. 2: Temperature differences at the core outlet for each fuel element position

used in the calculation corresponds to a decay heat distribution at the Begin of Cycle of a generic Konvoi reactor core. It was determined using the reactor dynamics code DYN3D based on the following assumptions: coolant mass flow rate 400 kg/s from bottom to top, no crosswise mixing, decay power 80 MW (approx. 2% of the nominal power, 1600 s after SCRAM), no boiling. The calculation showed a maximum coolant temperature difference at the outlet over all fuel element positions of $\Delta T_{max} = 60.5$ K. The average coolant temperature difference between the inner and outer sector (Fig. 2) was $\Delta T_{averaged} = 23.4$ K. These temperature differences between the inner and outer regions of the core are the source of the inner coolant circulation, which influences the presence of the so-called "brake through channels" in the core. In the CFD calculation a coolant temperature difference between the inner and outer region of the core of only $\Delta T_{averaged} = 10$ K was assumed to be on the conservative side.

3. CFD code, initial and boundary conditions

The CFD code for simulating the insulation transport studies was ANSYS CFX [3]. In the current study, the CFD simulations were performed according to the Best Practice Guidelines, with respect to model validation against experiments and grid studies [4]. A convergence criterion of 10^{-4} was considered to ensure negligibly small iteration errors. In the recent calculations shown below, the High-Resolution (HR) discretization scheme of ANSYS CFX was used to discretize the convective terms in the model equations. A second-order implicit scheme was used to approximate the transient terms. The time step size was 0.1 s. The fibre material, which had a different density, was used as a second phase. In a multi-phase flow, the phases have different velocities and temperature fields. The Shear Stress Transport (SST) turbulence model was used to model the effects of turbulence on the mean flow. The initial conditions were modelled using a quasi-steady state calculation, including the results of the decay heat calculation of DYN3D (previous section). In this calculation no ECC injection or

external source was assumed. As a result, an inner coolant circulation started, with upwards directed flow in the inner region and downwards directed flow in the outer region. In the lower plenum the downwards flowing coolant is redirected into the centre of the core and flowing upwards. Then the injection of the ECC water started in all four loops with a mass flow rate of $\dot{m}$ = 150 kg/s and a temperature of T = 330 K. The rock wool concentration was assumed to be 1500 ppm in all four loops with a density of the dry material of 2800 kg/m³. The injection time for the ECC water with an assumed mass of 5 kg insulation material was 2 s. Afterwards ECC water without insulation material (rock wool concentration = 0 ppm) was further injected in all four loops.

4.   Results

At the beginning of the switch-over of the ECC cooling to sump mode the coolant circulates in an inner convection loop in the core. After the start of the sump-cooling mode, the CFD simulations showed that the coolant which was collected in the containment sump and which is injected into the hot legs, is distributed in channels that correspond with the falling water regions in the outer core region, while hotter and therefore lighter coolant is rising in the centre of the core. Fig. 3 shows the nozzle plane of the RPV. The rock wool concentration is plotted (red: rock wool concentration = 1.5×10^{-3}, blue: rock wool concentration = 0). Fig. 4 illustrates the current mass load of rock wool at the upper spacer grid at 50 s after start-up of ECC injection (red: current mass load of rock wool = 1.3 [kg/m²], blue: current mass load of rock wool = 0 [kg/m²], grey: rock wool isosurfaces). The insulation material, which can be carried with the ECC water, accumulates at the spacer grids corresponding to the down flowing channels. Therefore, the fibre material at the uppermost spacer grid plane is not evenly distributed. Four zones of rock wool deposit are developed at the spacer grid. Later on, when the flow trough the channels is reduced due to the accumulation of fibre material the flow is redirected into other regions of the spacer grid. Then the insulation material can also be distributed there. It was found in the calculations that the pressure loss is not higher than 8 kPa with 2.7 kg (at 70 s) disposed fibre material at the spacer grid plane. The CFD calculation did not include steam production in the core or re-suspension of the insulation material during back flow. This would definitely enhance the coolability of the core.

5.   Summary and Outlook

The aim of the numerical simulations carried out in this study was to determine how and where mineral wool fibres transported to the core by ECC water during a LOCA are deposited across the grid spacers of the fuel elements of a German PWR. The spacer grid is modelled as a strainer which completely retains the insulation material carried by the coolant and reaching the plane of the spacers. The accumulation of the insulation material gives rise to the formation of a compressible fibrous cake whose permeability to the coolant flow is calculated in terms of the local amount of deposited material and the local value of the superficial liquid velocity. The calculations showed that the fiber material at the uppermost spacer grid plane is not evenly distributed. First, it is accumulated at the positions of the break-through channels. Later when the inner circulation in the core has stopped, the insulation material can also be distributed into other regions of the spacer plane. Further investigations are necessary to determine the accumulation of insulation material for a longer period of time. Also steam production in the core or re-suspension of the insulation material during back flow should be considered. Moreover, the geometry modeling should be improved taking into account the real structures in the upper plenum and the geometry of the ECC injection nozzle ("Hutze").
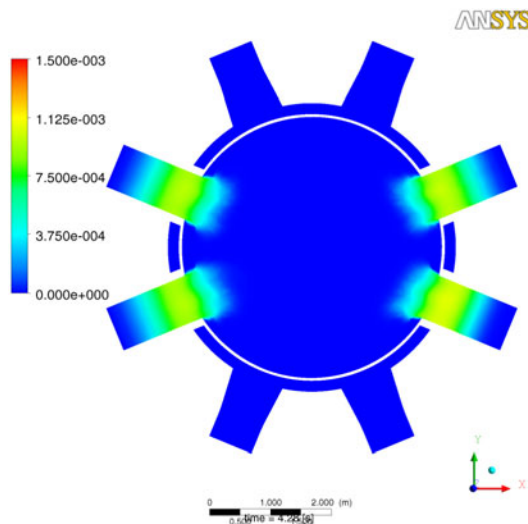
Fig. 3: Rock wool concentration [ppm] 4.3s after start-up of ECC injection, nozzle plane
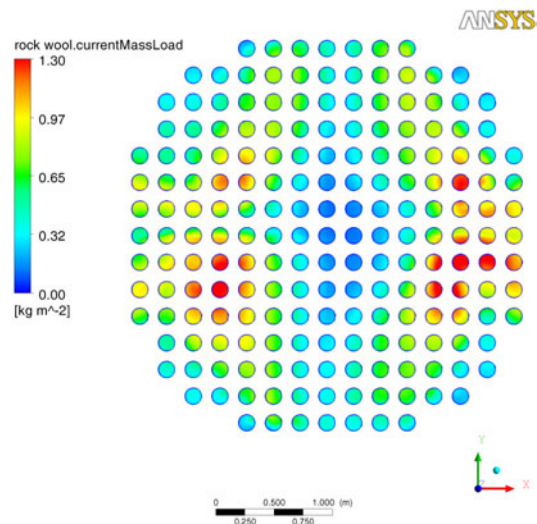
Fig. 4: Rock wool mass load [kg/m²] upper spacer grid 50s after start-up of ECC injection

References

[1]   OECD, ed., 2004. NRC/NEA Workshop on debris impact on emergency coolant recirculation, no. 5468 in Proceedings of the OECD NEA

[2]   A. Grahn; E. Krepper; S. Alt; W. Kästner, Implementation of a strainer model for calculating the pressure drop across beds of compressible, fibrous materials, Nuclear Engineering and Design 238 (2008), pp. 2546-2553

[3]   ANSYS CFX Solver Manual, CFX-12, 2009

[4]   U. Rohde; T. Höhne; S. Kliem; B. Hemström; M. Scheuerer; T. Toppila; A. Aszodi; I. Boros; I. Farkas; P. Muehlbauer; V. Vyskocil; J. Klepac; J. Remis; T. Dury, Fluid mixing and flow distribution in a primary circuit of a nuclear pressurized water reactor – Validation of CFD codes, Nuclear Engineering and Design 237(2007)15-17, 1639-1655

[5]   R. Hertlein; W. Herr, A new model for countercurrent flow in the upper part of a PWR core, NURETH-4, Karlsruhe October 1989, Proceedings Vol.1, p. 88-95

Acknowledgments

MODELING OF TURBULENCE IN BUBBLY FLOWS

Eckhard Krepper, Martin Schmidtke, and Dirk Lucas

1.   Introduction

In CFD modelling the concept of time averaging the Navier Stokes equations proposed by Reynolds has proven successful for the description of turbulent flows for many industrial applications. Questions arise, when the influence of bubbles on turbulence has to be considered. The correct simulation of this influence is quite important since in bubble size population balance models the liquid turbulence influences the bubble fragmentation. Vice versa the liquid turbulence flow structures influence the gas distribution. The latter phenomenon is described as a turbulent dispersion force.

In the present paper the common concept for modelling the influence of bubbles on liquid turbulence quantities proposed by Sato (1981) is described and analysed. Based on this analysis a proposal is derived, describing this influence by sources in the turbulence equations.

Unfortunately in the literature only few experimental data on two phase flow turbulence can be found. Shawkat et al. (2007, 2008) has measured radial profiles of void fractions, gas and liquid velocities and velocity fluctuations. These data were used to validate the described models.

2.   Experiments performed by Shawkat

Shawkat et al. (2007, 2008) have performed measurements in a air/water flow of a vertical upward pipe with diameter of 0.2 m and a height of 8.0 m. Besides radial profiles of gas volume fractions velocities and velocity fluctuations were measured. For the comparison with the model here the axial and radial velocity fluctuations were averaged and transformed in a profile of turbulent kinetic energy.

3.   The concept proposed by Sato

In the k-ε turbulence model for a single phase flow the turbulent viscosity μ_T is defined as a relation between turbulent kinetic energy k and turbulent eddy dissipation ε by:

$$\mu_T = C_\mu \rho_L \frac{k^2}{\varepsilon} \tag{1}$$

with ρ_L as the liquid density. $C_\mu = 0.09$

Sato (1981) proposed for the case of two phase flow, to consider the influence of bubbles by increasing the turbulent viscosity by

$$\mu_S = C_S \rho_L \alpha_G d_b \left| \vec{U}_G - \vec{U}_L \right| \tag{2}$$

where α_G is the gas volume fraction and $\vec{U}_G$ respective $\vec{U}_L$ the gas and liquid velocity, $C_S = 0.6$ and d_b is the bubble size. The integral viscosity is calculated from a laminar part μ_L, the turbulent viscosity μ_T and the bubble induced contribution proposed by Sato μ_S.

$$\mu = \mu_L + \mu_T + \mu_S \qquad (3)$$

This model approach has been used for long time as a CFD standard and yields good agreement between measurements and CFD calculations as far as for the radial gas fraction profiles or velocity profiles are considered. A more detailed knowledge about the turbulence quantities in two phase flow are necessary, when bubble breakup ore coalescence have to be considered.

A comparison to Shawkats measurements shows a reasonable agreement for the single phase case (Fig. 1, blue asterisks and blue solid line) but a strong underestimation of the turbulent kinetic energy in the pipe centre.
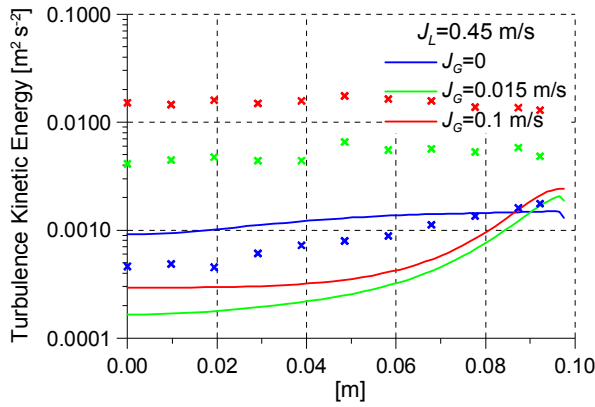
Fig. 1: Measured and calculated profiles for turbulent kinetic energy, measurements marked by asterisks
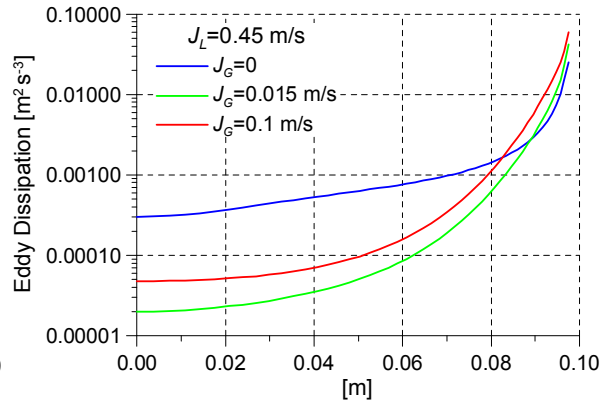
Fig. 2: Calculated profiles for the eddy dissipation

Also the turbulence eddy dissipation in the centre is very low (see Fig. 2) which results in a quite high turbulence viscosity in the centre (see Fig. 3).
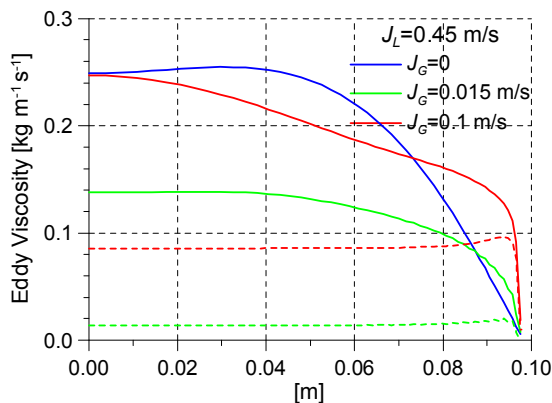
Fig. 3: Calculated profiles for turbulent eddy viscosity, the dotted lines mark the Sato contribution
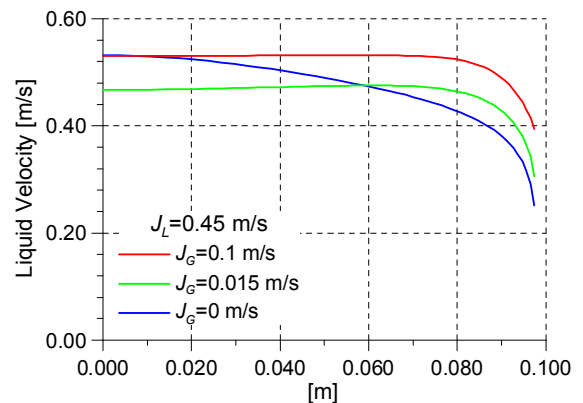
Fig. 4: Calculated profiles for the liquid velocity

4. Consideration of turbulence modulation by sources in the K and Epsilon equations

4.1. Navier stokes equations for two phase flow and bubble induced sources for turbulence kinetic energy

In the K-Epsilon turbulence model for a liquid continuous phase the presence of a dispersed gaseous phase can be considered in the equation for the turbulence kinetic energy k:

$$\frac{\partial}{\partial t}\left(\alpha_L \rho_L k_L\right) + \nabla \cdot \left(\alpha_L \rho_L \vec{v}_L k_L\right) = \nabla \cdot \left(\alpha_L \frac{\mu_T}{\sigma_k} \nabla k_L\right) + P_L - \rho_L \varepsilon_L + S_L^k \tag{4}$$

and for the eddy dissipation ε:

$$\frac{\partial}{\partial t}\left(\alpha_L \rho_L \varepsilon_L\right) + \nabla \cdot \left(\alpha_L \rho_L \vec{v}_L \varepsilon_L\right) = \nabla \cdot \left(\alpha_L \frac{\mu_T}{\sigma_\varepsilon} \nabla \varepsilon_L\right) + \frac{\varepsilon_L}{k_l}\left(C_{1\varepsilon} P_L - C_{2\varepsilon} \rho_L \varepsilon_L\right) + S_L^\varepsilon \tag{5}$$

S_L^k in equ. (4) describes the bubble induced source in the k-equation. Assuming all frictional work of a rising bubble is converted into turbulent kinetic energy this source can be calculated by

$$S_L^k = -\vec{F}_k^d \cdot \alpha_G \left|\vec{U}_G - \vec{U}_L\right| \tag{6}$$

where $\vec{F}_k^d$ is the drag force, α_G the gas volume fraction and $\vec{U}_G$ respective $\vec{U}_L$ the gas-respective the liquid velocity. For the Source in the Epsilon-equation equ. (5) is obtained:

$$S_L^\varepsilon = C_{\varepsilon 3} \frac{S_L^k}{\tau} \tag{7}$$

4.2. Bubble induced sources for turbulence eddy dissipation

Unfortunately there is no theoretical justification in the literature for the corresponding source S_L^ε in the Epsilon-equation, equ. (7). Most approaches consider S_L^ε proportional to S_L^k. The relaxation time τ in most cases is calculated on a dimensional background. Different concepts have been proposed.

Morel (Yao 2004) assumed an additional dependency on the bubble size d_b because the wakes behind the bubbles are assumed to be originally of the same diameter. The larger these wakes, the larger will be the time for their energy to cascade towards the smallest turbulence scales before to be dissipated. So, if bubbles are quite large, the turbulence generated is their wakes will have longer life duration:

$$\tau = \left(\frac{d_b^2}{\varepsilon_L}\right)^{1/3} \tag{8}$$

Troshko and Hassan (2001) propose the consideration of the coefficients of virtual mass C_{VM} and the drag force C_D:

$$\tau = \frac{2C_{VM}d_b}{3C_D\left|\vec{U}_G - \vec{U}_L\right|} \tag{9}$$

In the practical application of these approaches, the proposal of Troshko and Hassan, see equ. (9), causes some stability problems because of the velocity difference in the denominator. Both approaches need an additional adjustment of the factor $C_{\varepsilon 3}$, see equ. (7).
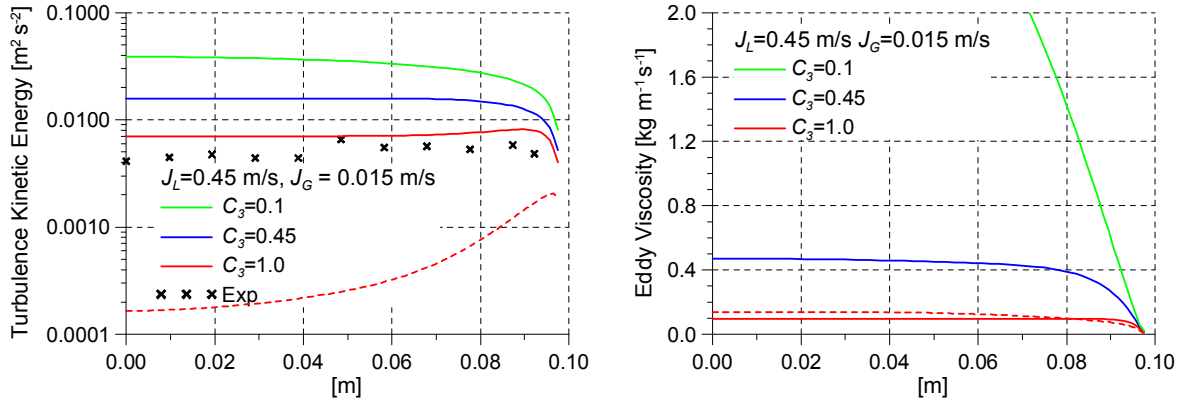
Fig. 5: Calculated profiles for turbulent kinetic energy (left) and for eddy viscosity (right) for different values of C_3, the dotted lines mark the Sato approach (comp. Fig 1)

The application of the Morel approach, see equ. (8), shows a much better agreement to the Shaw kat experiments than the Sato approach. Fig. 5 shows the profiles of turbulent kinetic energy and of eddy viscosity for different values of C_3. For comparison the corresponding values according to Sato are added as dotted lines. For $C_3 = 1.0$ a good agreement to Shawkat's measurements is found. Furthermore this value shows an agreement to the turbulent viscosity according to Sato's proposal.

5.   Validation by Shawkat's experiments

Different tests were calculated applying the approach of Morel with $C_3 = 1.0$ and compared to Shawkats measurements. The results are shown in Figures 6 to 8. For comparison the values gained by the Sato approach are added by dotted lines (comp. Fig. 1 and 2).
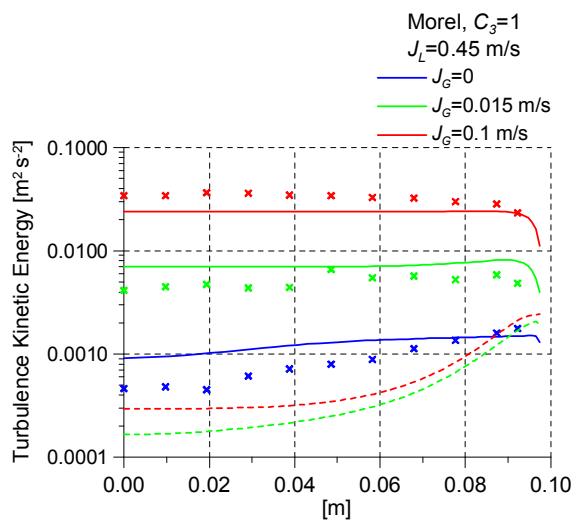
Fig. 6: CFD simulation of the profiles for turbulent kinetic energy
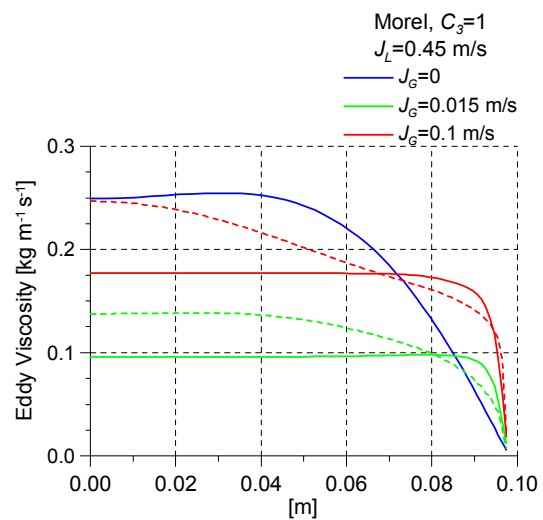
Fig. 7: Profiles for turbulent viscosity
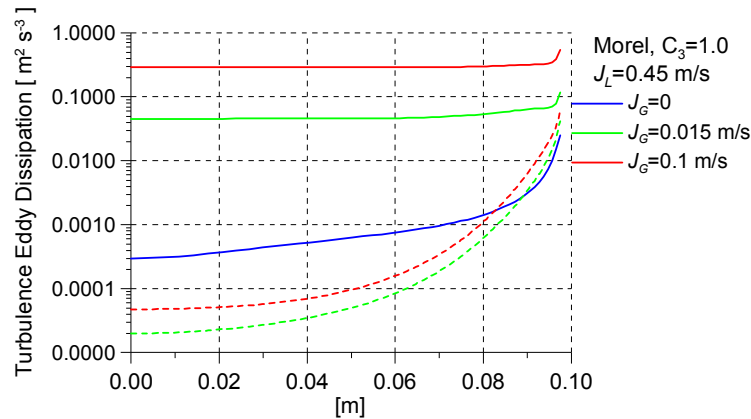
Fig. 8: CFD simulation of the profiles for turbulent eddy dissipation

Fig. 7 to 9 shows only a small illustrative part of the performed validation calculations. All simulation show similar tendencies.

6.   Conclusions and outlook

The presented approaches considering the influence of bubbles on turbulence have a physical confirmation for the production of turbulent kinetic energy by bubbles and for the formulation of the corresponding sources for the turbulent dissipation. The approaches yield a much better agreement to measured turbulent kinetic energies.

The simulated turbulent viscosity remained almost the same level calculated using the Sato approach. Additional work, which is not presented here, investigates the diffusive effect of the turbulent dispersion force and shows that the assumed model approaches are justified.

The turbulent eddy dissipation influences bubble breakup. The correct simulation of these values will have an essential influence on models for bubble breakup and coalescence, which are the basis of bubble population balance models.

References

[1]   A. Burns, T. Frank, I. Hamill, J.-M. Shi (2004) The Favre Averaged Drag Model for Turbulent Dispersion in Eulerian Multi-Phase Flows, 5th International Conference on Multiphase Flow, ICMF'04, Paper No. 392

[2]   D. Lucas, J.-M. Shi, E. Krepper, H.-M. Prasser (2004) Models for the forces acting on bubbles in comparison with experimental data for vertical pipe flow, 3rd International Symposium on Two-Phase Flow Modelling and Experimentation, 22.-24.09.2004, Pisa, Italy

[3]   M. Politano, P. Carrica, J. Converti (2003) A model for turbulent polydisperse two-phase flow in vertical channels, Int. J. of Multiphase Flow , 29, 1153

[4]   Y. Sato, K. Sekoguchi (1975) Liquid velocity distribution in two phase bubble flow. Int. J. Multiphase Flow, vol. 2, pp. 79-95.

[5]   Y. Sato, M. Sadatomi, K. Sekoguchi (1981) Momentum and heat transfer in two-phase bubble flow-I, Int. J. of Multiphase Flow, vol. 7, pp. 167-177.

[6]   M. Shawkat, C.Y. Ching, M. Shoukri (2007) On the liquid turbulence energy spectra in two-phase bubbly flow in a large diameter vertical pipe, Int. J. Multiphase Flow, 33, 300

[7] M. Shawkat, C.Y. Ching, M. Shoukri (2008) Bubble and liquid turbulence characteristics of bubbly flow in a large diameter vertical pipe, Int. J. of Multiphase Flow, 34, 767

[8] A.A. Troshko, Y.A. Hassan (2001) A two-equation turbulence model of turbulent bubbly flows, Int. J. of Multiphase Flow, 27, 1965

[9] W. Yao, C. Morel (2004) Volumetric interfacial area prediction in upward bubbly two-phase flow, Int. J. of Heat and Mass Transfer, 47, 307

Acknowledgement

PROTOTYPE COUPLING OF THE CFD CODE ANSYS CFX WITH THE 3D NEUTRON KINETIC CORE MODEL DYN3D

Sören Kliem, Ulrich Rohde, Jochen Schütze[1], and Thomas Frank[1]

1.   Introduction

Analyses of postulated reactivity initiated accidents in nuclear reactors are carried out using 3D neutron kinetic core models. The feedback is usually calculated using 1D thermal hydraulic models for channel flow, partly with the possibility of cross flow between theses channels. A different possibility is the use of subchannel codes for the determination of the feedback. The code DYN3D developed at Forschungszentrum Dresden-Rossendorf is an example for a 3D neutron kinetic core model. In its basic version, the code contains models for the solution of the 3D neutron diffusion equation in two energy groups for fuel assemblies with rectangular and hexagonal cross section [1]. Recently the code was extended to an arbitrary number of energy groups. Further, a simplified transport approximation for the flux calculation was implemented for fuel assemblies with quadratic cross section [2].

The computational fluid dynamics (CFD) code ANSYS CFX [3] is the reference CFD code of the German CFD Network in Nuclear Reactor Safety. One of the goals of the co-operation inside this network is the development of CFD software for the simulation of multi-dimensional flows in reactor cooling systems. This includes the coupling of the CFD code ANSYS CFX with the 3D neutron kinetic core model DYN3D.

2.   Coupling of ANSYS CFX and DYN3D

The coupling approach is based on the selection of best-in-class software tools for the simulation of each of the phenomena to be described by the coupled codes. For this, the module predicting the coolant flow within DYN3D is replaced by a fully three-dimensional CFD simulation using ANSYS CFX. A detailed and spatially resolved modeling of the whole reactor core down to the fuel pin level in the CFD code is not feasible for practical applications at present and in the foreseeable future. It is possible to achieve acceptable computation times only by modeling the reactor core as a porous region. This reduced resolution of the structures in the core affects the thought location of the interface between the CFD code and the neutron kinetics core model. An incorporation of the bare neutron kinetics model of DYN3D only, as it was done in the internal coupling of ATHLET and DYN3D [4], is not possible because the heat transfer from the fuel pins to the coolant cannot be calculated by ANSYS CFX due to the above mentioned restrictions. Therefore, it was decided to define the physical data interface at the level of the volumetric heat release rate into the fluid. The CFD code ANSYS CFX calculates the fluid dynamics in the reactor coolant inside the core. It provides the velocity, temperature, density and boron concentration fields to DYN3D. Based on these parameters DYN3D determines the nuclear power, calculates the fuel temperature distribution and the heat transfer to coolant. The volumetric heat source is given back to ANSYS CFX. It should be noted that in the current prototype, the coupling is restricted to single-phase flow conditions.

In the coupled calculation, ANSYS CFX acts as the master program; DYN3D is implemented as a set of subroutines. A 3D volume mesh-to-mesh transfer of field quantities between

---

[1]ANSYS Germany GmbH Otterfing and Darmstadt

ANSYS CFX and DYN3D had to be implemented taking into account the largely different mesh resolutions used in the two codes. A 3D volume mesh-to-mesh transfer for arbitrary data fields was implemented in CFX. The conservation of the data during transfer is properly ensured. The DYN3D coarse nodalisation is represented by a separate, coarsely meshed zone in CFX. This coarsely meshed zone is also available for post-processing DYN3D data in CFX-Post. Both zones co-exist side-by-side in CFX.

For steady-state calculations an iteration scheme between ANSYS CFX and DYN3D was implemented. In the DYN3D stand-alone case the thermal hydraulics is brought to convergence at each iteration step before going to the solution of the neutron-kinetic equations. In the coupled code calculation the approach is different: DYN3D is called at the end of each iteration step of ANSYS CFX. In this way, the number of iterations between the codes increases, but this implementation requires less total computation time as the dominant part of the computation time is spent for ANSYS CFX.

At the current stage of the implementation no iteration between ANSYS CFX and DYN3D is carried out during transient calculation. An explicit coupling approach is applied. DYN3D is called at the end of each time-step.

3.   Verification

3.1.   Steady-state problem

For the verification of the steady-state calculation procedure, a mini-core consisting of nine real size PWR fuel with a power of 50 MW was set-up (Fig. 1). As usual, the resolution of the DYN3D grid is one node per fuel assembly in radial direction. 14 nodes were used over the height. The CFX calculation grid contains 14,308 nodes. The fluid flow solver in ANSYS CFX was set up so as to only allow purely 1D flow in parallel channels in order to ensure the comparability with the DYN3D stand alone results.
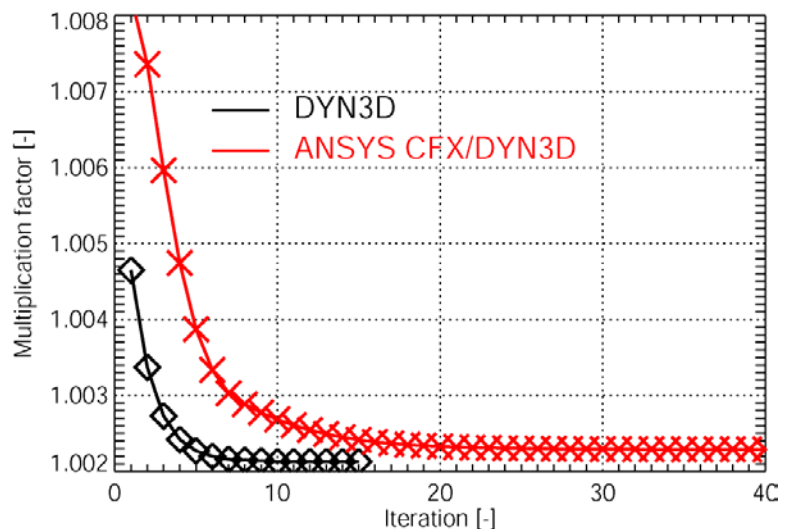
Fig. 1: Scheme of the mini-core   Fig. 2: Convergence of steady-state calculations

Fig. 2 shows the convergence of the effective multiplication factor in both calculations. The number of iterations is higher in the coupled calculation. This is due to the above mentioned different iteration scheme, where the neutron-kinetic module is called at every iteration step in CFX. In the stand alone version of DYN3D, the neutron-kinetic module is called only when

the thermal hydraulics has reached convergence. Here, the internal thermal hydraulic iterations are not counted. The resulting K_{eff}-values differ by 9.8 pcm, only. The reason for the differences was found in different material property packages. CFX uses the current standard for water properties IAPWS-IF97 while DYN3D uses the former standard IFC-67.

3.2. Transient problem

For the verification of the implementation of the transient calculation option the withdrawal of the control rod from the central fuel assembly at hot zero power was selected. The initial position of the control rod was selected with 1.50 m from lower edge. The time for full withdrawal was set to 20 s. Time-explicit coupling had been implemented so far, only. Calculations were carried out with variation of the time step size. The results of the calculations with time steps of 10 and 1 ms are shown on Fig. 3 and Fig. 4. For comparison purposes the iteration within each time step in the DYN3D stand-alone code was deactivated.
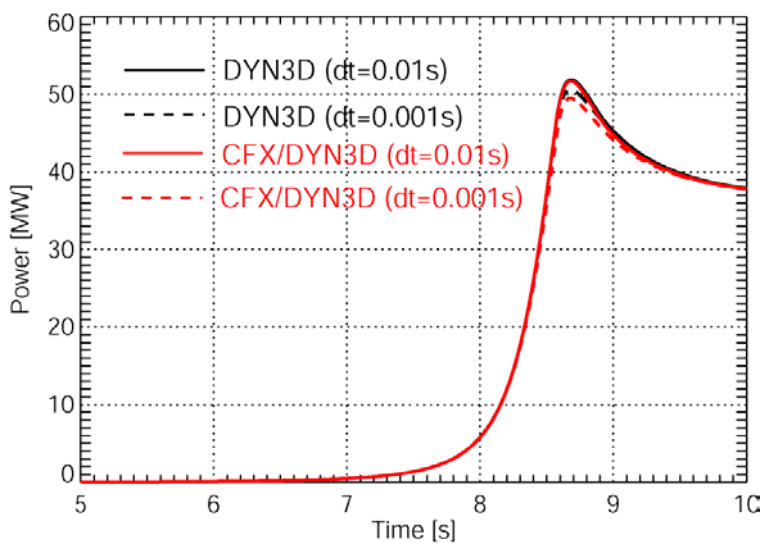
Fig. 3: Core power behavior in the DYN3D and CFX/DYN3D calculations

The power starts to rise remarkably after 7 s. A power peak occurs which is compensated by the Doppler feedback. Due to continuing control rod extraction the power will rise further. Here, only the first 10 s are analyzed. This includes the first power maximum and the power decrease due to fuel temperature increase.

The overall behavior of the core power is identical in all four calculations. Differences are to be seen in the maximum value reached. This maximum reduces with decreasing time step size in both codes. Both codes converge to different maximum values. This was proven by further reduction of the time step. The difference in the maximum core power is about 1 MW. This difference is acceptable considering the following: The introduced positive reactivity during the transient is slightly below 1 $. In the reactivity range around 1 $ the power behavior is very sensitive to changes in the feedback parameters. Therefore, smallest differences between the different transient flow solvers can have significant effect on the time-dependent feedback. One such difference is already known to lie in different water material property packages.

Further investigation on the transport of a temperature perturbation through the reactor core confirmed that the DYN3D flow solver shows some additional difference in comparison to the ANSYS CFX flow solver.

4. Conclusions and future work

The coupling of the CFD code ANSYS CFX with the neutron-kinetic core model DYN3D was successfully accomplished. The new coupled code system ANSYS CFX/DYN3D allows

for more realistic analyses of coupled thermal hydraulics – neutron kinetics problems. Steady-state and transient verification calculations for a small-size test problem confirmed the correctness of the implementation of the coupling.
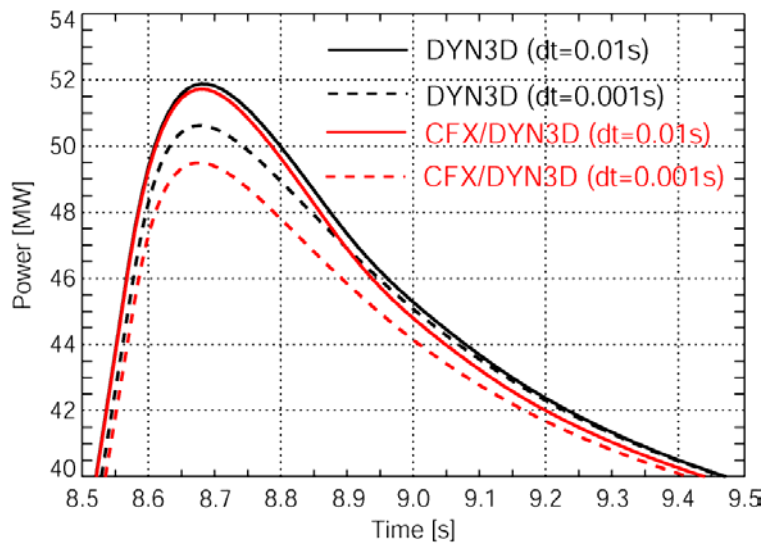
Fig. 4: Core power behavior in the DYN3D and CFX/DYN3D calculations (zoom)

Further verification and validation is needed before its application to accident scenarios. In the near future the semi-implicit time domain coupling should be introduced in the coupling. The extension of the coupling to two-phase flow conditions is a further precondition to carry out realistic accident analyses. In this field additional methodical work has still to be done, e.g. on the splitting of the volumetric heat source between liquid heat-up and vaporization and on two-phase flow treatment in the porous body approach. Further work will also be done on the automated mesh generation for the coupled code.

References

[1]   U. Grundmann, U. Rohde, S. Mittag (2000), DYN3D – Three Dimensional Core Model for Steady-State and Transient Analysis of Thermal Reactors, Proc. PHYSOR2000, Pittsburgh, USA
[2]   C. Beckert, U. Grundmann (2008), Development and verification of a nodal approach for solving the multigroup SP3 equations, Annals of Nuclear Energy, 35/1, pp. 75-86
[3]   ANSYS Inc. (2009), ANSYS 12.0 User's Guide, Canonsburg, PA, USA
[4]   Y. Kozmenkov, S. Kliem, U. Grundmann, U. Rohde, F.-P. Weiss (2007), Calculation of the VVER-1000 coolant transient benchmark using the coupled code systems DYN3D/RELAP5 and DYN3D/ATHLET, Nucl. Eng. Design, 237, pp. 1938-1951

Acknowledgment

APPLICATION OF ANALYTICAL SOLUTIONS TO YALINA EXPERIMENTS SC3A AND SC3B

Bruno Merk, Varvara Glivici-Cotruţă, and Frank-Peter Weiss

1.   Introduction

Different current and planned experiments (YALINA [1], Guinevere [2]) are designed to study the zero power neutron physical behavior of accelerator driven systems (ADS). The detailed analysis of the kinetic space-time behavior of the neutron flux is important for the evaluation of these ADS experiments. Up to now, the analysis for all these experiments is based on the zero dimensional standard methods [3] - Sjöstrand method [4] and Slope method [5]. Zero dimensional analysis relies on separation of space and time and does not provide reliable results for cases with space-time dependent external source [6]. Our proposal is to handle this problem by solving more elaborate approximations of the transport equation - the time dependent Telegrapher's equation [7] or the space-time dependent diffusion equation [8]. Solutions for the Telegrapher's equation have already been provided for a Dirac type external source [9], for the start up, [14], and for the switch off [6] of an external source. The Telegrapher's equation and the diffusion equation without delayed neutron production are solved completely analytically by using the Green's function method [10]. For the comparison with the experimental results, obtained at the YALINA-Booster facility, a special external source (switch on followed by a switch off after a finite time period) is used for the application with the Green's function. The derived solutions for the space-time dependent neutron flux (diffusion and P_1 transport) are compared to the detector responses at different locations in the fast area of the YALINA-Booster core [12]. The final aim is a fast method for the analysis of the experiments and the calculation of integral parameters comparable to those defined for critical reactors.

2.   Comparison with Experiments

The developed analytical approximation solution for the space-time dependent neutron flux following the finite source pulse [13] is compared with the results from two different experimental setups, SC3A and SC3B [15], at the YALINA-Booster facility in Belarus.

The basic core of the YALINA-Booster facility consists of the central target region, surrounded by the region with 90% enriched uranium metal rods in a lead matrix. This central region is surrounded by another fast region consisting of lead with 36% enriched uranium oxide(UOX) rods. In this region the three experimental channels (EC1B, EC2B, and EC3B) are located (see Fig. 1). The fast region is decoupled from the surrounding thermal region by the so-called "valve", consisting of one row of natural uranium metal rods and one row of boron carbide rods. The thermal region consists of a polyethylene matrix with holes, which are filled either with 10% enriched UOX fuel or with air. The core is surrounded by a graphite reflector.

The SC3A and SC3B configurations of the YALINA-Booster facility are used for the comparison with the analytical solution. In the SC3A configuration the 90% enriched uranium metal fuel of the inner fast zone is replaced by 36% enriched uranium oxide fuel. In the SC3B configuration this inner fast region is empty, and 13 of 10% enriched uranium oxide fuel rods at the boundary of the core in the thermal part are added, to compensate for the loss in criticality. The 2D HELIOS transport calculation has been corrected with a leakage term in

the third dimension to reach a comparable result to a MCNP calculation [13]. This model is used for the production of the, in the analytical solution, needed cross section set is needed. Cross section sets are derived for the reference element and the whole fast system only without the natural uranium and boron carbide row. The external source is not taken into account in the HELIOS calculation for the cross section preparation.
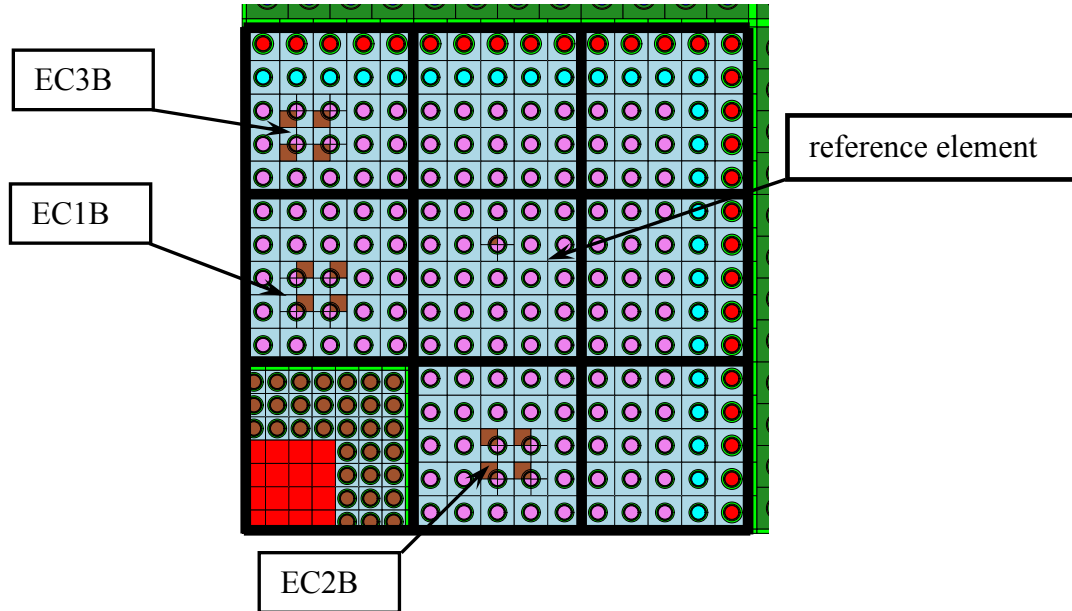
Fig. 1: Central fast area of the YALINA-booster core

The results of the analytic approximation solution for the three different detector positions (EC1B, EC2B, and EC3B) are compared to the detector response [11] in the experiment in Fig. 2. The cross sections are taken for the reference element. It is observable, that the real source in the experiment (blue diamonds) does not have the ideal shape in the experiment, like it is defined in the mathematical model. This fact causes observable differences in the results for the experiment and the analytical solution. Nevertheless, there is a good agreement between the analytical results with the experimental ones. The detector response for the three different detector positions - EC1B (red), and EC2B (black) and EC3B (green) - is given by diamonds at different time points of the experiment.
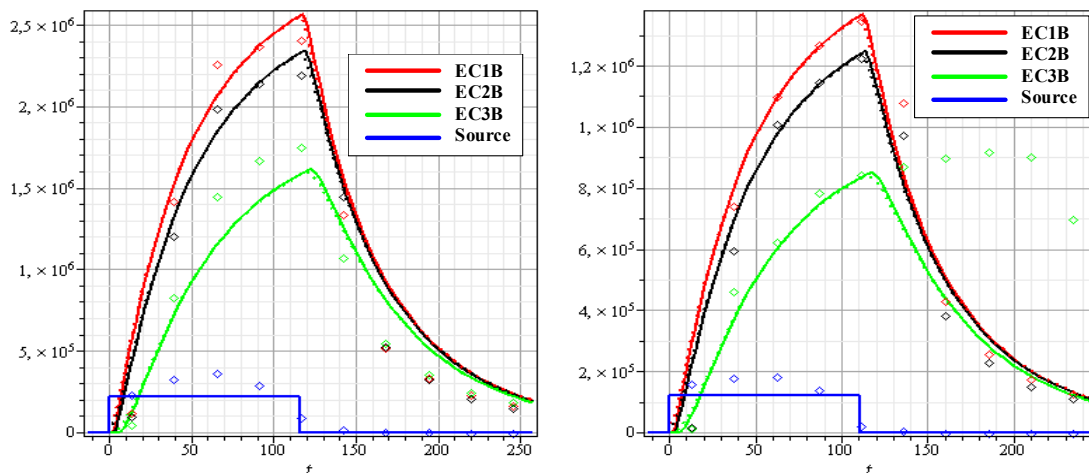
Fig. 2: Comparison of the analytical results for the space-time dependent neutron flux, using the reference element cross section set, with the experimental results for the SC3A (left) and SC3B (right) configurations of the YALINA-Booster facility

The time behavior of the neutron flux, calculated with the analytical time dependent P_1 transport solution at the different positions of the detector, is given by the full lines. The comparison with the experiment demonstrates, that the developed solution without space and time separation can reproduce the behavior of the neutron flux at the different positions of the detectors. In the calculation, the rise in the neutron flux, caused by the steep switch on of the external source is stronger. After roughly 10 neutron generations the neutron production due to multiplication the one of the external neutron source exceeds. The calculated neutron flux rises as long as the external source is in operation, and would reach a steady state value if the external source would be operated long enough. The neutron flux decays very rapidly in an exponential manner after the switch off of the external source. The response at the outermost detector is somewhat lower in the calculation; the reason will be given later. Over all, the agreement between the calculation and the experiment is slightly better for the SC3B than for the SC3A. Especially the analytical calculation result for the position EC3B in SC3B experiment is in rather good agreement with the experimental result.
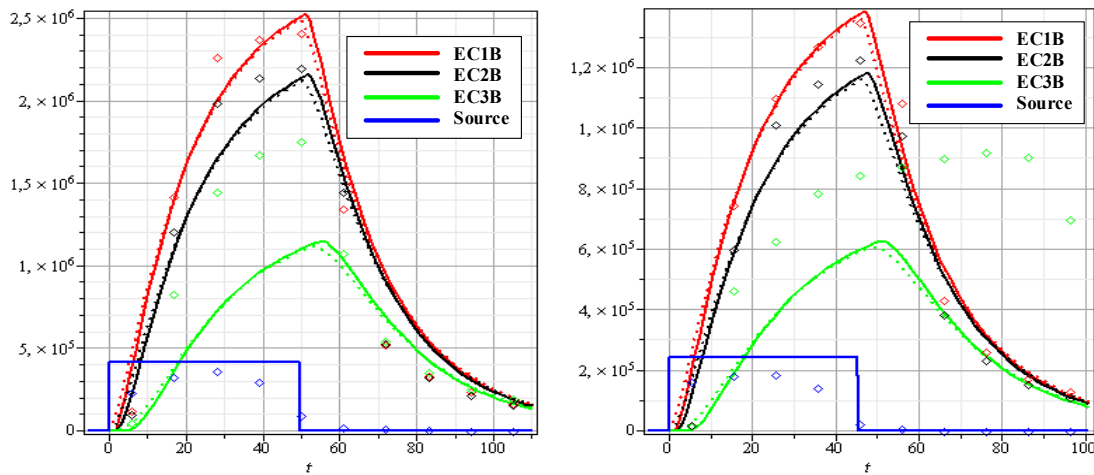
Fig. 3: Comparison of the analytical results for the space-time dependent neutron flux with the experimental results for the SC3A (left) and SC3B (right) configurations of the YALINA-Booster facility, using the fast system cross section set

Fig. 3 shows the analysis of the same experiment, but this time, with a changed cross section set. Now for the calculations with the analytic approximation solution the cross section set for the fast system is used. The agreement between the experimental results (diamonds) and the analytical results (lines), compared to the results for the reference element cross section set, is worse for all detector positions. The time shape of the analytic solution, as well as the spatial distribution, does not agree in a same manner as in the case of the reference element cross section set.

3.   DISCUSSION OF THE YALINA-BOOSTER CONFIGURATION

For a more detailed analysis of the differences shown in the last paragraph, cross sections sets are produced and compared for each fuel element in the fast system of SC3B. For Fig. 4 shows the $\nu\Sigma_f$ cross section for each fuel element in the fast region. The central element (at the front of the figure) is empty, like it is given in the SC3B configuration which is without filling the inner part of the booster region. The three inner elements have a macroscopic $\nu\Sigma_f$ cross section between 0.0051 and 0.058 cm^{-1}. The $\nu\Sigma_f$ cross section in the elements of the outer row is significantly higher, between 0.01 and 0.016 cm^{-1}. The maximum appears in the corner element, which is surrounded on two sides by the thermal system.
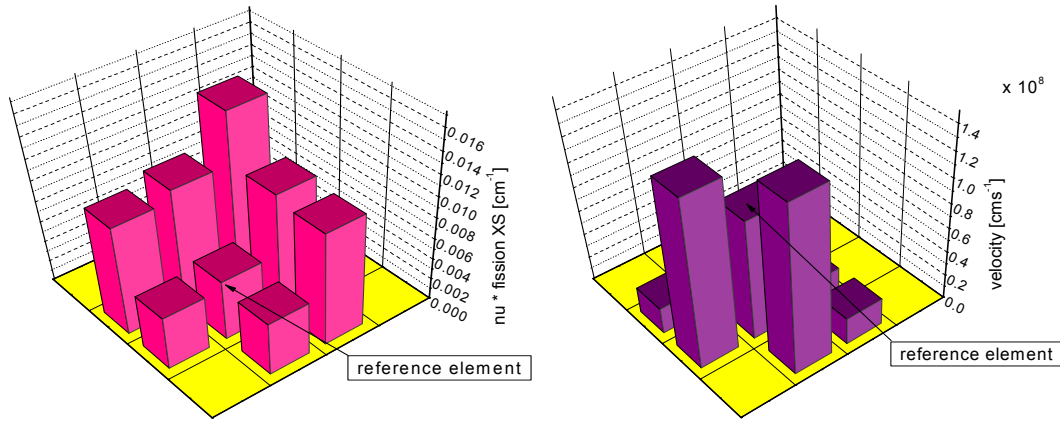
Fig. 4: Neutron production cross section (left) and neutron velocity (right) for the different fuel elements and areas in the fast part of YALINA-booster for SC3B

Nevertheless, the material configuration is identical in all eight elements. The only reason for the strong increase of the $\nu\Sigma_f$ cross section can be a significantly different energy distribution of the neutron flux. The right figure shows the distribution of the average neutron velocity for the eight different fuel element positions. The average neutron velocity in the inner ring varies between $13.8 \cdot 10^7$ cm/s at the two innermost elements close to the central external source region, and $9.9 \cdot 10^7$ cm/s in the reference element. In the outer ring the neutron velocity is significantly lower - between $2.2 \cdot 10^7$ cm/s and $1.2 \cdot 10^7$ cm/s - in the corner element. This distribution of the average velocity indicates that thermal neutrons leak through the 'valve', from the moderated thermal area into the fast region. The presence of thermal neutrons, which causes the lower average neutron velocity, explains the significantly higher macroscopic $\nu\Sigma_f$ cross section, since the microscopic fission cross section of uranium is several decades higher for thermal neutrons.
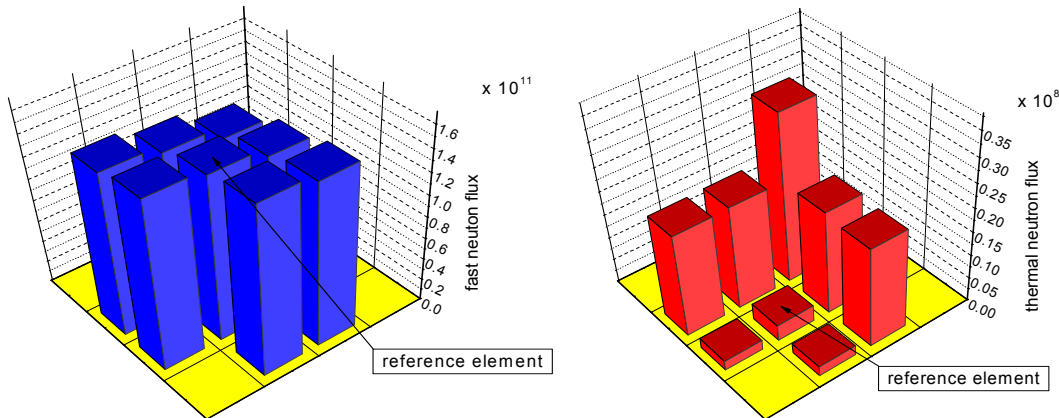
Fig. 5: Fast neutron flux (left) and thermal neutron flux (right) in the different fuel elements and areas in the fast part of YALINA-booster for SC3B

Finally, the fast and the thermal neutron flux distributions are given in Fig. 5. The cut-off energy is the traditional value of $6.2506 \cdot 10^{-1}$ eV. The spatial distribution of the fast neutron flux (left figure) shows the expected distribution. The fast flux distribution is cosine like, since the external source is not taken into account in the transport calculation for cross section generation. This result is in strong contrast to the result for the thermal neutron flux (right figure). The thermal neutron flux shows a distribution which is neither expected, nor typical for a reactor core, since the thermal neutron flux is the highest in the corner of the fast zone.

This kind of distribution can only be explained by the ingress of thermal neutrons from the moderated outer region through the "valve" into the fast area. The influence of the thermal neutrons on the cross section preparation is like already mentioned very strong, since the microscopic cross section, e. g., fission of U-235, is several hundred times higher than for fast neutrons.

4.   Conclusions

The newly developed methodology represents an encouraging basis for a new method for the analysis of ADS experiments. The developed method for the solution of the time dependent P_1 transport equation without separation of space and time, based on Green's functions, appears to be promising. A special solution for a finite pulse of the localized external neutron source has been developed. The cross section set is produced with the HELIOS 1.9 code.

The comparison of the results of the analytic approximation with experimental ones from the YALINA-Booster facility has been successful for the SC3A and the SC3B setups. Very promising results have been obtained, and a good agreement between the experiment and the calculation has been achieved in space, as well as in time. The dependence of the quality of the result of the analytical solution on the cross section set has been investigated.

The special configuration of the YALINA-Booster facility is discussed. The two region core configuration (the fast and the thermal zones) has important influence on the results. The $\nu\Sigma_f$ cross section and the average neutron velocity in the fast zone have been evaluated for all fuel element positions, and significant differences have been found for the different fuel element positions with identical fuel elements. In the next step, the two group neutron flux is investigated for all fuel element positions in the fast zone. The significantly increased thermal neutron flux in the corner position close to the moderated region shows the insufficient efficiency of the thermal neutron "valve". The appearance of the thermal neutrons from the moderated region causes significant problems in the cross section preparation, since the cross sections for uranium is several times higher for thermal neutrons than for fast neutrons. Due to the described effects, the YALINA configuration causes significant problems for cross section preparation, since the standard onset one fuel element in an infinite grid cannot be used at all. A full system calculation is needed for a precise and reliable cross section preparation.

References

[1]   A.I. Kievitskaia, et al., Experimental and theoretical research on transmutation of long-lived fission products and minor actinides in a subcritical assembly driven by a neutron generator, 3rd Int. Conf. on ADTTA, Praha, (1999)

[2]   H.Aït Abderrahim, P.Baeten, The GUINEVERE-project at VENUS, Project Status, ECATS meeting, Cadarache, 31. Jan. (2008)

[3]   C. Persson et. al, Analysis of reactivity determination methods in the subcritical experiment Yalina, Nuclear Instr. and Meth. in Physics Research A 554 (2005)

[4]   N. G. Sjöstrand, Measurements on a subcritical reactor using a pulsed neutron source, Arkiv för Fysik, 11, pp. 13 (1956)

[5]   B. E. Simmons, J. S. King, A Pulsed Neutron Technique for Reactivity Determination, Nucl. Sci. Eng., 3, pp. 595. (1958)

[6]   B. Merk, F. P. Weiß, A three scale expansion solution for a time dependent neutron transport problem with external source, Nuclear Science and Engineering 163, pp. 152-174 (2009)

[7]   A. M. Weinberg, E. P. Wigner, The Physical Theory of Neutron Chain Reactors, The University of Chicago Press, Chicago (1958)

[8]   B. Merk, F.P.Weiß, A Two Group Analytical Approximation Solution for an External Source Problem without Separation of Space and Time, submitted Annals of Nuclear Energy (2009)

[9]   B. Merk, Time Dependent Analytical Approximation Solutions for a Pulsed Source Problem: P1 Transport versus Diffusion, IEEE Nuclear Science Symposium, Dresden (2008)

[10]   B. Merk, An Analytical Solution for a One Dimensional Time Dependent Neutron Transport Problem with External Source, Transport Theory and Statistical Physics, 37: 5-7, pp.535-549 (2008)

[11]   Calle Berglöf, YALINA-Booster: Pulsed Neutron Source Characterization, 2nd EUROTRANS ECATS Progress Mtg, Aix-en-Provence, France, Jan 28-29 (2009)

[12]   V. Bécares Palacios et al., Analysis of PNS measurements at the YALINA-Booster subcritical facility, 2nd EUROTRANS ECATS Progress Meeting, Aix-en-Provence, France, Jan 28-29 (2009)

[13]   B. Merk, V. Glivici-Cotruță, F. P. Weiß, A Solution for the Telegrapher's Equation with External Source: Development and First Application, submitted to Nuovo Ciemento

[14]   B. Merk, An Analytical Approximation Solution for a Time-Dependent Neutron Transport Problem with External Source and Delayed Neutron Production, Nuclear Science and Engineering 161, pp. 49-67 (2009)

[15]   B. Merk, V. Glivici-Cotruță, F. P. Weiß, A Solution for the Telegrapher's Equation with External Source: Application to YALINA - SC3A and SC3B, PHYSOR 2010, Pittsburgh, USA (2010)

Acknowledgement

ON THE USE OF A MODERATION LAYER TO ENHANCE THE FEEDBACK COEFFICIENTS IN A SODIUM COOLED FAST REACTOR

Bruno Merk and Frank-Peter Weiss

1. Introduction

Reduction of the sodium void effect is an important point in the design of sodium cooled fast reactors. Already in the 70ies studies were performed to reduce the sodium void coefficient [1]. These studies were mostly performed on the basis of full core calculations to optimize the core geometry to reduce the sodium void coefficient. No calculations on fuel element basis were performed due to the limited computer resources at this time. Current publications concentrate mostly on the design [2] and basic discussions on the nature of the sodium void coefficient and give rough suggestions what should be tested to reduce the sodium void coefficient [3].

New possibilities arise due to the rapid development of the computational tools for two dimensional fuel element calculations in light water reactor (LWR) technology in the late 90ies. These tools based on unstructured mesh, like HELIOS [4], offer the chance to investigate the sodium void effect on fuel element level in more detail, including multigroup visualization of integral and resolved spectra and cross sections.

Nevertheless, it is important to focus not only on the sodium void coefficient, but rather to investigate all major feedback coefficients in these calculations.

2. Sodium void effect

The calculations to study the influence of changes in the fuel rod and element composition are preformed on a fuel element, based on the European fast reactor (EFR) design [6, 8], additional values are taken from a standard reference [7].
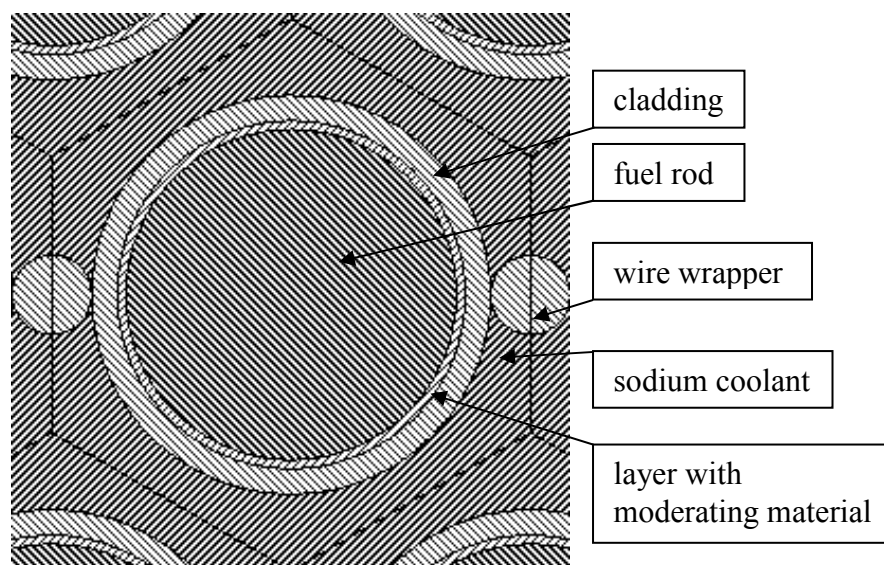
Fig. 1: Unit cell out of a fuel element based on the European fast reactor (EFR) design

Fig. 1 shows a unit cell out of the full fuel element, which was used for the calculations. In addition to the standard elements of a unit cell – fuel rod, cladding, sodium coolant and spacer wire – a small layer consisting of moderating material and resonance absorber is introduced. The layer is placed between the fuel pellet and the cladding. The function of this small layer is to reduce the sodium void effect coinciding with the force up of the absolute value of the negative fuel temperature effect and the reduction of the positive coolant effect (consisting of coolant density and temperature effect).

Fig. 2 shows the neutron spectrum in the calculated fast reactor fuel element, based on the EFR design and the, over the fuel element averaged macroscopic cross sections. It is easily visible in this figure, that the neutron flux spectrum in a sodium cooled fast reactor is mainly concentrated in a dip of the cross section curves. Changes in the neutron flux spectrum to lower energies as well as to higher energies will lead to an increased neutron production, which leads to an increase in the power production.
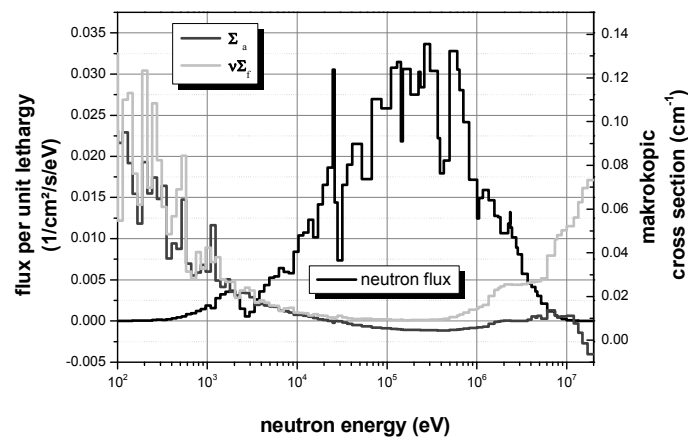
Fig. 2: Integral neutron flux spectrum and macroscopic cross sections averaged in the calculated fuel element of a sodium cooled fast reactor

In the case of sodium voiding three major effects occur: the absorption of neutrons in the sodium is decreased, the neutron spectrum will become harder and the neutron leakage out of the reactor core increases [5]. The last described effect, the increased leakage is not considered in infinite system calculations performed with cell and lattice codes. The other two effects can be analyzed with the help of Fig. 3. The change in the neutron spectrum caused by voiding of the sodium coolant is shown in both figures. There are two different characteristics: a significant increase of the neutron flux around 3 keV and a decrease of the neutron flux below 200 keV together with an increase of the neutron flux above this value.

The significant increase of the neutron flux around 3 keV is correlated with the absorption resonance in the sodium at this value (see Fig. 3 left). The absence of the sodium coolant due to voiding reduces the absorption of neutrons in the coolant, thus the neutron flux in this energy range increases significantly. More neutrons are available for the chain reaction and the multiplication factor rises. The neutrons are less slowed down since the number of collisions in the coolant is significantly reduced due to the absence of the sodium. This leads to the mentioned harder neutron spectrum. The increased neutron flux in higher energies correlates with the increase of the neutron production cross section(see Fig. 3 right). This leads to a higher multiplication factor, too.
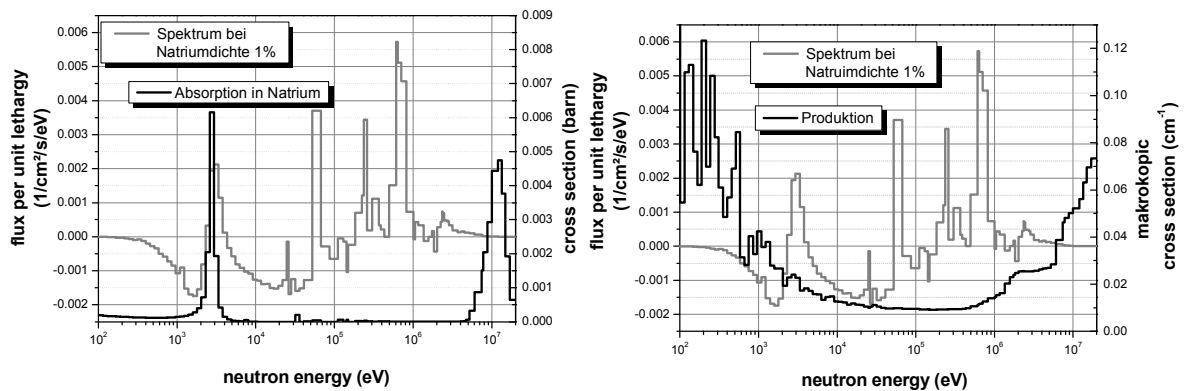
Fig. 3: Change in the neutron flux spectrum due to voiding of the sodium coolant in relation with the absorption cross section in the sodium coolant (left) and the macroscopic neutron production cross section $\nu\Sigma_f$ - Σ_a (right)

3. Effect of Moderating Layer

The left part of Fig. 4 shows the change of k_{inf} over burnup, calculated for a fast reactor unit cell. The black line with squares shows the reference result. Inventing the layers 2 and 3 containing 0.1 mm and 0.2 mm Uranium hydride (UH) leads to a reduction of the initial k_{inf} but to a comparable burnup swing. Layer 3 consisting of 0.6 mm B4C does not reduce the initial k_{inf} and the burnup swing is reduced, compared to the reference solution. The right part of Fig. 4 shows the effect of voiding the sodium coolant (the density is reduced to 1%) on the k_{inf}. The effect of sodium voiding on the k_{inf} for the reference solution rises significantly during burnup. Introducing the UH layers (layer 1 and layer 2) leads to a significant reduction of the initial void effect and a slightly reduced rise during burnup. The B4C layer has a slightly smaller effect on the initial sodium void than UH, but the rise of the void effect during burnup is slower.
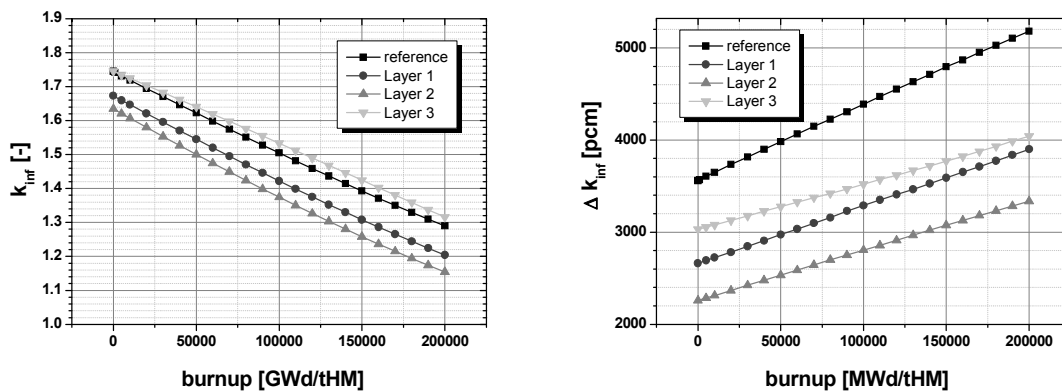
Fig. 4: Change in the infinite multiplication factor (left) and in the sodium void effect on k_{inf} over the burnup(right)

The change of the fuel temperature effect and the coolant effect (temperature and density change) on k_{inf} over burnup for the reference case and for the system with uranium hydride layer is shown in Fig. 5. Introducing of a 0.2 mm thick uranium hydride layer enhances the negative fuel temperature effect by roughly a factor of 4 and halves the positive moderator effect. The effect of the layer reduces only slightly over burnup. Both changes improve the stability of the fast reactor operation and the safety of the system significantly.
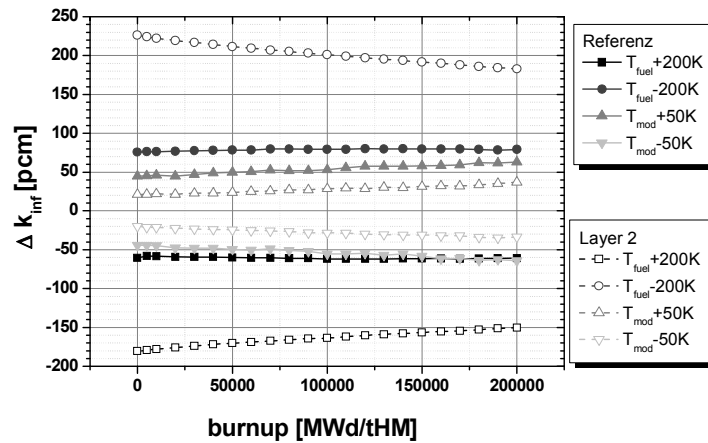
Fig. 5: Change of the fuel temperature and the coolant effect on k_{inf} over burnup for the reference case and for the system with uranium hydride layer

4.   Conclusions

Introducing the suggested moderating layer leads to significantly improved feedback coefficients, compared to the current fast sodium cooled reactors. The sodium void effect, as well as the fuel temperature and moderator effect is changed. All changes increase the stability and thus the safety of the system. Using the suggested layer design offers the possibility to enhance the safety characteristics without changing power density and distribution, fuel configuration, fuel element geometry and coolant streaming paths. Only minor changes occur to the breeding capabilities and the production of minor actinides. The idea offers new degrees of freedom for the optimization of the transmutation potential.

References

[1]   R. N. HILL and H. KHALIL, Evaluation of LMR Design Options for Reduction of Sodium Void Worth, Proc. of Int. Conf. on Physics of Reactors, 1980 Marseille, France, Vol. 1, p. 11-19

[2]   G. RIMPAULT et al., Towards GEN IV SFR design: Promising ideas for large advanced SFR Core Designs, International Conference on the Physics of Reactors, Interlaken, Switzerland, 2008

[3]   L.BUIRON et al., Innovative Core Design For Generation IV Sodium-Cooled Fast Reactors, Proceedings of ICAPP 2007, Nice, France 2007

[4]   HELIOS Methods, Studsvik Scandpower Nov. 2003

[5]   H. Hummel and D. Okrent, Reactivity Coefficients in Large Fast Power Reactors, ANS 1970

[6]   IAEA Fast Reactor Database - 2006 Update

[7]   A. E. Waltar, A. B. Reynolds, Fast Breeder Reactors, Pergamon Press, New York, USA (1981)

[8]   A. Pay, E. Francillon, B. Steinmetz, D. Barnes, N. Meda, http://www.iasmirt.org/iasmirt-3/SMiRT10/DC_250515, 10th International Conference on Structural Mechanics in Reactor Technology , Anaheim, CA, USA, August 14-18, 1989

ESTIMATION OF THE SOLUBILITY LIMIT OF CHROMIUM IN IRON AT 300°C FROM SANS EXPERIMENTS

Frank Bergner, Andreas Ulbricht, and Cornelia Heintze

1. Introduction

Essential modifications to the standard binary Fe-Cr phase diagram [1] have been recently suggested on the basis of a review of experimental work reporting Cr ordering and/or α' precipitation ([2] and references therein). In [2] attention is focussed on both the Fe-rich part of the phase diagram, which is important for ferritic/martensitic Cr steels, and low temperatures, where Cr diffusion is limited. As thermal aging is not sufficient to reach phase equilibrium at temperatures below about 700 K, particle-irradiated Fe-Cr alloys are especially referred to. The underlying assumption is that ordering/phase separation is irradiation-accelerated instead of irradiation-induced and that the phase boundary is therefore not affected by irradiation [2]. The boundary of the miscibility gap in the Fe-rich part was constructed such as to separate the regions of reported ordering/solubility from regions of reported precipitation.

In the present investigation a more direct experimental approach to the boundary of the miscibility gap is outlined and applied in order to determine the solubility limit of Cr in Fe at 300°C. This approach is based upon the application of small-angle neutron scattering (SANS) to neutron-irradiated binary Fe-12.5at%Cr and Fe-9at%Cr alloys. It relies on the assumption that the observed saturation of the volume fraction of irradiation-induced scatterers with increasing neutron exposure corresponds to the thermodynamic equilibrium at irradiation temperature.

2. Experiment

The investigated Fe-Cr alloys were delivered by SCK•CEN, Mol, Belgium [3]. They were produced by furnace melting of commercial purity Fe and Cr and irradiated in the BR2 reactor at a temperature of 300°C up to neutron exposures of 0.6 and 1.5 displacements per atom (dpa). Material treatment, irradiation conditions and properties of the unirradiated material are reported in more detail in [3]. SANS measurements were performed at the SANS-2 facility of GKSS, Geesthacht, Germany. Samples with dimensions of 7 x 7 x 1 mm^3 were placed in a saturation magnetic field perpendicular to the incident neutron beam direction. A wavelength, λ, of 0.58 nm and three sample-detector distances of 1, 4 and 16 m with corresponding beam collimation lengths were used in order to cover a wide range of scattering vectors, Q, from 0.1 to 3 nm^{-1}. SANS data reduction was carried out using the SANDRA software package [4]. The magnetic and nuclear contributions to the total scattering were separated using the angular dependence of the scattering in the saturation magnetic field. In order to avoid difficulties related to the complex magnetic behaviour of the Fe-Cr system, the present investigation is based on the nuclear contribution.

3. Results

The magnetic and nuclear scattering cross sections measured for the neutron-irradiated samples and the unirradiated control of Fe-12.5at%Cr are shown in Fig. 1 as a function of the scattering vector, Q. A pronounced irradiation-induced increase of the scattering cross sections is observed in the range $Q > 0.3$ nm^{-1}. The A-ratio originally defined as ratio of the

scattering cross sections, $d\Sigma/d\Omega$, perpendicular and parallel to the magnetic field direction [5] was calculated from the magnetic (mag) and nuclear (nuc) contributions according to equ. (1):

$$A = \frac{\left(d\Sigma/d\Omega\right)_{\perp}}{\left(d\Sigma/d\Omega\right)_{\parallel}} = \frac{\left(d\Sigma/d\Omega\right)_{mag}}{\left(d\Sigma/d\Omega\right)_{nuc}} + 1 \tag{1}$$

We have observed that the A-ratio measured for Fe-12.5at%Cr is independent of the magnitude of Q and that the average values are $A = 2.07 \pm 0.05$ and $A = 2.05 \pm 0.05$ for neutron exposures of 0.6 dpa and 1.5 dpa, respectively. These results are consistent with scattering caused by α' particles dispersed in the α matrix, for which the range of A-ratios from 2.09 to 2.13 was reported [6]. The A-ratio calculated for pure Cr precipitates in α-Fe of 2.03 [6] is also in the experimentally observed range of A-ratios.

In order to calculate the size distribution of scatterers, a two-phase matrix-inclusion topology composed of homogeneous spherical scatterers randomly dispersed in the matrix is assumed. For a number of N scatterers of radius, R, in the probed volume, V_p, the coherent scattering cross section can be expressed as:

$$\left(\frac{d\Sigma}{d\Omega}\right)(Q,R) = \frac{N(R)}{V_p}\Delta\eta^2 V^2(R)\left|F(Q,R)\right|^2 = c_R(R)\Delta\eta^2 V(R)\left|F(Q,R)\right|^2 \tag{2}$$

$$\left|F(Q,R)\right|^2 = \frac{9\left(\sin QR - QR\cos QR\right)^2}{\left(QR\right)^6} \tag{3}$$
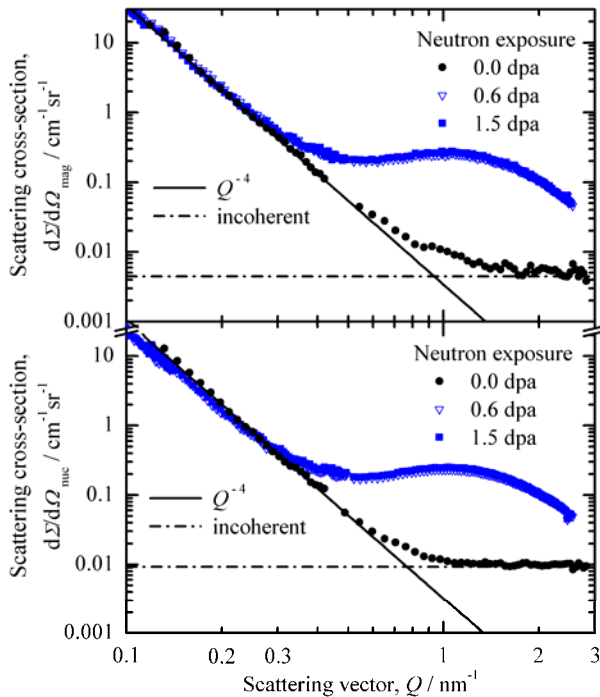
Fig. 1: Magnetic and nuclear scattering cross sections measured for the unirradiated control sample and two irradiated conditions of Fe-12.5at%Cr
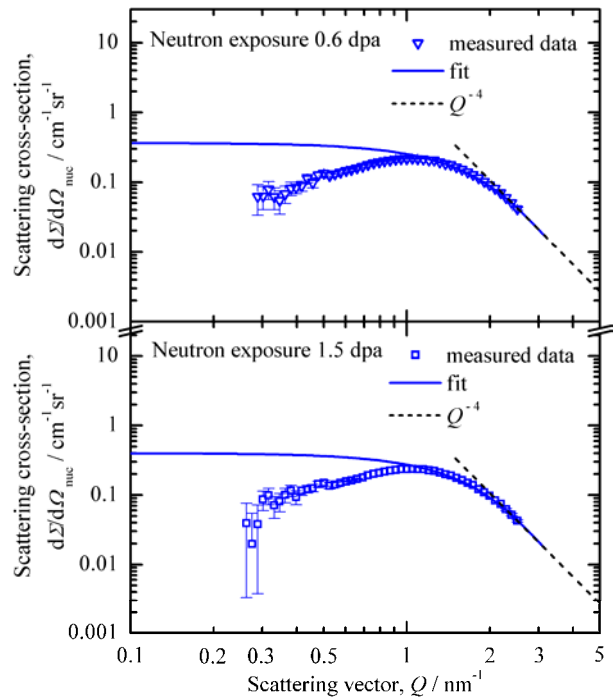
Fig. 2: Difference nuclear scattering cross sections for Fe-12.5at%Cr irradiated up to 0.6 and 1.5 dpa with the unirradiated control taken as reference

$V(R) = 4\pi R^3/3$ is the volume of a sphere, F is the form factor and $c_R(R)$ is the volume fraction of scatterers per size increment, i.e. the particle volume size distribution function. The scattering contrast, $\Delta\eta^2$, is considered below. The indirect transformation method was applied to obtain $c_R(R)$ without assuming a certain type of distribution. The resulting fit of the measured nuclear difference scattering curves is shown in Fig. 2. It is important to note that the decrease of the scattering cross section at decreasing Q is caused by interference effects typical for concentrated alloys. Therefore, the range of fit was restricted to Q-values beyond the maximum.

We have found that the size distributions, Fig. 3, are single-peaked and almost agree for both neutron exposures. This means that the total volume fraction of scatterers as a function of neutron exposure saturates at a dpa-level below or at about 0.6 dpa. The observed saturation is assumed to be related to thermodynamic equilibrium (at the irradiation temperature of 300°C) having been reached.
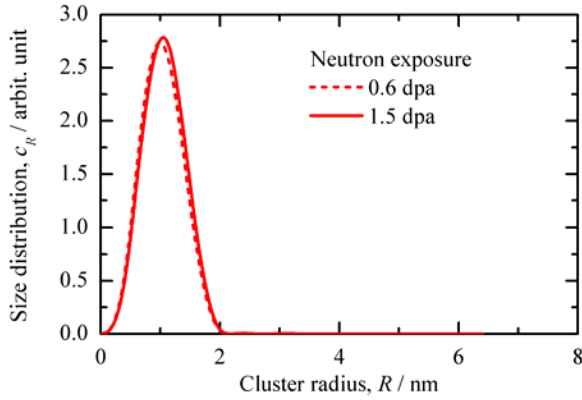
Fig. 3: Particle volume size distribution functions of irradiation-induced scatterers
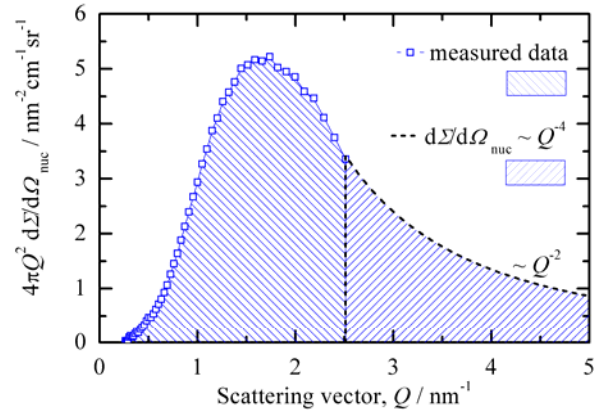
Fig. 4: Representation of the same data as in the lower part of Fig. 2 to clarify the method of calculation according to equ.(4)

In order to avoid uncertainties caused by interference effects and to obtain a quantitative estimation of the total volume fraction occupied by the α' phase, we consider the SANS invariant introduced by Porod [7] for nuclear scattering:

$$\Im = 4\pi \int_0^\infty \frac{d\Sigma}{d\Omega} \cdot Q^2\, dQ = (2\pi)^3 c(1-c)\Delta\eta^2 \tag{4}$$

c is the total volume fraction of scatterers identified above as α'-particles and $\Delta\eta^2$ is the nuclear scattering contrast. The calculation of the integral from experimental results has to be taken with care. Our approach is depicted in Fig. 4 for Fe-12.5at%Cr irradiated up to 1.5 dpa. At high values of Q, we assume a Q^{-4} dependence of the difference scattered intensity according to Porod's law to be applicable. This is supported by the tail of the measured curve in Fig. 2. At the lowest values of Q, the contribution to the value of the integral is small and can be neglected. The result of the calculation is $\Im = (16.06 \pm 0.8)$ cm^{-1} nm^{-3}.

4.   Discussion

The nuclear contrast according to equ. (2) can be expressed as

$$\Delta\eta^2 = \left\{ \frac{2}{a_{\alpha'}^3}\left[x_{Cr,\alpha'}b_{Cr} + \left(1 - x_{Cr,\alpha'}\right)b_{Fe}\right] - \frac{2}{a_{\alpha}^3}\left[x_{Cr,\alpha}b_{Cr} + \left(1 - x_{Cr,\alpha}\right)b_{Fe}\right] \right\}^2 . \tag{5}$$

Though the lattice parameters of pure Fe ($a = 0.2866$ nm) and pure Cr ($a = 0.2884$ nm) differ only slightly, the lattice parameters of α and α' were allowed to depend on the respective Cr concentrations according to Vegard's rule. The standard phase diagram [2] indicates a solubility of Fe in α' of about 2.5 at% in qualitative agreement with recent calculations [8]. Therefore, $x_{Cr,\alpha'} = 97.5$ at% is taken as fixed. $x_{Cr,\alpha}$ is the (still unknown) atomic fraction of Cr in α and b is the nuclear scattering length of Cr ($b_{Cr} = 3.635$ fm) or Fe ($b_{Fe} = 9.45$ fm).

Equ. (4) poses a relation between the unknown volume fraction of α' and the nuclear contrast, which is linked with the unknown composition of α. In order to calculate both, c and $x_{Cr,\alpha}$, an additional relationship is required. This is imposed by the lever rule for the fractions of α and α' in the α-α' two-phase region of the Fe-Cr phase diagram. An iterative procedure was used in [9] in order to extract estimations for c and $x_{Cr,\alpha}$. The results are $x_{Cr,\alpha} = (8.5 \pm 0.2)$ at% and $c = (4.3 \pm 0.4)$ vol%. The obtained solubility limit of Cr in α at a temperature of 300°C is located at significantly higher Cr fractions than assumed in the standard phase diagram [1], but it is in good agreement with the indication phase boundary derived in [2]. Our result allows the volume fraction of α' particles in neutron-irradiated Fe-12.5at%Cr to be specified in absolute units.

References

[1]   J.-O. Andersson and B. Sundman (1987), CALPHAD 11, 83
[2]   G. Bonny, D. Terentyev and L. Malerba (2008), Scripta Mater. 59, 1193
[3]   M. Matijasevic and A. Almazouzi (2008), J. Nucl. Mater. 377, 147
[4]   P. Biemann, M. Haese-Seiller and P. Staron (2000), Physica B 276-278, 156
[5]   G. Solt, F. Frisius, W.B. Waeber (1989), in: L.E. Steele (Ed.), Radiation Embrittlement of Nuclear Reactor Pressure Vessel Steels: An International Review, ASTM STP 1011, American Society for Testing and Materials, Philadelphia, p. 229
[6]   M.H. Mathon, et al. (2003), J. Nucl. Mater. 312, 236
[7]   G. Porod (1982), in: O. Glatter, O. Kratky (Eds.), Small Angle X-ray Scattering, Academic Press, London, p. 17
[8]   M.Yu. Lavrentiev et al. (2007), Phys. Rev. B 75, 014208.
[9]   F. Bergner, A. Ulbricht and C. Heintze (2009), Scripta Mater. 61, 1060

MECHANICAL PROPERTIES OF SPARK-PLASMA SINTERED IRON-CHROMIUM COMPACTS STRENGTHENED BY NANODISPERSED YTTRIA PARTICLES

Peter Franke[1], Cornelia Heintze, Frank Bergner, and Thomas Weißgärber[2]

1.   Introduction

Ferritic/martensitic high-Cr steels are candidate materials for future applications in both generation-IV fission and fusion reactor components [1], [2]. Oxide dispersion strengthening (ODS) of this class of materials is a promising way to extend the range of operation towards maximum temperatures of about 650°C [3]. This extension is possible because of the improved creep resistance under irradiation. However, ODS is only one hardening contribution among others arising from carbides, Cr-rich α'-phase particles and other microstructural features. Moreover, irradiation creep is only one issue among a number of different complex and interrelated phenomena such as the brittle-ductile transition and the effect of Helium generated by nuclear reactions.

In order to separate the effect of ODS on the irradiation behaviour from the effect of other microstructural features it is important to investigate model alloys of less complexity such as ODS-FeCr produced by hot extrusion [4] or hot isostatic pressing (HIP) [5]. The present work is devoted to the mechanical properties of ODS Fe-9wt%Cr alloys produced by powder metallurgy (PM) including reactive milling and spark plasma sintering (SPS). The Cr-content of 9wt% is located close to the lower boundary of the Fe-Cr miscibility gap [6], i.e. extensive formation of α' is not expected. The range of material conditions covers contents of nanodispersed yttria of 0 (reference), 0.3wt% and 0.6wt%. Different milling times were applied. The results obtained for the density, elastic properties, hardness, tensile behaviour and brittle-ductile transition are reported and the effect of ODS content and PM process parameters is discussed. The investigation is part of an effort directed towards an improved understanding of the effect of ODS on the irradiation behaviour of Fe-Cr model alloys.

2.   Experiments

2.1.   Material

The details of the production process of the ODS-Fe-9wt%Cr alloys are described in [7]. The PM process starts from commercial-purity elemental powders of Fe and Cr and Y_2O_3 powders received from two different manufacturers. The median diameters of the Y_2O_3 particles are 800 nm and 60 nm for manufacturers A and B, respectively. Milling was done with a Netzsch planetary ball mill under argon atmosphere without milling additions. The milling time varied in the range from 5 to 20 hours. In addition to the Fe-9wt%Cr reference alloy, ODS alloys with 0.3wt% and 0.6wt% Y_2O_3 were produced. The set of powder mixtures is summarized in Table 1, where the designations of the final material variants are given for later reference.

SPS was applied for consolidation of the powder mixtures in order to produce compacts of 100 mm diameter and 6 mm thickness. The maximum temperature and press force applied

---

during the SPS process are 1250°C and 314 kN, respectively. The process parameters were maintained for the whole set of material variants.

Chemical analyses performed by means of spectrometry and EDX after consolidation revealed <0.069wt%C, <0.0017wt%S and <0.0006wt%P and confirmed the Cr content of 9wt% in all cases.

2.2. Samples

According to the cutting scheme presented in Fig. 1, a number of samples were machined by means of a wire travelling electroerosive discharging machine for each of the material variants listed in Table 1. A number of 12 subsized notched impact bars (KLST specimens according to DIN 50115), 6 tensile bars and 12 blocks for basic characterization (e.g. elastic properties) and future irradiation experiments are included in the sets of samples.
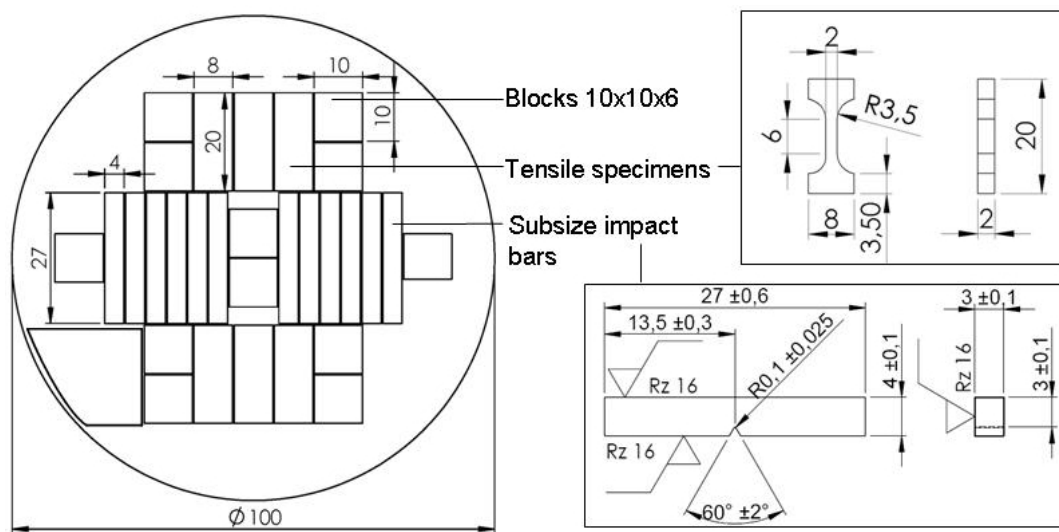
Fig. 1: Cutting scheme and drawings of the tensile and impact bars

Table 1: Summary of nominal compositions and material designations

	Fe-9wt%Cr	Fe-9wt%Cr-0.3wt%Y_2O_3-A	Fe-9wt%Cr-0.3wt%Y_2O_3-B	Fe-9wt%Cr-0.6wt%Y_2O_3-B
5 hours milling	FeCr5	ODS0.3A5	ODS0.3B5	ODS0.6B5
10 hours milling	FeCr10	ODS0.3A10	ODS0.3B10	ODS0.6B10
20 hours milling	FeCr20	ODS0.3A20	ODS0.3B20	ODS0.6B20

2.3. Experimental Procedure

The density, ρ, was measured gravimetrically according to the DIN ISO 3369 standard using high precision scales. The porosity was calculated as the relative deviation of the measured density from the theoretical value. The ultrasonic pulse echo technique was applied in order to determine the sound velocity of both longitudinal, c_L, and shear waves, c_T. To this end a pulser/receiver and a digital sampling oscilloscope were used in order to measure the pulse travel time. Finally, Poisson ratio, ν, Young's modulus, E, shear modulus, G, and bulk modulus, B, were calculated according to textbook equations.

Vickers hardness, HV10, was measured. Tensile tests were performed at both room temperature and 250°C. The strain was determined optically using a video extensometer.

The impact testing covered the temperature range from -190 to +250°C. The notched bars were manually moved from the temperature bath to the support of the pendulum within a maximum time of 5 s. The impact pendulum has a capacity of 15 J. The fracture surfaces of the broken halves of the impact bars were characterized by means of scanning electron microscopy (SEM).

3. Results and discussion

The basic measuring results are compiled in Table 2.

Table 2: Measured density, porosity, Young's modulus, hardness, proof stress, transition temperature (in terms of the inflection point of a fitted tanh-curve) and upper shelf energy of the compacts

Material	ρ / kg m^{-3}	p / %	E / GPa	HV10	$R_{p0.2}$ / MPa	T_0 / °C	USE / J
FeCr5	7.604	2.38	215	244 ± 2	540 ± 10	24 ± 24	1.5
FeCr10	7.288	6.43	187	239 ± 4	580 ± 30	*	0.4
FeCr20	7.284	6.48	188	234 ± 7	860 ± 60	*	0.3
ODS0.3A5	7.592	2.37	215	238 ± 4	540 ± 10	42 ± 22	2.4
ODS0.3A10	7.635	1.81	216	278 ± 4	650 ± 10	-5 ± 28	1.7
ODS0.3A20	7.405	4.77	197	306 ± 7	760 ± 90	*	0.5
ODS0.3B5	7.647	1.66	217	216 ± 6	540 ± 10	32 ± 15	2.3
ODS0.3B10	7.622	1.98	217	280 ± 2	670 ± 20	*	1.2
ODS0.3B20	7.416	4.63	205	293 ± 9	780 ± 90	*	0.4
ODS0.6B5	7.574	2.43	214	249 ± 5	610 ± 10	5 ± 30	1.4
ODS0.6B10	7.507	3.30	210	321 ± 12	705 ± 20	*	0.7
ODS0.6B20	7.540	2.87	212	322 ± 10	790 ± 20	*	0.5

* Fit of a tanh-function impossible because of low level of USE. Fractography indicates transition from cleavage fracture to shear fracture in the covered temperature range.

We have observed that there is an empirical correlation between milling time and porosity under the present conditions (Table 2). This correlation was interpreted in [7] in terms of process parameters according to the following reasoning: The same sintering pressure was applied independently of the milling time. However, a pressure increasing with milling time would have to be applied in order to obtain a constant porosity. This increase of pressure is needed in order to overcome the work hardening introduced by the milling process.

In Fig. 2, the measured values of Young's modulus are plotted as a function of porosity. Values reported for monolithic binary Fe-Cr alloys are given for comparison [8-10]. A second degree polynomial was fitted to the measured data. It may serve as an interpolation formula. The given upper bound according to [11] has a sound physical basis. Arbitrary aggregates of metal/porosity can take any value less or equal to the upper bound. However, for a dilute system of isolated pores in a metal matrix, the Young's modulus is expected to approach the upper bound curve, and the distance from this curve is related to the aspect ratio of the pores [12]. Indeed, whereas most of the compacts contain near-spherical pores (Fig. 3, left), the largest deviations from the upper bound are observed for cases with network-forming elongated pores (Fig. 3, right). Obviously, the sintering process is not finished in the latter case.
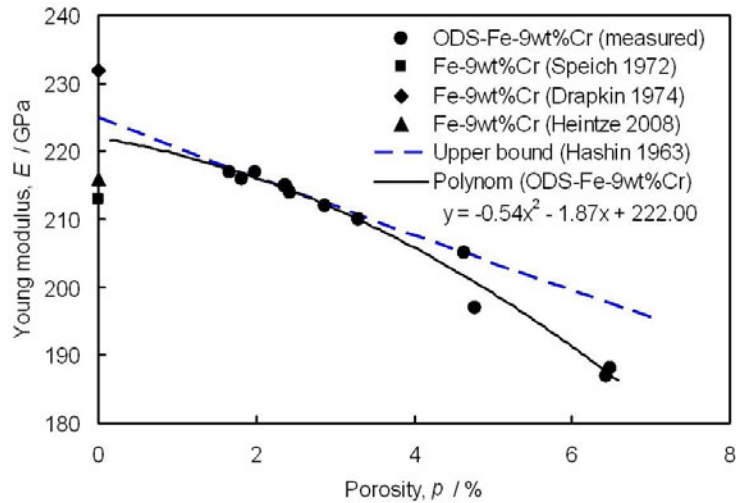
Fig. 2: Young's modulus as a function of porosity
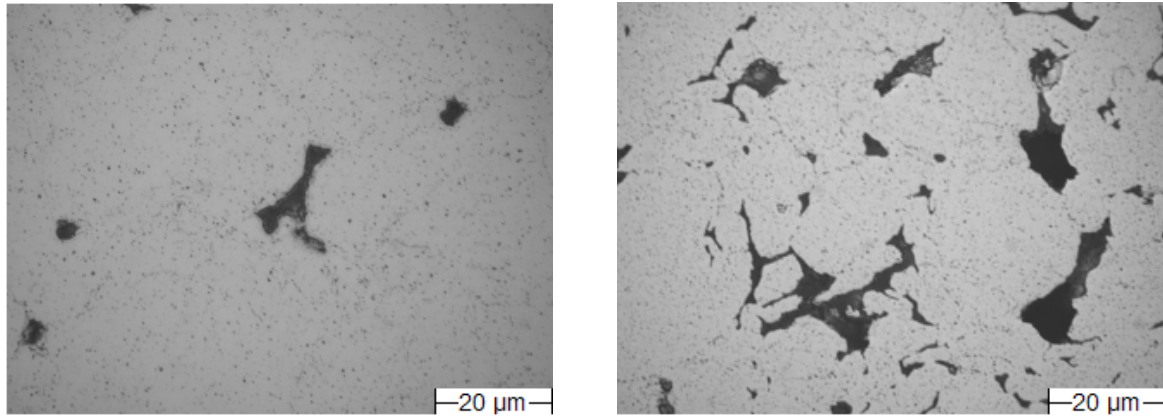
Fig. 3: Polished sections for ODS0.3A10 (left) and FeCr20 (right)

It can be concluded that the process parameters do influence the elastic properties. This effect is primarily introduced via porosity and secondarily via pore shape. As expected, the ODS content is too small to manifest itself in the measured elastic properties. Similar trends as for the Young's modulus are observed for shear and bulk modulus. The Poisson ratio is approximately 0.28 for the whole set of materials.

Both Vickers hardness HV10 and 0.2% proof stress $R_{p0.2}$ exhibit clear trends as a function of milling time (except HV10 for ODS-free FeCr) and as a function of ODS content (except HV10 for milling time of 5 h and $R_{p0.2}$ for milling time of 20 h). The increase of hardness and proof stress with milling time indicates that work hardening and/or uniform distribution of ODS particles achieved by milling overcompensates for the weakening induced by porosity.

A pronounced brittle-ductile transition was only observed in a few cases as indicated in Table 2. Two extreme examples are shown in Fig. 4. If it was possible to fit a tanh-curve to the data, the upper shelf energy (USE) was determined and the inflection point was taken as a measure of the transition temperature T_0 (Table 2). In all other cases, the question arises whether the transition is outside of the available temperature range (-190 to 250°C) or whether the "upper shelf" energy is too small to be distinguished from the lower shelf. SEM fractographs (Fig. 5) confirm that cleavage fracture is observed at the lowest test temperatures and shear fracture at the highest temperatures for each of the materials. Hence, the transitions take place inside the covered range of test temperatures, but in some cases the "upper shelf"

50

energy is too small in order to give rise to a pronounced transition. In the latter cases the average impact energy at the highest test temperatures (with fractographic evidence for shear fracture) was taken as a measure of the "upper shelf" energy.
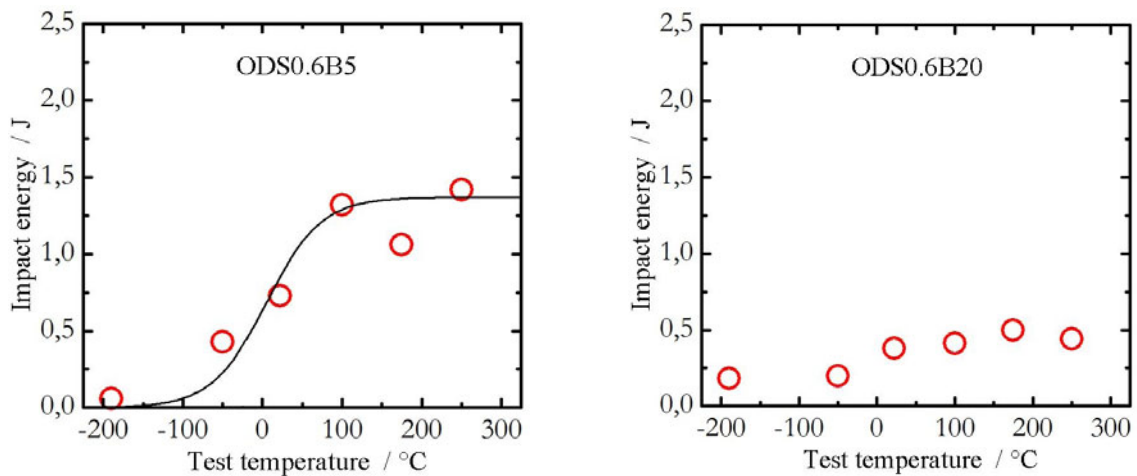
Fig. 4: Impact energy versus test temperature for ODS0.6B5 (left) and ODS0.6B20 (right)

A clear increase of USE with decreasing porosity (Table 2) is observed, in particular at porosities smaller than 3%. The dependence can be described reasonably well by a two-phase linear regression model [13] reflecting a weak dependence at high porosities and a much stronger dependence at porosities below 3% indicating a decisive role of porosity in ductile fracture. The transition temperatures found in the present work are much higher than those reported for ferritic/martensitic steels (Eurofer97: -90°C) but slightly below the transition temperatures observed for the respective ODS variants produced by HIP (ODS-Eurofer: 60 to 100°C) [3].
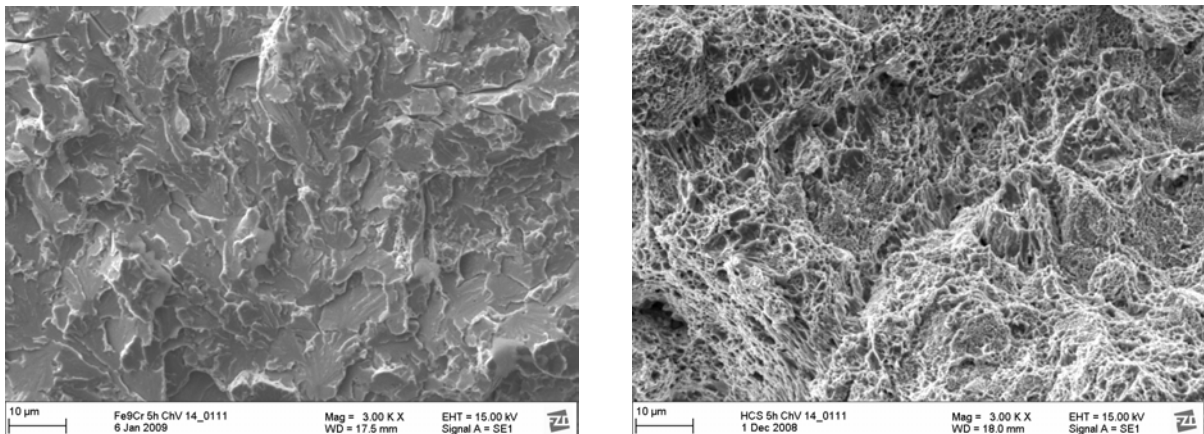
Fig. 5: Fracture appearance for FeCr5 tested at -190°C (left) and ODS0.3A5 tested at 175°C

4.   Conclusions

The present investigation reveals clear trends for the mechanical properties of spark plasma sintered compacts of ODS-Fe-9wt%Cr as a function of composition and process parameters. The dependence of the elastic properties and fracture behaviour on process parameters is dominated by the effect of porosity. This effect is consistent with the state-of-the-art physical understanding. For hardness and proof stress, the effect of porosity turns out to be overcompensated by work hardening and/or uniform distribution of ODS particles achieved

by powder milling. For each of the involved variants a transition from cleavage fracture to shear fracture was observed in the covered temperature range. In a few cases this transition of the fracture mechanism manifests itself in a pronounced brittle-ductile transition.

As indicated in the introduction, the investigation is part of an effort directed towards an improved understanding of the effect of ODS on the irradiation behaviour of Fe-Cr model alloys. As the irradiation-induced damage takes place essentially on the nm-lengthscale, a small fraction of near-spherical pores on the μm-scale should be tolerable. For the purpose of reliable mechanical property characterization, it seems to be necessary to restrict to the materials with porosities essentially below 3% or to reduce porosity correspondingly. Reduction of porosity can be achieved by increasing the sintering pressure during the SPS process for new ODS materials or by adding a HIP process for the existing compacts. The latter is expected to be effective for porosities of the existing compacts below 5%.

References

[1]   R. L. Klueh and A. T. Nelson (2007), Ferritic/martensitic steels for next-generation reactors, J. Nucl. Mater. 371, 37

[2]   I. Cook (2006), Materials research for fusion energy, Nature Materials 5, 77

[3]   R. Lindau, et al. (2005), Present development status of EUROFER and ODS-EUROFER for application in blanket concepts, Fusion Engng. Design 75–79, 989

[4]   A. Alamo, V. Lambard, X. Averty and M. H. Mathon (2004), Assessment of ODS-14%Cr ferritic alloy for high temperature applications, J. Nucl. Mater. 329–333, 333

[5]   V. de Castro et al. (2009), Microstructural characterization of Y_2O_3 ODS–Fe–Cr model alloys, J. Nucl. Mater., in press

[6]   G. Bonny, D. Terentyev and L. Malerba (2008), On the α–α' miscibility gap of Fe–Cr alloys, Scri. Mater. 59, 1193

[7]   P. Franke (2009), Diploma thesis, TU Bergakademie Freiberg

[8]   G. R. Speich, A. J. Schwoeble and W. C. Leslie (1972), Elastic constants of binary iron-base alloys, Metall. Trans. 3, 2031

[9]   B. M. Drapkin (1973), The variation of Young's modulus of Fe-Cr, Problemy Prochnosti 4, 78

[10]   C. Heintze, F. Bergner and A. Ulbricht (2009), Characterization of Fe-Cr alloys using SANS, nanoindentation and ultrasound, to be presented at Euromat 2009

[11]   Z. Hashin and S. Shtrikman (1963), A variational approach to the theory of the elastic behaviour of multiphase materials, J. Mech. Phys. Solids 11, 127

[12]   B. Köhler, F. Bergner, B. Bilger and B. Rehmer (1990), Influence of shape, size and volume fraction of graphite inclusions on the propagation of ultrasound in cast iron, Mater. Sci. Forum 62-64, 815

[13]   P. Franke, C. Heintze, F. Bergner and T. Weißgärber (2010), Mechanical properties of spark plasma sintered Fe-Cr compacts strengthened by nanodispersed yttria particles, Materials Testing 52, 133

EXPERIMENTAL MODELLING OF THE CONTINUOUS CASTING PROCESS: THE LIMMCAST-PROGRAM

Klaus Timmel, Sven Eckert, and Gunter Gerbeth

1. Introduction

Continuous casting is the process whereby molten steel is solidified into billets, blooms or slabs for subsequent rolling in a mill. About 92% of the worldwide annual output of crude steel was produced using the continuous casting process [1]. The molten steel flow in the mould has a great influence on the obtained steel quality. In particular, an inappropriate flow regime can lead to the entrapment of oxides, slag or gas bubbles and their transport into the solidification zone. Therefore, the quest for better product quality and higher productivity makes the flow control in tundish and mould, and the initial solidification control in the mould to important issues with respect to an optimization of the continuous casting technology.

The continuous casting process is sketched in Fig. 1. From the ladle, the hot metal is poured into a holding bath called tundish. The tundish serves as a buffer vessel for regulating the metal feed to the casting machine, stabilizing the flow out, and cleaning the metal. The stopper rod regulates the flow from the tundish through the submerged entry nozzle (SEN) into the water cooled copper mould, where the initial solidification starts. The partial solidified steel strand is then withdrawn and further cooled down.
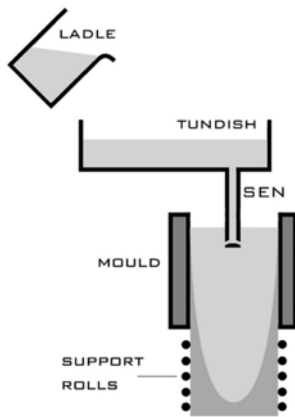
Fig. 1: Principle of the continuous casting process

The application of electromagnetic fields provides a considerable potential to control the fluid flow in the mould cavity and to influence the solidification in the strand. In principle, two categories of electromagnetic control techniques have been proposed to improve the quality of the steel in the continuous casting process: electromagnetic stirrers (EMS) and electromagnetic brakes (EMBR). First strategies for EM applications in steel casting were mainly guided from simplified pictures of the magnetic field impact on the global flow field. Many numerical investigations have been reported until now to improve the understanding of the magnetic field influence on the mould flow (see for instance [2-5]). However, the problem has to be considered as challenging because of the complexity of the geometry, the highly turbulent flow or specific peculiarities occurring in case of MHD turbulence. Obviously, a validation of the numerical predictions by liquid metal experiments is indispensible. However, related experimental studies are rather scarce until now. Several plant trials were carried out [6, 7] to test the efficiencies of electromagnetic brakes in the real casting process. Because of the lack of suitable measuring techniques for liquid steel at 1500°C such trials cannot provide any reliable knowledge to validate numerical calculations. A Japanese group reported some experimental studies employing simple mercury models [8, 9]. With our work we want to continue the strategy of cold metal models. The main value of such cold metal laboratory experiments consists in the capabilities to obtain quantitative flow measurements with a reasonable spatial and temporal resolution. New ultrasonic or

electromagnetic techniques for measuring the velocity in liquid metal flows came up during the last decade allowing for a satisfying characterisation of flow quantities in the considered temperature range until 300°C [10].

2. The LIMMCAST facility

The experimental programme of the LIMMCAST facility at FZD aims to model the essential features of the flow field occurring during the continuous casting of steel, namely the flow field in the tundish, the submerged entry nozzle (SEN) and the mould cavity as well as the solidification of the material in the strand. The facility has been designed and assembled during the last two years. The operation has been started in March 2009 with the first filling of the facility. After verification of the instrumentation, process measuring and control technology the experimental programme will start in 2010. The low melting point alloy Sn60Bi40 is used as model liquid. The liquidus temperature of 170°C allows for an operation of the facility in a temperature range between 200 and 400°C. All components being in direct contact with the melt are made from stainless steel.

An overall heating power of about 200 kW is installed at the outer wall of the loop system and the components to achieve the operating temperature. The melt inventory is stored in two vessels with a capacity of 250 l for each vessel. For operation the alloy is melted and pushed with Argon from the storage vessels into a loop of circular pipes. The present situation of the facility comprises two test sections. Test section I, which contains the tundish, the SEN and the mould, will be used for physical modelling of the continuous casting process. The investigations will be explicitly focussed on the behaviour of the isothermal melt flow. A further test section has been installed as closed piping system and serves for material tests or verifications of various measuring techniques. A third test section will be realised in future, where a solidification of the strand will become possible.

Fig. 2: View of the LIMMCAST facility

An overall view of the LIMMCAST facility is shown in Fig. 2. An electromagnetic pump is used to pump the liquid metal into the tundish. The flow rate is measured by an electromagnetic flow meter [11]. From tundish the melt pours through a pipe with an inner diameter of 35 mm into the mould with a rectangular cross section of 400×100 mm^2. Special adapters at the lid of the mould allow for a direct access for measuring techniques to the liquid metal in the mould. Flow velocities will be measured using the UDV method. High temperature sensors with acoustic wave guides [12] will be attached to the free surface of the melt to determine the vertical component of the liquid velocity.

Further adapters are available for visual inspections of the free surface. Moreover, local probes can be positioned inside the melt to measure velocity fluctuations or void fraction distributions in case of gas bubbling.

3. Mini-LIMMCAST: a small-scale GaInSn facility

During the construction and commissioning period of the large scale LIMMCAST facility, the small-scale set-up Mini-LIMMCAST was employed which uses the eutectic alloy GaInSn that is liquid at room temperatures. At this set-up we started a preliminary experimental program which is focused on quantitative flow measurements in the mould and in the submerged entry nozzle (SEN). This way we expected to gain valuable experiences for the detailed design and the operation of the larger LIMMCAST facility. A selection of first representative results from the flow measurements will be shown within this report.

3.1. Setup

Fig. 3 shows a sketch of the experimental setup. A stainless steel cylinder serves as the tundish which contains about 3.5 l of the GaInSn alloy. The melt is discharged through a Plexiglas tube with an inner diameter of 10 mm into the mould with a rectangular cross section of 140×35 mm^2 also made of Plexiglas. Two nozzle ports are situated about 80 mm
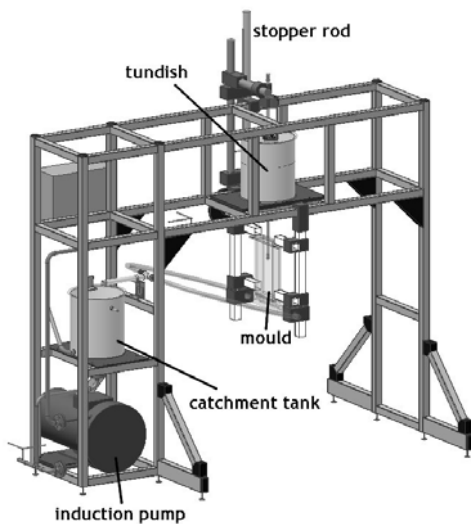
Fig. 3: Schematic view of the Mini-LIMMCAST facility
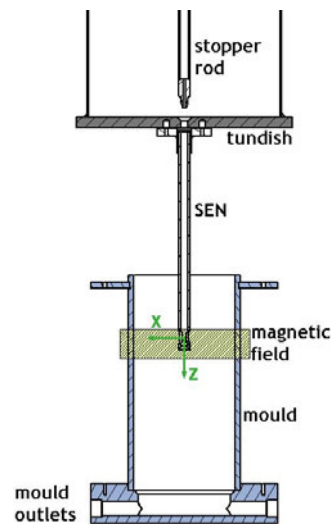
Fig. 4: Detailed view on tundish with stopper rod, SEN and mould

below the free surface in the mould. From the mould the liquid metal flows through a U-bend channel into a storage vessel. The vertical position of the vessel inlet controls the free surface level in the mould. The experiments presented here were performed in a discontinuous mode, i.e. after filling the tundish with the melt the stopper rod was lifted to drain the fluid into the mould. During this process the liquid level of both the tundish and the mould were monitored using a laser distance sensor. The liquid flow rate has been derived from the descent of the surface level in the tundish. A schematic view of the section comprising the outlet of the tundish with stopper rod, the SEN and the mould can be seen in Fig. 4.

A DC magnet supplies a transverse magnetic field. Measurements of the field strength have shown that the field is homogenous between the pole faces within a tolerance of about 5%. The pole faces of the magnet cover the wide side of the mould completely. The vertical extension of the pole shoes is 40 mm, whereas the position of the upper edge of the pole faces coincides with the nozzle outlet. For the simulation of the solidified shell in the real casting

process, brass plates were placed on the wide side walls of the mould. The induced currents in the liquid metal are now able to close through the rigid, electrical conducting walls.

The ultrasound Doppler velocimetry (UDV) was used for measuring the fluid velocity in the mould. This method is based on the pulse-echo technique and delivers instantaneous profiles of the local velocity along the ultrasonic beam and can be applied to attain experimental data from a bulk flow in opaque liquids [13]. In the last twenty years the UDV technique became an accepted method for flow investigations in various liquid metals (see [10] and references therein). In the previous experiments we have applied the DOP2000 velocimeter (model 2125, Signal Processing SA, Lausanne) equipped with up to ten 4MHz transducers (TR0405LS, acoustic active diameter 5 mm). The transducers were arranged within a vertical line array which was attached at the outer wall and located at the midsection of the narrow mould side. The distance between two adjacent transducers was 10 mm. Profiles of the horizontal velocity were recorded along the wide side of the mould between the narrow side wall and the submerged entry nozzle The internal multiplexer of the DOP2000 has been used for a sequential acquisition of data from all sensors with an overall scan rate of 5 Hz.

3.2.   Some results from the flow measurements

The influence of a transverse DC magnetic field on the jet flow discharging from a submerged nozzle into a rectangular cavity has been investigated. The pole faces of the magnetic field span the entire wide side of the mould below the SEN ports. In the measurements considered here the position of the magnetic field was chosen that the upper edge of the pole faces coincide with the vertical location of the nozzle ports. Linear profiles of the vertical flow velocity were acquired in a domain between 20 mm above and 70 mm below the midpoint of the SEN between the nozzle ports which is taken as point of origin for the coordinate system in all measurements which will be presented below.
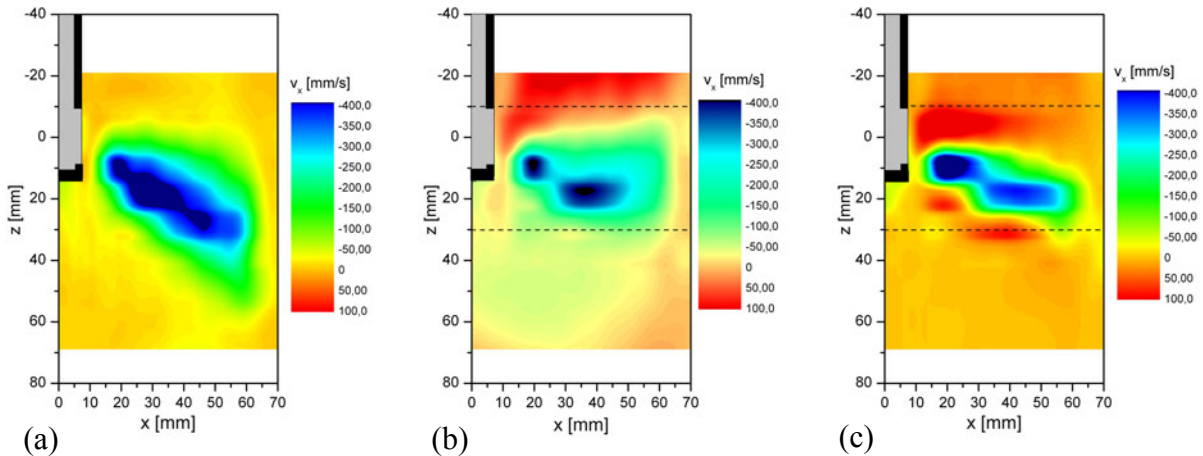
Fig. 5: Time-averaged, horizontal flow at the nozzle outlet (a) without magnetic field,
(b) B = 310 mT, non-conducting channel (c) B = 310 mT, conducting channel

Fig. 5 contains time-averaged plots showing the UDV measurements of the horizontal velocity field. The liquid metal jet emerging from the nozzle port can be clearly identified in all displayed flow structures (blue regions represent a flow from the SEN towards the narrow wall). Nevertheless there are remarkable differences in the flow fields. The application of the magnetic field in a non-conducting mould as displayed in Fig. 5(b) provokes a recirculating flow at the upper part of the nozzle outlet (horizontal green lines indicate the position of the magnet pole faces). The inclination angle of the jet becomes flat. The impingement point at

the opposite side wall is shifted upwards by about 20 mm. The intensity of the velocity within the jet is only slightly reduced. The addition of a conducting wall creates another flow structure. A further recirculation zone is established below the liquid metal jet and the horizontal flow below the pole shoes becomes uniform.

Fig. 6 shows time series of the local velocity recorded in the inner jet region and a measuring position below the discharging jet, respectively. The ultrasonic sensor detects a turbulent flow with strong irregular velocity oscillations if no magnetic field is applied. The highest velocities within the jet region (see Fig. 6(a)) were found in the case B = 0. Although, the mean velocity is lowered for both imposed magnetic fields, the velocity fluctuations were not reduced, but, even increased by the magnetic field in the non-conducting vessel. An effective damping of turbulent velocity fluctuations can only be observed at a position below the jet (see Fig. 6(b)) in a conducting mould.

4.   Conclusion

We investigated the impact of a steady magnetic field on the liquid metal flow in the continuous casting mould. The imposition of the magnetic field causes regions of reverse flow on both sides of the central jet. Furthermore, the exit angle of the jet becomes more flat. Thus, the penetration depth of the discharging flow into the lower part of the mould is reduced. The flow measurements presented here, did not confirm the expectation of a smooth reduction of the velocity fluctuations at the nozzle outlet due to the magnetic field.

(a)   (b)
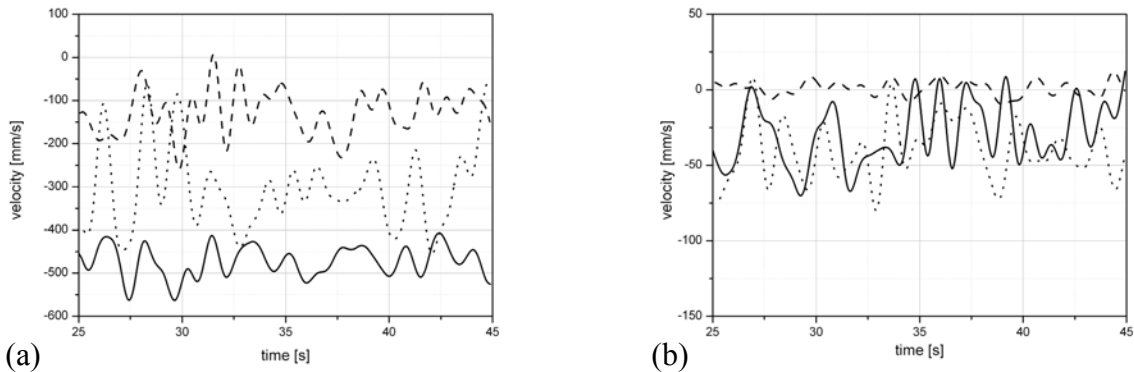
Fig. 6: Time series of the local velocity for B= 0 (solid lines), B= 310 mT in the non-conducting mould (dotted lines) and B = 310 mT in the conducting channel (dashed lines): (a) inside the jet; (b) below the jet

The application of tailored magnetic fields is the key issue for an effective optimisation of the continuous casting process, but it requires further investigations of the interplay between the mould flow and the magnetic field, in particular experimental data are needed to verify the electromagnetic braking effect.

The availability of liquid metal cold models appears as an important tool for an experimental investigation of complex flows structures and transport processes being relevant for the continuous casting process. Moreover, the model experiments at LIMMCAST and Mini-LIMMCAST will provide valuable experimental data for the validation of numerical flow simulations.

References

[1]   World Steel Association, „Steel Statistical Yearbook 2008", (2008)
[2]   B.G. Thomas, L. Zhang: ISIJ Int. 41 (2001), 1181-1193
[3]   K. Takatani, K. Nakai, N. Kasai, T. Watanabe, H. Nakajima: ISIJ Int. 29 (1989), 1063-1068
[4]   B. Li, F. Tsukahashi: ISIJ Int. 46 (2006), 1833-1838
[5]   K. Cukierski, B.G. Thomas (2008), Metall. Mater. Trans. 39B, 94-107
[6]   P. Gardin, J.-M. Galpin, M.-C. Regnier, J.-P. Radot (1996), Magnetohydrodynamics 32, 189-195
[7]   K.H. Moon, H.K. Shin, B.J. Kim, J.Y. Chung, Y.S. Hwang, J.K. Yoon: ISIJ Int. 35 (1996), S201-S203
[8]   K. Okazawa, T. Toh, J. Fukuda, T. Kawase, M. Toki (2001), ISIJ Int. 41, 851-858
[9]   H. Harada, T. Toh, T. Ishii, K. Kaneko, E. Takeuchi (2001), ISIJ Int. 41, 1236-1244
[10]   S. Eckert, A. Cramer, G. Gerbeth: Velocity measurement techniques for liquid metal flows, in "Magnetohydrodynamics - Historical Evolution and Trends", S. Molokov, R. Moreau, H.K. Moffatt (Eds.), Springer-Verlag (2007), 275-294
[11]   J. Priede, D. Buchenau, G. Gerbeth: Magnetohydrodynamics (2010) in press
[12]   S. Eckert, G. Gerbeth, V.I. Melnikov (2003), Exp. Fluids 35, 381-388
[13]   Y. Takeda (1991), Nucl. Eng. Design 126, 277-284

Acknowledgment

ROLE OF THE SOFT-IRON IMPELLERS IN THE FRENCH VON-KÁRMÁN-SODIUM (VKS) DYNAMO EXPERIMENT

André Giesecke, Frank Stefani, and Gunter Gerbeth

1. Introduction

Cosmic magnetic fields are responsible for numerous astrophysical phenomena like sunspots, acceleration of charged particles (cosmic rays), synchrotron radiation, formation of stars or black holes and they might even influence the large scale structures in galactic clusters. The understanding of the interplay of magnetic field and astrophysical objects is essential for our picture of the universe and requires a detailed knowledge of the field generation mechanism - the so called dynamo process. Experimental dynamos, although of much smaller size compared to stellar, planetary or galactic dynamos, provide an ideal playground for studies on magnetic field self-excitation as they are able to explore parameter regions that are hardly accessible to numerical simulations.

Fig. 1: Opened container of the VKS dynamo experiment. An internal copper wall is mounted within the stainless steel cylinder and separates the flow active region from the side layers

Besides this astrophysical motivation, experimental dynamo work also gives insight to a wide range of different fundamental physical processes that are involved in the field generation mechanism. Among others, this includes (rotating) fluid dynamics, turbulence, non-linear phenomena or statistical effects like irregularly occurring reversals.

Since 2006, only the third (after Riga and Karlsruhe in 1999) successful example of a laboratory dynamo has been realized in the French *von-Kármán-Sodium* (VKS) dynamo experiment [1]. In this experiment a turbulent flow of liquid sodium is driven by counterrotating impellers that are located at the two end-caps of a cylindrical domain (Fig. 1). Note: the soft-iron impeller at the rear with eight bended blades that have been optimized to obtain an ideal ratio of poloidal to toroidal velocity. The basic (axisymmetric) flow that is generated by this set-up consists of two toroidal cells and a poloidal/meridional recirculation in each cylindrical hemisphere (Fig. 2).

Fig. 2: Sketch of the experimental setup and the geometric structure of the basic flow

This type of flow is known as a good candidate for self excitation of a magnetic field, and, indeed, dynamo action was obtained 2006 at a critical magnetic Reynolds number of $\text{Rm}^{\text{crit}} \approx 32$. However, the results of the VKS experiment have initiated intense debates, because of a couple of characteristic features that up to now are far away from being understood. This concerns the surprising low critical magnetic Reynolds number at which dynamo action sets in and the occurrence of the dominant axisymmetric field mode. Furthermore, despite of all experimental efforts dynamo action is obtained only if impellers are utilized that are made of soft iron with a large relative permeability. So far dynamo action is not observed if stainless steel impellers are used for flow driving which is probably the most discussed "feature" of the VKS dynamo.

2.   Model setup

The kinematic mean field induction equation that describes the temporal development of the magnetic flux density $\boldsymbol{B}$ reads:

$$\partial_t \boldsymbol{B} = \nabla \times \left(\boldsymbol{u} \times \boldsymbol{B} + \alpha \boldsymbol{B} - \frac{1}{\sigma} \nabla \times \frac{\boldsymbol{B}}{\mu_0 \mu_{\mathrm{r}}} \right), \tag{1}$$

where $\boldsymbol{u}$ denotes the flow velocity, σ the electrical conductivity, μ_0 the vacuum permeability and μ_{r} the relative permeability. The term $\alpha\boldsymbol{B}$ represents an additional source term caused by the α-effect [2]. Equ. (1) is solved numerically applying a hybrid finite volume/boundary element method [3]. The grid based scheme intrinsically maintains the solenoidal character of the magnetic field and allows to consider insulating boundaries as well as non-uniform material coefficients like electrical conductivity or permeability.

A mean axisymmetric flow is prescribed using analytic expressions given by [4]. This flow roughly describes the behaviour of the mean velocity as shown in Fig. 2 but neglects the fluctuations due to the strong turbulence. A detailed picture of the geometric configuration and the structure of the velocity field is visualized in Fig. 3. Note the presence of the outer layers that surround the dynamo active region. The side layer contains stagnant liquid sodium that is physically separated from the flow active domain and provides for a reduction of the critical magnetic Reynolds number [5]. A less desired impact results from the so called lid layers that are located behind each impeller disk. The liquid sodium contained in these layers is driven by the backside of the impeller resulting in a predominantly azimuthal flow which is known to be extremely detrimental for dynamo action [5]. These perturbing layers are the main reason for the decision to utilize soft iron impellers because this yields a shielding of the self generated magnetic field in the bulk of the container from the flow in the lid layers.
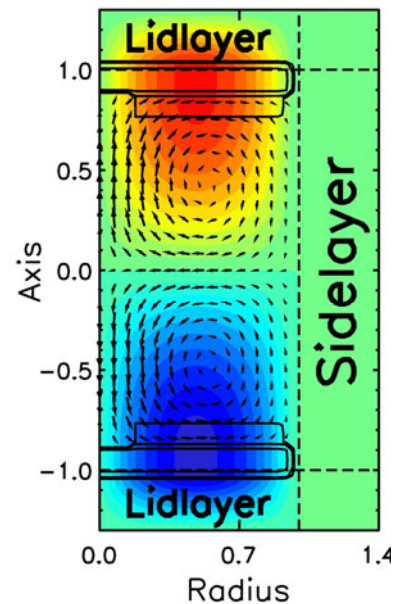
Fig. 3: Structure of the prescribed axisymmetric velocity field. The color coded pattern represents the azimuthal velocity and the arrows show the poloidal velocity field. The black solid lines represent the shape of the impeller system (disk and blades)

60

Beside the above discussed behaviour of the large scale flow, the interaction of rotational driving and small scale flow fluctuations (that are of the same order as the mean flow) cannot be neglected because a conducting flow subject to a helical turbulence generates an electromotive force that can be parametrized by the so called α-effect [2]:

$$\mathcal{E} = \langle u' \times b' \rangle = \alpha B - \eta_{\text{tur}} \nabla \times B. \tag{2}$$

Magnetic field generation based on the α-mechanism has extensively been applied in galactic, stellar and planetary dynamo models. In the induction equ. (1) the α-term acts as an additional source term that describes the induction effects of unresolved small scale flow fluctuations. A first attempt to understand the behaviour of the VKS dynamo has been proposed by [6] in terms of a so called αω-dynamo. In this model the poloidal field component essentially is generated from an α-effect that represents the joint induction effects of (assumed) helical outflow in between the impeller blades (Fig. 4).
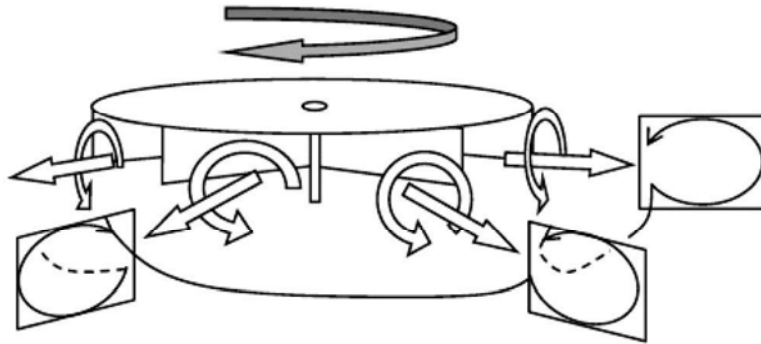
Fig. 4: Sketch of the (assumed) helical outflow in between the impeller blades providing the source for the α-effect (illustration courtesy of [7])

The dynamo cycle is closed by an ω-effect caused by shear which provides for the regeneration of the toroidal field by stretching of meridional magnetic field lines.

However, in [8] we could demonstrate by means of numerical simulations that this model is not capable of explaining the field generation process in the VKS experiment. It turned out that the magnitude of the α-effect which is necessary to obtain growing axisymmetric solutions as observed in the experiment lies far above any realistic value. As a consequence it became inevitable to consider the effect of the high magnetic permeability ($\mu_r \approx 65$, [9]) of the flow driving impellers which has been done in a numerical model for the VKS dynamo for the first time in [10]. The structure of the utilized permeability distribution is sketched by the three dimensional model in Fig. 5. The permeability distribution consists of a solid disk and a non-axisymmetric variation $\sim \cos 8\varphi$ that
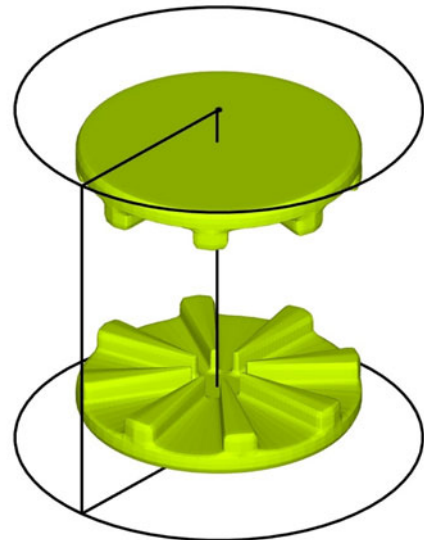
Fig. 5: Structure of the permeability distribution. The fluid permeability outside the domain indicated by the isosurface is set to $\mu_r=1$

61

represents the impeller blades. Note that no bending is included in the blade structure and no particular flow boundary conditions are enforced on the (assumed) interface between impeller and fluid.

3. Results

The numerical solution of equ.(1) provides magnetic fields that exhibit exponentially growth (or decay): $|B| \sim e^{\gamma t}$ where γ denotes the field amplitude growth rate. Fig. 6 presents the growth rates for the axisymmetric field ($m = 0$, solid curves) and the simplest non-axisymmetric mode $|B| \sim \cos\varphi$ ($m = 1$, dashed curves) for simulations without any α-effect. The growth rate of the ($m = 1$) mode hardly depends on the permeability whereas the axisymmetric mode is significantly enhanced with increasing μ_r. In the experimentally relevant regime (between $Rm = 30$ and $Rm = 50$) the ($m = 0$)-mode dominates. However, for large values of μ_r the ($m = 0$) growth rate saturates slightly below the dynamo threshold and - as expected by Cowling's theorem - no growing axi-symmetric solutions are obtained. For sufficiently large but experimentally inaccessible magnetic Reynolds number, i.e. $Rm \geq 60$, the ($m = 1$) mode dominates again and exhibits dynamo action with an equatorial oriented dipole field at a critical value of $Rm^{crit} \approx 63$.

An axisymmetric growing solution can be obtained if an additional α-effect is included. As the growth rate of the ($m = 0$) mode has been shifted close to zero by the influence of the hight permeability, now a quite small amplitude for the α-effect is sufficient to excite growing axisymmetric fields (Fig. 7). The growth rates exhibit a rather sensitive behaviour and even a small variation in α results in large changes of the corresponding growth rates. The critical value of α that is necessary for growing axisymmetric fields decreases for increasing μ_r and lies far below the critical value at $\mu_r=1$ (insert plot in Fig. 6). A characteristic field geometry is reflected in the strong concentration of field energy close to the impeller disk (Fig. 8a). An increase of the magnetic Reynolds number results in a re-emerging of the well
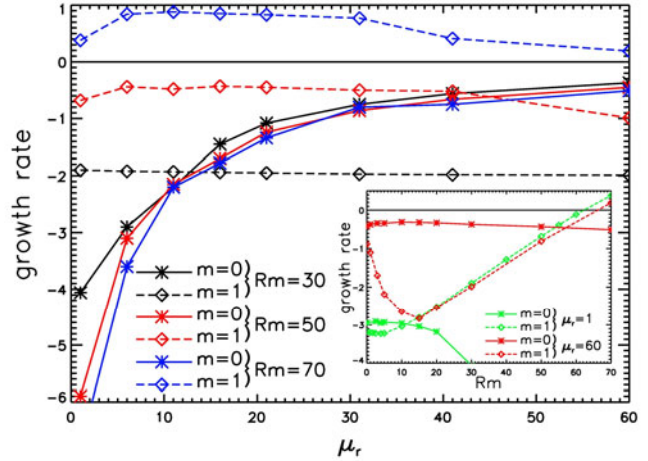
Fig. 6: Growth rates of the field amplitude (without α-effect). Solid curves represent the results for the axisymmetric mode (m=0) and dashed curves show the (m=1)-mode. The inset plot presents the growth rates for $\mu_r=1$ and $\mu_r=60$ in dependence on Rm.
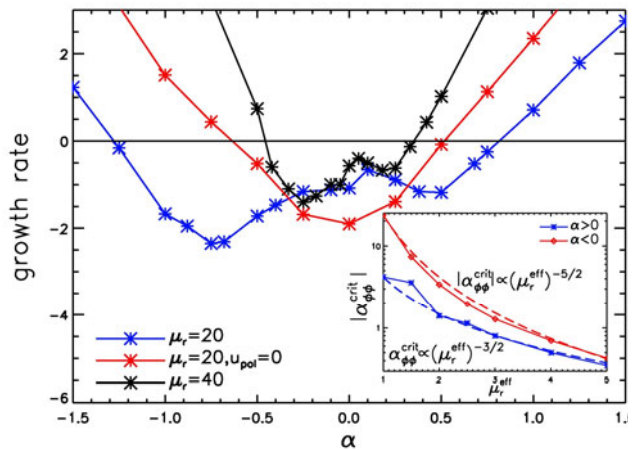
Fig. 7: Growth rates of the axisymmetric mode for Rm=30 in dependence on a prescribed homogenous α-effect. In all cases the (m=1)-mode lies below the growth rates of the axisymmetric solution.

known ($m = 1$) dominated field structure (Fig. 8b) where dynamo action predominantly takes place in the bulk of the cylinder which explains the impassivity of the ($m = 1$)-mode towards the high μ_r disks located close to the end caps. At a Reynolds number of Rm = 30 and without any α-effect the field decays and the eigenmode is essentially determined by an axisymmetric toroidal field component (Fig. 8c).

4. Summary and outlook

For the first time, we have now treated the high permeability of the soft-iron impellers in the VKS dynamo in a more or less realistic manner [10]. Our simulations conclusively show that the magnetic material properties essentially determine the behavior of the field generation process and allow for explanations of the three unsolved questions mentioned above. In particular, it is demonstrated that the presence of the high-permeability material within the dynamo active region significantly favors the axisymmetric field which has been the most controversial result of the VKS experiment because an axisymmetric field violates Cowlings's theorem which is the most fundamental (anti-)dynamo theorem in dynamo theory.
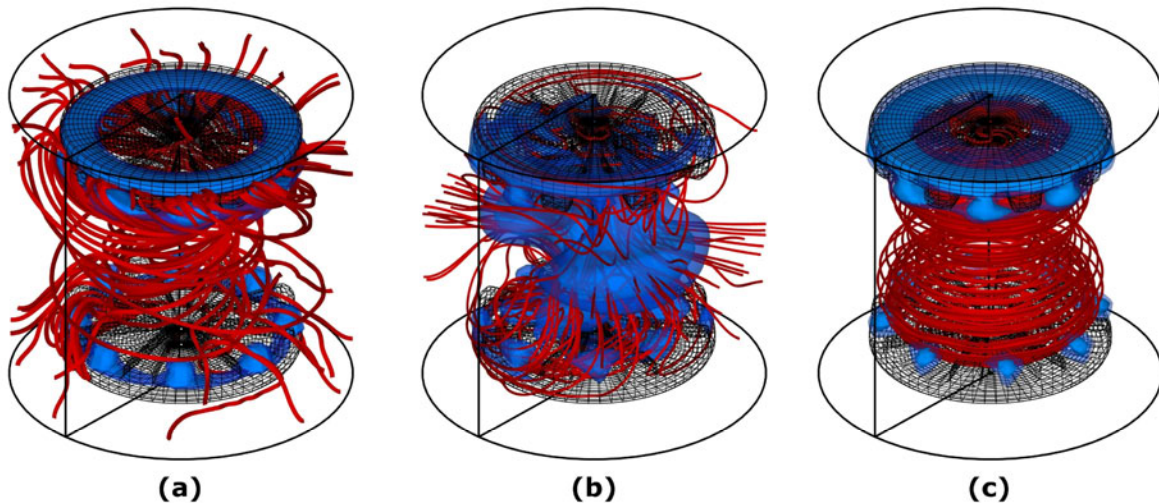
Fig. 8: Distribution of magnetic energy density (blue colored isosurfaces at 10% of the maximum value) and geometric structure of the magnetic field (red streamlines) for μ_r=20: (a) Rm=30, α=-1.5, growing axisymmetric mode;(b) Rm=70, α=0, growing (m=1)-mode; (c) Rm=30, α=0, decaying axisymmetric mode. Note the (m=8) modulation induced by the impeller blades.

Our outcome gives insight into the general functioning of the dynamo effect in inhomogeneous media and suggests that the VKS dynamo might not be characterized as a purely homogenous dynamo.

References

[1]   R. Monchaux, M. Berhanu, M. Bourgoin, M. Moulin, P. Odier, J.-F. Pinton, R. Volk, S. Fauve, N. Mordant, F. Pétrélis, A. Chiffaudel, F. Daviaud, B. Dubrulle, C. Gasquet, L. Marié, F. Ravelet (2007), Generation of a Magnetic Field by Dynamo Action in a Turbulent Flow of Liquid Sodium, Phys. Rev. Lett., 98, 044502
[2]   F. Krause and K.-H. Rädler (1980), Mean-field magnetohydrodynamics and dynamo theory Oxford: Pergamon Press

[3]   A. Giesecke, F. Stefani, G. Gerbeth (2008), Kinematic simulation of dynamo action by a hybrid boundary-element/finite-volume method, Magnetohydrodynamics, 44, 237

[4]   L. Marié, C. Normand, F. Daviaud (2007), Galerkin analysis of kinematic dynamos in the von Kármán geometry, Phys. Fluids, 18, 017102

[5]   F. Stefani, M. Xu, G. Gerbeth, F. Ravelet, A. Chiffaudel, F. Daviaud, J. Léorat (2006), Ambivalent effects of added layers on steady kinematic dynamos in cylindrical geometry: application to the VKS experiment, Eur. J. Mech. B Fluids, 25, 894

[6]   F. Pétrélis, N. Mordant, S. Fauve (2007), On the magnetic fields generated by experimental dynamos, Geophys. Astrophys. Fluid Dyn., 101, 289

[7]   R. Laguerre, C. Nore, A. Ribeiro, J. Léorat, J.-L. Guermond, F. Plunian (2008), Impact of Impellers on the Axisymmetric Magnetic Mode in the VKS2 Dynamo Experiment, Phys. Rev. Lett., 101, 104501

[8]   A. Giesecke, C. Nore, F. Plunian, R. Laguerre, A. Ribeiro, F. Stefani, G. Gerbeth, J. Leorat, J.-L. Guermond (2010), Generation of axisymmetric modes in cylindrical kinematic mean-field dynamos of VKS type, Geophys. Astrophys. Fluid Dyn., 104, 249

[9]   G. Verhille, N. Plihon, M. Bourgoin, P. Odier, J.-F. Pinton (2010), Induction in a von Kármán flow driven by ferromagnetic impellers, New Jour. Phys., 12, 033006

[10]   A. Giesecke, F. Stefani, G. Gerbeth (2010), Role of Soft-Iron Impellers on the Mode Selection in the von Kármán-Sodium Dynamo Experiment, Phys. Rev. Lett., 104, 044503

Acknowledgments

Summaries of research activities

Accident Analysis of Nuclear Reactors

The research is aimed at the enhancement of the predictive capability of computer simulations of accident scenarios in presently operating and future nuclear reactors. This is achieved by improvements of the neutron kinetics methods and by coupling of the FZDs reactor dynamics model DYN3D to thermo-hydraulics system codes and to computational fluid dynamics (CFD) simulations. This is performed primarily within the European code platform NURESIM.

In particular, it is the objective to promote the basic understanding of coolant mixing phenomena relevant for boron dilution and pressurized thermal shock scenarios in Light Water Reactors (LWR) and to adequately simulate inherent feedback mechanisms ensuring the controllability of accidents with assumed failure of the reactor scram system.

Moreover, the field of applicability of the reactor dynamics simulations will be extended to innovative reactor concepts. New code versions of DYN3D are going to be developed and validated for such designs. Analytical methods of time-dependent neutron transport theory are developed to basically understand the propagation of neutron pulses in accelerator driven sub-critical systems for transmutation of minor actinides.

S. Kliem,
S. Mittag,
U. Rohde,
F.Schäfer,
S. Baier,
Y. Kozmenkov,
H. Hristov,
Y. Bilodid,
A. Gommlich,
P. Tusheva

Development, Validation and Application of the Code Complex DYN3D - ATHLET

One direction of the improvement and extension of the reactor dynamics code DYN3D is multi-physics coupling with Computational Fluid Dynamics (CFD), system codes like ATHLET for nuclear power plant modelling and fuel rod behaviour simulation tools. Currently, DYN3D is coupled with the CFD code ANSYS-CFX using the porous body approach for the fluid dynamics of the reactor core. A coupling between DYN3D and the French 3D two-phase thermo-hydraulics code FLICA-4 is performed within the development of a European code platform in the NURISP project. This software platform is based on the SALOME software environment which allows a unified coupling of various codes for different applications. The role of DYN3D as a European reference code for the simulation of reactivity initiated accidents within this platform has further been consolidated. New users, which participate in the extension and validation of the code within the European project NURISP, are KIT (Karlsruhe) and KTH (Stockholm).

Particular investigations on the behaviour of Light Water Reactors (LWR) loaded with thorium fuel in Anticipated Transients Without Scram (ATWS) have been performed. In thorium fueled LWR, plutonium which is used as fissile nuclide in the beginning of a fuel cycle, is almost completely burned during the cycle, while only a minimum amount of Minor Actinides will be generated. In ATWS simulations by the help of DYN3D it was shown, that ATWS can safely be mastered also for thorium loadings.

The expertise of the institute on thermo-hydraulic system codes and coupled neutronics/thermo-hydraulics code complexes is increasingly appreciated by industries. A number of accident scenario studies for an NPP with a Boiling Water Reactor (BWR) were performed by order of E.ON. For these analyses, a NPP simulator developed by GRS based on the thermo-hydraulic code ATHLET with an interactive graphical user surface was used as an advanced tool in these analyses.

B. Merk, *S. Mittag,* *E. Fridman,* *A. Ferrari,* *J. Konheiser,* *S. Dürigen,* *V. Glivici-Cotruta*	**Neutronics for innovative reactor concepts** Currently a special version of DYN3D for gas-cooled High Temperature Reactors (HTR) is under development. The adaptation of the code for Liquid Metal Fast Reactors (LMFR) was started. For both versions, a neutron transport approach based on the SP$_3$ approximation in trigonal fuel geometry is going to be implemented. It allows the consideration of anisotropy of the neutron flux taking into account the first angular momentums of the flux distribution.

Analytical methods of the time-dependent neutron transport theory, based on the solution of the transport equation in P$_1$ approximation by the help of Green's functions have been developed. The obtained solutions allow a more accurate interpretation of detector counting rates in pulsed sub-critical systems (ADS). This work is funded within the European project EUROTRANS.

H. Kryk, *E. Krepper,* *A. Grahn,* *G. Cartland-* *Glover,* *W. Hoffmann*	**Development of CFD models for the simulation of fibre loaded coolant flow** Insulating material (mineral wool) may be released from pipes and components during loss-of-coolant accidents in NPP and will be transported with the coolant towards the reactor sump. There it might lead to blockage of the sieves separating the suction chambers of the safety injection pumps from the sump leading to failure of the late phase emergency core cooling.

Within a research project funded by BMWi aimed at the simulation of the behaviour of mineral wool particles in the sump pool flow, models were developed for the transport, sedimentation and re-suspension of isolation material as well as for the transient build-up of the differential pressure at clogged sump screens. The models were implemented into the 3-dimensional flow simulation code ANSYS-CFX. Furthermore, water jets impacting on a liquid pool were investigated both experimentally and numerically. The study was focussed at the effect of entrained air on the flow field in the pool and the transport of fibres.

During the last year, the work has been extended to the investigation of chemical effects, such as corrosion of zinc plated containment components, on the water chemistry and the clogging behaviour of sump screens. First experiments have shown, that, other than expected, no products of low solubility will be released at zinc plated surfaces in a boric acid environment, as it would be the case with iron, but zinc borate, which is soluble up to a zinc concentration of 100 grams per litre and which has the unusual property of decreasing solubility with increasing temperature.

A very small amount of insulation material may penetrate the sump screens and enter the reactor core where it finally accumulates at the spacer grids separating the fuel elements. Elaborate CFD calculations have shown that insulation material preferably deposits on the upper spacer grid plane at the locations of so-called break-through channels. However, at elevated quantities, the insulation material is distributed more evenly across the spacer grid plane. Nevertheless, the pressure difference over the deposited material remains sufficiently small to ensure enough emergency cooling water to enter the reactor core. The

results have been used in safety analyses for regulatory purposes.

The work is done in co-operation with the University of Applied Sciences Zittau/Görlitz, where experiments are performed, while FZ Dresden-Rossendorf is responsible for the CFD modelling.

Materials and Components Safety

The change in the toughness behaviour of reactor pressure vessel materials is investigated as it results from neutron and gamma irradiation. The consequences are evaluated with respect to the safety of light water reactors (LWRs). For this purpose, material and fracture mechanical parameters of irradiated specimens have to be measured under hot cell conditions. The interpretation of the experiments is supported by finite element calculations. The microstructural reasons and mechanisms of the neutron embrittlement are studied by small angle neutron scattering and nano indentation experiments supported by nano-scaled modelling. These microstructural methods are also applied to materials which are currently developed for new reactor concepts (GEN-IV reactors).

H.-W. Viehrig, *U. Rindelhardt,* *E. Altstadt,* *C. Zurbuchen,* *J. Schuhknecht*	**Investigation of reactor pressure vessel material of the dismantled Greifswald NPP** A reference temperature of T_0 = -107 °C according to the Master Curve Concept was measured for the base material of unit 1, which had been irradiated, annealed and re-irradiated. The relative high scatter of the K_{Jc} values could be explained by metallographic and SEM investigations. The fracture faces showed a mixture of intergranular and transgranular cleavage fracture. The microstructure consisting of Martensite and Bainite was characterized by a heterogeneous grain size distribution with grains larger than 0.1 mm.
	The reference temperature of the weld material of unit 2 (irradiated and annealed) was -38°C at the inner surface and increased through the different filling layers up to +6°C. This variation of T_0 over the wall thickness is comparable with the results of unit 1 where however the mean T_0 was about 40 K higher due to the re-irradiation. The overall low T_0 values measured at the specimens of units 1 and 2 proved the large scale thermal treatment to be successful
Supported by *BMWi*	

H.-W. Viehrig, *C. Zurbuchen,* *E. Altstadt*	**Application of the Master Curve Concept to irradiated material** The project in cooperation with the Swiss "Eidgenössisches Nuklearsicherheitsinspektorat" (ENSI) was successfully finished. Using specimens manufactured from the base metal 22 NiMoCr 3 7 of the Biblis C RPV (which had not been put in operation), the influence of the specimen size, the crack geometry and the loading rate on the reference temperature T_0 was analysed. It was shown, that fracture toughness values measured with different specimen thicknesses can be mutually re-calculated. The applicability of the MC concept with dynamic loading was proven.
Supported by *ENSI*	

F. Bergner, *A. Ulbricht,* *C. Heintze,* *R. Küchler,* *P. Franke*	**Analysis of the irradiation induced micro-structural changes in RPV steels and GEN IV materials** Aiming at the investigation of long term irradiation effects, low Cu steel were irradiated to different neutron fluences and characterised by SANS and tensile tests. A late blooming effect was found, i.e. and irradiation hardening progressing slowly until a certain threshold fluence reached. Beyond this threshold an significant acceleration of the deterioration of the mechanical properties was stated.
	During the neutron irradiation of Fe-Cr alloys, there is an accelerated formation of the Cr rich α' phase in Fe until the solubility limit of Cr in

Fe is reached. This phenomenon could be used to measure for the first time the solubility limit at 300 °C based on a sophisticated analysis procedure of SANS measurements.

In cooperation with the Institut für Strahlenphysik of FZD and the MLU Halle, first PAS measurements were performed at the EPOS facility using neutron and ion irradiated materials.

In cooperation with IFAM Dresden ODS Fe-Cr alloys were produced and characterised. By means of SANS measurements it could be demonstrated that the ODS particles have a size between 5 and 20 nm and thus show the desired nano scale dimensions.

Using ion-irradiated binary Fe-Cr alloys and a ferritic-martensitic Cr steel, systematic studies of the effects of the Cr content (up to 12.5%), the fluence (up to 10 dpa) and the temperature (up to 500 °C) upon the nanohardness were performed. The irradiation induced embrittlement is characterised by a saturation like behaviour for Fe-9at%Cr and Fe-12.5at%Cr but not for Fe-2.5at%Cr. The findings could be explained by results obtained with neutron irradiated specimens of these materials. The dislocation loops detected by TEM and the Cr rich α' particles observed by SANS indicate that the irradiation hardenin

*F. Bergner,
U. Birkenheuer,
A. Gokhman,
R. Küchler*

Modelling of the irradiation induced embrittlement
Within the validation of the computer code V3C for the defect simulation by rate theory, it could be shown that in a Fe-0.3%Cu alloy new defects develop up to a neutron dose of 0.02 dpa and that beyond this dose the Ostwald ripening starts to develop. These results are in agreement with SANS measurements. First investigations of the irradiation induced damage for the concentrated Fe-Cr alloys have started.

Thermal fluid dynamics of multiphase systems

The general aim of the work done in the field of thermal fluid-dynamics is the qualification of Computational Fluid Dynamics (CFD) codes for the simulation of complex two-phase flows with relevance for industrial applications. This qualification process includes the development, test and optimization of closure models for the interaction between the phases, i.e. mass, momentum and heat transfer as well as the validation based on experimental data. For the special case of dispersed bubbly flow, all interfacial transfers strongly depend on the local bubble size distribution. For this reason, the gas phase has to be split into a number of size groups in case of poly-dispersed flows. Transfers between these groups are amongst others determined by bubble coalescence and fragmentation. For stratified flows in horizontal components models for the transfers at the free interface and for the coupling of the turbulence fields are required. Experimental data are required with a high resolution in space and time and are generated by combining large scale experiments at high pressure and temperature at the TOPFLOW facility with innovative two-phase measuring instrumentation including tomography methods. Such measuring techniques are developed in the framework of this project.

E. Krepper,
Y. Liao,
M. Schmidtke,
D. Lucas

CFD models for bubbly flows

A new turbulence model which allows to consider bubble induced turbulence was implemented into the CFD code ANSYS-CFX. It allows a much more accurate simulation of turbulence parameter in poly-dispersed bubbly flows as shown by the comparison with experimental data. This is quite important since turbulence parameters are one input for the models for bubble coalescence and breakup, but also for the momentum exchange between the phases. The previously developed basic model for bubble coalescence and breakup which includes sub-models for the different mechanisms was implemented into CFX and adapted in connection with the Inhomogeneous MUSIG (**MU**lti Bubble **SI**ze **G**roup) model and new turbulence model. The experimental database on upwards air-water pipe flow, obtained at the TOPFLOW facility is used for the validation. There is already a good agreement for some flow conditions, however discrepancies for other combinations of gas and liquid superficial velocities demonstrate, that the generality of the models is still not satisfying. The extensions of the Inhomogeneous MUSIG model to enable simulations for cases with mass transfer are now implemented into CFX. To generate a suitable database for the validation, new experiments were conducted at the TOPFLOW facility for the condensation of steam bubbles injected into sub-cooled water flowing upwards in a vertical DN200 pipe. First simulations for these data show the characteristically trends are well reflected.

Supported by
BMWi

T. Höhne,
P. Apanasevich

CFD models for stratified flows

Simulations using ANSYS-CFX were done for co-current and counter-current flows as well as flows under counter-current flow limitation (CCFL) for experiments conducted at the hot leg model of the TOPFLOW facility. They aim on the validation of improved two-phase closure models for stratified flows which are developed at FZD in collaboration with ANSYS and which are now implemented in the code. Based on the Algebraic Interfacial Area Density (AIAD) model, a new model for the momentum transfer at a free surface was developed,

implemented and tested in CFX-12. It includes a time and space dependent drag force depending on the local morphology of the flow. The simulations applying this new model show an improved agreement with the experimentally observed phenomena. E.g., using this model for CCFL situations, the blocking of the channel caused by the gas flow can be well reproduced.

First CFD simulations were done in frame of the European project "NURISP" to simulate experiments on Pressurized Thermal Shock (PTS) which will be conducted at the TOPFLOW facility. From these pre-test simulation valuable inputs for the experimental procedure were obtained.

Ch. Vallee, D. Lucas, Deendarlianto

Counter-Current-Flow-Limitation effects in a PWR hot leg geometry
Investigations regarding the unexpected shift between flooding curves for air-water and steam-water flows observed in TOPFLOW experiments on a 1:3 scaled model of a Pressurized Water Reactor (PWR) hot leg have shown that the proposed correction factor for the Wallis parameter can also improve the agreement between the steam-water experiments previously conducted at the UPTF facility at different pressure levels. Jointly conducted experiments at Kobe University using a 1:15 scaled Plexiglas model of the Japanese PWR hot leg show also an influence of the viscosity, but this is much lower than that observed in our experiments. One possible reason is the small scale or the different pipe geometry of the Kobe experiment.

U. Hampel, M. Bieberle, F. Fischer, U. Sprewitz

Ultra fast X-ray tomography
The ultrafast X-ray tomography scanner ROFEX at the TOPFLOW DN50 titanium pipe was put into operation. Fist measurements using a frame rate of 2500 pictures per second for bubbly flows in stagnant liquid showed the capabilities of this new technique. Now a non-invasive measuring instrument complementary to the wire-mesh sensors is available for investigations on multiphase flows and the generation of CFD-grade data. The methodology of the ultra fast X-ray tomography was further developed in the frame of DFG-funded project "Ultraschnelle Röntgentomographie". New methods for the reconstruction of the gas-liquid interface basing on a level-set algorithm were developed. Also possibilities for a 3D-tomography were studied basing on the two-step target, which allows the measurement of bubble velocities.

U. Hampel, A. Bieberle, D. Hoppe, E. Schleicher, C. Zippe

Gamma ray tomography for void fraction measurements in fuel rod assemblies
Extensive measurements were done at an electrically heated Boiling Water reactor (BWR) rod bundle mockup under thermal-hydraulic reactor operation conditions using a high-resolution gamma ray tomography system. It is being utilized at the KATHY thermal hydraulic test facility of AREVA NP Germany. The data evaluation based on new developed algorithms considering e.g. scattered radiation and mechanical deformation of the bundle. In the result a spatial resolution

of 2 mm was achieved. The comparison done by AREVA with simulations showed a good agreement of the void fraction distributions. The measuring technique is unique worldwide and allows a better assessment of fuel element designs regarding safety-related and economical aspects.

M. Schubert,
H. Kryk,
G. Hessel

Hydrodynamic phenomena in porous media
Two-phase flows phenomena in porous media are important aspects in many chemical engineering processes (e.g. trickle bed reactors) and nuclear safety-related problems (e.g. cooling of meltdown debris).

For the first time, fluid dynamics in porous packings were studied applying spatial and temporal high-resolution capacitance wire-mesh sensor techniques. Therefore, local liquid holdups and liquid interstitial velocities in the cross-section of a randomly packed bed were measured. It was shown, that frequency distribution of the local velocities strongly depends on phase throughput. Furthermore, dynamic characteristics, namely pulse frequency and pulse velocity of the natural pulse flow regime occurring at higher flow rates were analyzed.

Magneto-Hydrodynamics

Magnetohydrodynamics investigates the interaction of electrically conducting fluids (liquid metals and semiconductors, electrolytes) with magnetic fields. In various applications, the use of magnetic fields provides a comfortable contact-less possibility to control the transport processes in such melts. Moreover, problems as MHD turbulence, the homogeneous dynamo or the magnetorotational instability are the subject of intense basic research.

I. Grants,
V. Galindo,
G. Gerbeth

Flow Stability Investigations

The vertical Gradient Freeze (VGF) crystal growth technique works with a stabilizing temperature gradient, i.e. it is cold at the bottom and hot in the upper part of the melt. Travelling magnetic fields (TMF) have been suggested for an intensification of the melt flow in order to influence the phase boundary of the growing crystal or the dopant distributions. The performed numerical and experimental flow stability investigations showed that by a TMF of suitable amplitude and frequency stable, laminar flows can be obtained which even provide a change of the flow direction close to the phase boundary. The latter is known to lead to an improvement of the dopant distribution in VGF growth of GaAs.

Supported by
DFG

A. Giesecke,
F. Stefani,
G. Gerbeth

The French VKS Dynamo

In the French VKS dynamo liquid sodium is pumped in a close cylindrical vessel by two propellers. After years of preparations, this dynamo became operating in 2006. Surprisingly, magnetic field self-excitation started at about half of the pre-calculated melt velocity. In addition, the induced magnetic field turned out to be axisymmetric in a good approximation, which is in direct contradiction to the so-called anti-dynamo theorem of Cowling. An explanation of these basic open aspects has been derived by taking into account the magnetic permeability of the ferromagnetic propeller. It turned out, however, that this high permeability of the propellers lead to the observed magnetic field induction almost independent of the flow field in the liquid sodium. Though the VKS dynamo showed very interesting phenomena such as reversals and excursions, it is only partly a hydromagnetic dynamo.

Supported by
DFG

K. Timmel,
X. Miao,
S. Eckert,
G. Gerbeth

Liquid Metal Model of Steel Casting

The large-scale liquid metal model of the continuous casting of steel, using a tin-bismuth alloy in the range of 170°C – 300°C, started its operation as planned. This was only possible thanks to the intense cooperation and support by Zentralabteilung Research Technology. The flow rate in the loop and the melt level in the mould are controlled by the power of the electromagnetic pump and by the stopper rod on top of the submerged entry nozzle. This new liquid metal model of the steel casting process was a highlight of the world conference "Electromagnetic Processing of Materials" (EPM2009) which took place in Dresden in October 2009.

Supported by
DFG, EC

Th. Gundrum,
F. Stefani,
G. Gerbeth

Experiments on the Magneto-Rotational Instability (MRI)

The experiments at the improved set-up PROMISE-2 convincingly confirmed the theoretical predictions on the distinction between

convective and absolute instabilities caused by the symmetry breaking helical magnetic field. This helical MRI (HMRI) occurs already at much lower melt velocities than the standard MRI (SMRI) of a pure vertical magnetic field. The reason for the different scaling behaviours of HMRI and SMRI is that SMRI is essentially a destabilized slow magneto-Coriolis wave, while HMRI is essentially a weakly destabilized inertial oscillation. Nevertheless, both instabilities are connected continuously, a fact that has been explained recently in terms of the appearance of an exceptional point where both modes coalesce and exchange their branches

*Ch. Zhang,
S. Eckert,
G. Gerbeth*

Liquid Metal Gas Bubble Flows in Magnetic Fields
Complex flow phenomena were observed if gas bubbles are injected into metal melts and exposed to external magnetic fields. The drag coefficient of a single gas bubble in a steady magnetic field strongly depends on the bubble size. For small bubbles this drag increases for growing field strength, the opposite is the case for larger bubbles. Alternating magnetic fields in combination with bubble injection provide an attractive method for an efficient mixing of metal melts. In particular, an upwards travelling magnetic field superimposed to a central bubble injection was found to lead to a multitude of vortices with alternating flow direction and, thus, a high level of turbulent fluctuations.

Transient Two-Phase Flow Test Facility TOPFLOW

The TOPFLOW (Transient **TwO** **P**hase **FLOW**) test facility is one of the major research facilities at Forschungszentrum Dresden – Rossendorf. It is mainly used for the investigation of generic and applied steady state and transient two-phase flow phenomena in either steam-water or air-water mixtures. TOPFLOW has a maximum heating power of 4 MW and allows operation at pressures up to 7 MPa and temperature up to 285°C in pipes and vessel geometries of industrial relevance. It has become the experimental reference facility of the German CFD (Computational Fluid Dynamic) Research Alliance. Since 2006 two major research projects are run at the TOPFLOW facility. One is a BMWi funded project aiming at the development and validation of CFD models for disperse and stratified two-phase flows with heat and mass transfer. Within this project a series of novel two-phase flow experiments are conducted at TOPFLOW in different test sections. Furthermore, an international consortial project dedicated to the investigation of thermal hydraulic phenomena in a pressurised thermal shock scenario (PTS) is run.

M. Beyer,
T. Seidel,
H. Pietruske,
P. Schütz,
H. Rußig,
K. Linder,
S. Weichelt

Two phase flow experiments in the vertical test section DN200 with heat and mass transfer

Comprehensive investigations of non-adiabatic flow inside the test section "Variable gas injection" were started after successful commissioning of the DN200 high temperature wire mesh sensors. The experimental series is part of the TOPFLOW-II project funded by BMWi. Tests with steam condensation in subcooled water were accomplished at 1, 2 and 4 MPa system pressure. A first analysis of the data revealed a complex interplay of steam condensation and liquid heat up, so that the data with its unique resolution in space and time at pressures and temperatures up to 65 bar and 282°C will be of great relevance for future model development and CFD code validation.

For another subproject of the aforementioned BMWi project TOPFLOW-II a test facility was designed and an advanced instrumentation setup was configured. The test facility will serve for investigations on steam condensation at free surfaces and jets and will be operated in the TOPFLOW pressure vessel. The unique TOPFLOW pressure vessel technology provides the opportunity of a large-area observation of flow phenomena at pressures up to 5 MPa similar to previous experiments on counter- and cocurrent flow in a hot-leg model.

Supported by
BMWi

U. Hampel,
F. Fischer,
U. Sprewitz,
M. Beyer,
E. Schleicher,
P. Schütz,
M. Tschofen

Fast X-ray tomography of two-phase flow structures

After successful completion of the radiation protection setup of the 150 keV X-ray tomograph and grant of the operation licence in October 2009 the X-ray measurement system was mounted at the vertical test section DN50 and is now ready for operation. The vacuum system and the beam control were further optimized. The X-ray scanner provided for the first time image data for air/water flow without disturbing the flow itself. These data will be used in the future for CFD code validation and comparison with data from invasive wire mesh sensors. Furthermore, the assembly of a dual-plane detector was started. It allows the measurement of local gas velocities by cross-correlation of images from two consecutive planes.

Supported by
BMWi

U. Hampel,
E. Schleicher,
M. Beyer,
H. Pietruske,
M. Tschofen,
S. Weichelt,
C. Zippe

TOPFLOW – PTS (thermal hydraulics at pressurized thermal shock)

In this project thermal hydraulic phenomena occurring in an emergency core cooling scenario in pressurized water reactors during loss of coolant accidents are investigated. Of special interest is the mixing of hot and cold water in the cold-leg and the downcomer during emergency core cooling. Stationary and transient experiments with air-water and steam-water systems are run in a 1:2.5 downscaled simulator of a cold-leg pipe of a French pressurized water reactor. For a detailed experimental study of the thermal hydraulic phenomena diverse special instrumentation, including thermo-couple lances, wire mesh sensors, high speed video camera and infrared imaging, is operated within the TOPFLOW pressure vessel at pressures up to 5 MPa. In the reference period the commissioning tests for the entire test rig were completed and preliminary experiments were carried out for air-water flows.

Publications

Publications in journals

Al Issa, S.; Lucas, D.
Two phase flow 1D turbulence model for poly disperse upward flow in a vertical pipe
Nuclear Engineering and Design 239(2009)10, 1933-1943

Albeverio, S.; Günther, U.; Kuzhel, S.
J-selfadjoint operators with C-symmetries: extension theory approach
Journal of Physics A 42(2009), 105205

Aydin, B.; Schubert, M.; Lange, R.; Larachi, F.
Nicht-Newtonsche schäumende Flüssigkeiten in Rieselbettreaktoren – Hydrodynamische Charakterisierung und effiziente Schaumbegrenzung
Chemie Ingenieur Technik 81(2009)7, 969-978

Azzopardi, B.; Hampel, U.; Hunt, A.
Pipe dream
TCE - The chemical engineer (2009)820, 39-41

Bechta, S. V.; Granovsky, V. S.; Khabensky, V. B.; Krushinov, E. V.; Vitol, S. A.; Sulatsky, A. A.; Gusarov, V. V.; Almiashev, V. I.; Lopukh, D. B.; Bottomley, D.; Fischer, M.; Piluso, P.; Miassoedov, A.; Tromm, W.; Altstadt, E.; Fichot, F.; Kymalainen, O.
VVER vessel steel corrosion at interaction with molten corium in oxidizing atmosphere
Nuclear Engineering and Design 239(2009), 1103-1112

Bergner, F.; Ulbricht, A.; Heintze, C.
Estimation of the solubility limit of Cr in Fe at 300°C from small angle neutron scattering in neutron-irradiated Fe-Cr alloys
Scripta Materialia 61(2009), 1060-1063

Bergner, F.; Ulbricht, A.; Viehrig, H.-W.
Acceleration of irradiation hardening of low-copper reactor pressure vessel steel observed by means of SANS and tensile testing
Philosophical Magazine Letters 89(2009)12, 795-805

Bieberle, M.; Fischer, F.; Schleicher, E.; Koch, D.; Menz, H.-J.; Mayer, H.-G.; Hampel, U.
Experimental two-phase flow measurement using ultra fast limited-angle-type electron beam X-ray computed tomography
Experiments in Fluids 47(2009)3, 369-378

Biswas, K.; Hermann, R.; Wendrock, H.; Priede, J.; Gerbeth, G.; Büchner, B.
Effect of melt convection on the secondary dendritic arm spacing in peritectic Nd-Fe-B alloy
Journal of Alloys and Compounds 480(2009), 295-298

Boden, S.; Willers, B.; Eckert, S.; Gerbeth, G.
Observation of dendritic growth and fragmentation in Ga-In alloys by X-ray radioscopy
International Journal of Cast Metals Research 22(2009), 30-33

Cartland Glover, G. M.; Generalis, S. C.
Pattern competition in homogeneously heated fluid layers
Engineering Application of Computational Fluid Dynamics 3(2009)2, 164-174

Cramer, A.; Galindo, V.; Gerbeth, G.; Priede, J.; Bojareviecs, A.; Gelfgat, Y.; Andersen, O.; Kostmann, C.; Stephani, G.
Tailored magnetic fields in the melt extraction of metallic filaments
Metallurgical and Materials Transactions B 40(2009), 337-344

Cramer, A.; Lange, A.; Plevachuk, Yu.; Sklyarchuk, V.
Toward physical modeling of laser welding: thermophysics revisited
International Journal of Thermophysics 30(2009), 555-571

Cramer, A.; Zhang, X.; Gerbeth, G.
Macroscopic thermomagnetic convection: A more generic case and optimization
Magnetohydrodynamics 45(2009)4, 505-510

Da Silva, M. J.; Hampel, U.
A field-focusing imaging sensor for fast visualization of multiphase flows
Measurement Science and Technology 20(2009)10, 104009

Da Silva, M. J.; Thiele, S.; Hampel, U.
Neuartige kapazitive Sensoren für die Visualisierung von Mehrphasenströmungen
Technisches Messen 76(2009)4, 189-197

Eckert, S.; Nikrityuk, P. A.; Räbiger, D.; Willers, B.; Eckert, K.
Anwendung zeitmodulierter Magnetfelder zur Strömungskontrolle während der gerichteten Erstarrung metallischer Legierungen
Berg- und hüttenmännische Monatshefte 154(2009)3, 117-120

Eckert, S.; Räbiger, D.; Willers, B.; Nikrityuk, P. A.; Eckert, K.
Use of time-modulated AC magnetic fields for melt flow control during unidirectional solidification
International Journal of Cast Metals Research 22(2009), 78-81

Fischer, F.; Hampel, U.
Ultra fast electron beam x-ray CT scanner for two phase flow measurement
atw - International Journal for Nuclear Power (2009)7, 461-464

Fischer, M.; Gerbeth, G.; Giesecke, A.; Stefani, F.
Inferring basic parameters of the geodynamo from sequences of polarity reversals
Inverse Problems 25(2009), 065011

Grants, I.; Klyukin, A.; Gerbeth, G.
Instability of the melt flow in VGF growth with a traveling magnetic field
Journal of Crystal Growth 311(2009)17, 4255-4264

Hamidipour, M.; Schubert, M.; Larachi, F.
Rieselbettreaktoren unter Filtrationsbedingungen – Mechanismus der Ablagerung, Hydrodynamische Folgen, Methoden zur Begrenzung der Filterwirkung
Chemie Ingenieur Technik 81(2009)7, 979-988

Hampel, U.; Fischer, F.
Hochdynamische Prozesse im Röntgenblick
Nachrichten aus der Chemie (2009)1, 47-49

Hampel, U.; Otahal, J.; Boden, S.; Beyer, M.; Schleicher, E.; Zimmermann, W.; Jícha, M.
Miniature conductivity wire mesh sensor for gas-liquid two-phase flow measurement
Flow Measurement and Instrumentation 20(2009), 15-21

Heintze, C.; Recknagel, C.; Bergner, F.; Hernández-Mayoral, M.; Kolitsch, A.
Ion-irradiation-induced damage of steels characterized by means of nanoindentation
Nuclear Instruments and Methods in Physics Research B 267(2009), 1505-1508

Höhne, T.
CFD-simulation of the VVER thermal hydraulic benchmark V1000CT–2 using ANSYS CFX
Science and Technology of Nuclear Installations 2009(2009), Article ID 835162

Höhne, T.
Anwendung von CFD-Methoden für den Kern sowie den Primärkreislauf von LWR
atw - International Journal for Nuclear Power 8/9(2009), 546-548

Höhne, T.; Kliem, S.; Vaibar, R.
Experimental and numerical modeling of transition matrix from momentum to buoyancy-driven flow in a pressurized water reactor
Journal of Engineering for Gas Turbines and Power - Transactions of the ASME 131(2009)1, 012906

Höhne, T.; Moncalvo, D.; Friedel, L.; Jörgensen, B.
Nachrechnung eines Vollhub-Feder-Sicherheitsventils mit ANSYS CFX
Forschung im Ingenieurwesen - Engineering Research 73(2009)2, 99-103

Höhne, T.; Vallee, C.
Modelling of stratified two phase flows using an interfacial area density model
WIT Transactions on Engineering Sciences Volume 63(2009), 123-135

Hoppe, D.; Grahn, A.; Schütz, P.
Determination of velocity and angular displacement of bubbly flows by means of wire-mesh sensors and correlation analysis
Flow Measurement and Instrumentation 21(2009)1, 48-53

Hozoi, L.; Birkenheuer, U.; Stoll, H.; Fulde, P.
Spin-state transition and spin-polaron physics in cobalt oxide perovskites: ab initio approach based on quantum chemical methods
New Journal of Physics 11(2009), 023023

Kaji, R.; Azzopardi, B. J.; Lucas, D.
Investigation of flow development of co-current gas-liquid vertical slug flow
International Journal of Multiphase Flow 35(2009), 335-348

Kirillov, O.; Günther, U.; Stefani, F.
Determining role of Krein signature for 3D Arnold tongues of oscillatory dynamos
Physical Review E 79(2009), 016205

Kliem, S.; Mittag, S.; Rohde, U.; Grundmann, U.; Weiß, F.-P.
Simulation von ATWS-Transienten in Druckwasserreaktoren
atw - International Journal for Nuclear Power 54(2009)2, 100-110

Kliem, S.; Mittag, S.; Rohde, U.; Weiß, F.-P.
ATWS analysis for PWR using the coupled code system DYN3D/ATHLET
Annals of Nuclear Energy 36(2009), 1230-1234

Konheiser, J.; Mittag, S.; Zaritsky, S.
Neutron fluence calculations for embrittlement surveillance specimens in VVER-1000
Annals of Nuclear Energy 36(2009)8, 1235-1241

Krepper, E.; Beyer, M.; Frank, T.; Lucas, D.; Prasser, H.-M.
CFD modelling of polydispersed bubbly two phase flow around an obstacle
Nuclear Engineering and Design 239(2009), 2372-2381

Krepper, E.; Cartland-Glover, G.; Grahn, A.
CFD-modelling of insulation debris transport phenomena in water flow
Kerntechnik 74(2009)5-6, 255-264

Krepper, E.; Cartland-Glover, G.; Grahn, A.; Weiss, F.-P.; Alt, S.; Hampel, R.; Kästner, W.; Seeliger, A.
CFD-modeling and experiments of insulation debris transport phenomena in water flow
Nuclear Technology 167(2009)1, 46-59

Krepper, E.; Cartland-Glover, G.; Grahn, A.; Weiss, F.-P.; Alt, S.; Hampel, R.; Kästner, W.; Seeliger, A.
CFD-modeling of insulation debris transport phenomena in water flow
Nuclear Engineering and Design 240(2009), 2357-2364

Lange, A.; Cramer, A.; Beyer, E.
Thermoelectric currents in laser induced melts pools
Journal of Laser Applications 21(2009)2, 82-87

Liao, Y.; Lucas, D.
A literature review of theoretical models for drop and bubble breakup in turbulent dispersions
Chemical Engineering Science 64(2009)15, 3389-3406

Lucas, D.; Bestion, D.; Coste, P.; Pouvreau, J.; Morel, Ch.; Martin, A.; Boucker, M.; Bodele, E.; Schmidtke, M.; Scheuerer, M.; Smith, B.; Dhotre, M. T.; Niceno, B.; Lakehal, D.; Galassi, M. C.; Mazzini, D.; D'Auria, F.; Bartosiewicz, Y.; Seynhaeve, J.-M.; Tiselj, I.; ŠTrubelj, L.; Ilvonen, M.; Kyrki-Rajamäki, R.; Tanskanen, V.; Laine, M.; Puustinen, J.
Main results of the European project NURESIM on the CFD-modelling of two-phase Pressurized Thermal Shock (PTS)
Kerntechnik 74(2009), 238-242

Lucas, D.; Tiselj, I.; Hassan, Y.; Moretti, F.
Computational Fluid Dynamics (CFD) for gas-liquid flows
Science and Technology of Nuclear Installations 2009(2009), Article ID 725247

Manera, A.; Ozar, B.; Paranjape, S.; Ishii, M.; Prasser, H.-M.
Comparison between wire-mesh sensors and conductive needle-probes for measurements of two-phase flow parameters
Nuclear Engineering and Design 239(2009)9, 1718-1724

Mazzini, G.; Bomboni, E.; Cerullo, N.; Fridman, E.; Lomonaco, G.; Shwageraus, E.
The use of Th in HTR: state of the art and implementation in Th/Pu fuel cycles
Science and Technology of Nuclear Installations 2009(2009), 749736

Merk, B.
On the influence of spatial discretization in LWR-burnup calculations with HELIOS 1.9 – part I: Uranium oxide (UOX) fuel
Annals of Nuclear Energy 36(2009), 151-167

Merk, B.
An Analytical Approximation Solution for a Time-Dependent Neutron Transport Problem with External Source and Delayed Neutron Production
Nuclear Science and Engineering 161(2009)1, 49-67

Merk, B.
On the influence of spatial discretization in LWR-burnup calculations with HELIOS 1.9 – part II: mixed oxide (MOX) fuel
Annals of Nuclear Energy 36(2009), 168-182

Merk, B.; Weiß, F. P.
A Three-Scale Expansion Solution for a Time-Dependent P1 Neutron Transport Problem with External Source
Nuclear Science and Engineering 163(2009), 152-174

Metan, V.; Eigenfeld, K.; Räbiger, D.; Leonhardt, M.; Eckert, S.
Grain size control in Al-Si Alloys by grain refinement and electromagnetic stirring
Journal of Alloys and Compounds 487(2009)1-2, 163-172

Moncalvo, D.; Friedel, L.; Jörgensen, B.; Höhne, T.
Nachrechnung der Leistungsparameter eines Sicherheitsventils mit ANSYS CFX
Forschung im Ingenieurwesen - Engineering Research 73(2009)2, 99-103

Moncalvo, L.; Friedel, B.; Jörgensen, T.; Höhne, T.
Sizing of safety valves using ANSYS CFX-Flo
Chemical Engineering & Technology 32(2009)2, 1-6

Moretti, F.; Melideo, D.; Del Nevo, A.; D'Auria, F.; Höhne, T.; Lisenkov, E.
CFD validation against slug mixing experiment
Science and Technology of Nuclear Installations (2009), Article ID 436218

Munteanu, M. C.; Schubert, M.; Larachi, F.
Rieselbettreaktoren unter künstlichem Schwerkrafteinfluss – Prinzip, Umsetzung, Auswirkung und Anwendung
Chemie Ingenieur Technik 81(2009)7, 957-967

Nikrityuk, P. A.; Eckert, K.; Eckert, S.
The impact of turbulent flow on the solidification of metal alloys driven by a rotating magnetic field
International Journal of Cast Metals Research 22(2009)No 1-4, 236-239

Pal, J.; Cramer, A.; Gundrum, Th.; Gerbeth, G.
MULTIMAG - A MULTIpurpose MAGnetic system for physical modelling in magnetohydrodynamics
Flow Measurement and Instrumentation 20(2009), 241-251

Priede, J.; Buchenau, D.; Gerbeth, G.
Force-free and contactless sensor for electromagnetic flowrate measurements
Magnetohydrodynamics 45(2009)3, 451-458

Priede, J.; Gerbeth, G.
Absolute versus convective helical magnetorotational instability in a Taylor-Couette flow
Physical Review E 79(2009), 046310

Rindelhardt, U.
Wasserkraftnutzung an der Saale
EW: Das Magazin für die Energiewirtschaft (2009)19, 44-49

Rindelhardt, U.; Viehrig, H.; Konheiser, J.; Schuhknecht, J.; Noack, K.; Gleisberg, B.
RPV material investigations of the former VVER-440 Greifswald NPP
Nuclear Engineering and Design 239(2009)9, 1581-1590

Rindelhardt, U.; Viehrig, H.-W.; Konheiser, J.; Schuhknecht, J.
Weld material investigations of a VVER-440 reactor pressure vessel: Results from the first trepan taken from the former Greifswald NPP
Journal of Engineering for Gas Turbines and Power - Transactions of the ASME 131(2009), 22904

Schubert, M.; Larachi, F.
Phase holdups in three-phase semi-fluidized beds and the generalized bubble wake model
Industrial & Engineering Chemistry Research 48(2009)18, 8393-8401

Sklyarchuk, V.; Plevachuk, Y.; Yakymovich, A.; Eckert, S.; Gerbeth, G.; Eigenfeld, K.
Structure sensitive properties of Al-Si liquid alloys
International Journal of Thermophysics 30(2009), 1400-1410

Stefani, F.; Gerbeth, G.; Gundrum, T.; Hollerbach, R.; Priede, J.; Rüdiger, G.; Szklarski, J.
Helical magnetorotational instability in a Taylor-Couette flow with strongly reduced Ekman pumping
Physical Review E 80(2009), 066303

Stefani, F.; Gerbeth, G.; Gundrum, T.; Szklarski, J.; Rüdiger, G.; Hollerbach, R.
Liquid metal experiments on the helical magnetorotational instability
Magnetohydrodynamics 45(2009)2, 135-143

Stefani, F.; Giesecke, A.; Gerbeth, G.
Numerical simulations of liquid metal experiments on cosmic magnetic fields
Theoretical and Computational Fluid Dynamics 23(2009)6, 405-429

Talati, M.; Albaret, T.; Tanguy, A.
Atomistic simulations of elastic and plastic properties in amorphous silicon
EPL - Euro Physics Letters 86(2009), 66005

Talati, M.; Jha, Prafulla J.
Temperature Effect on Vibrational Properties of La0.7Sr0.3MnO3
International Journal of Modern Physics B 23(2009)23, 4767-4777

Thiele, S.; Da Silva, M. J.; Hampel, U.
Capacitance planar array sensor for fast multiphase flow imaging
IEEE Sensors Journal 9(2009)5, 533-540

Vallee, C.; Deendarlianto,.; Beyer, M.; Lucas, D.; Carl, H.
Air/water counter-current flow experiments in a model of the hot leg of a pressurised water reactor
Journal of Engineering for Gas Turbines and Power - Transactions of the ASME 131(2009)2, 022905

Vezzoni, B.; Cerullo, N.; Forasassi, G.; Fridman, E.; Lomonaco, G.; Romanello, V.; Shwageraus, E.
Preliminary evaluation of a nuclear scenario involving innovative gas cooled reactors
Science and Technology of Nuclear Installations 2009(2009), 940286

Viehrig, H.-W.; Schuhknecht, J.
Fracture Mechanics Characterisation of the WWER-440 Reactor Pressure Vessel Core Welding Seam
International Journal of Pressure Vessels and Piping 86(2009)4, 239-245

Viehrig, H.-W.; Schuhknecht, J.; Rindelhardt, U.; Weiss, F.-P.
Investigation of the beltline welding seam of the Greifswald WWER-440 unit 1 reactor pressure vessel
Journal of ASTM International 6(2009)5

Wondrak, T.; Stefani, F.; Gundrum, T.; Gerbeth, G.
Some methodological improvements of the contactless inductive flow tomography
International Journal of Applied Electromagnetics and Mechanics 30(2009)3-4, 255-264

Yin, W.; Peyton, A.; Stefani, F.; Gerbeth, G.
Theoretical and numerical approaches to the forward problem and sensitivity calculation of a novel contactless inductive flow tomography
Measurement Science and Technology 20(2009), 105503

Zhang, C.; Eckert, S.; Gerbeth, G.
The impact of a vertically travelling magnetic field on the flow in a cylindrical liquid metal bubble plume
Metallurgical and Materials Transactions B 40(2009)5, 700-711

Zhang, X.; Cramer, A.; Lange, A.; Gerbeth, G.
Model experiments on macroscopic thermoelectromagnetic convection
Magnetohydrodynamics 45(2009), 25-42

Zhu, Z.; Dorao, Carlos A.; Lucas, D.; Jakobsen, Hugo A.
On the coupled solution of a combined population balance model using the least-squares spectral element method
Industrial & Engineering Chemistry Research 48(2009), 7994-8006

Zorn, T.; Küchler, R.; Noack, K.; Dittmar, T.; Worch, E.
Zur Gipsauflösung in Batch- und Säulenversuchen
Grundwasser 14(2009)4, 287-295

Zurbuchen, C.; Viehrig, H.-W.; Weiß, F.-P.
Master Curve and Unified Curve applicability to highly neutron irradiated Western type Reactor Pressure Vessel steels
Nuclear Engineering and Design 239(2009)7, 1246-1253

Conference contributions and other oral presentations

Abdulkareem, L. A.; Hernandez-Perez, V.; Azzopardi, B. J.; Sharaf, S.; Thiele, S.; Da Silva, M. J.
Comparison of different tools to study gas-liquid flow
7th World Conference on Experimental Heat Transfer, Fluid Mechanics and Thermodynamics, 28.06.-03.07.2009, Krakow, Poland

Abdulkareem, L. A.; J. Azzopardi, B.; Thiele, S.; Hunt, A.; Da Silva, M. J.
Interrogation of gas/oil flow in a vertical pipe using two tomographic techniques
28th International Conference on Ocean, Offshore and Arctic Engineering, 31.05.-05.06.2009, Honolulu, USA

Al-Asqalani, A. T.; Posselt, M.; Bergner, F.; Birkenheuer, U.
Atomic-level computer simulations of copper-vacancy clusters in alpha-Fe
First international school on materials for nuclear reactors (MATRE-1), 18.-23.10.2009, Rochehaut-sur-Semois, Belgium

Albrecht, T.; Marlow, F.; Metzkes, H.; Stiller, J.
DNS and LES of separation control using oscillating Lorentz forces
6th International Conference on Electromagnetic Processing of Materials (EPM 2009), 19.-23.10.2009, Dresden, Deutschland

Altstadt, E.
Status of the Umbrella project LONGLIFE
5-th NULIFE Network meeting, 15.-17.09.2009, Les Renardieres, France

Altstadt, E.; Bergner, F.; Hein, H.; Gillemot, F.; Serrano, M.; Brumovsky, M.; Lidbury, D.; Marcelles, I.
FP7 project LONGLIFE: Treatment of long term irradiation embrittlement effects in RPV safety assessment
15th Workshop of the International Group on Radiation Damage Mechanisms in Pressure Vessel Steels (IGRDM-15), 11.-16.10.2009, Budapest, Ungarn

Azzopardi, B. J.; Abdulkareem, L. A.; Zhao, D.; Thiele, S.; Da Silva, M. J.; Beyer, M.; Hunt, A.
Comparison between electrical capacitance tomography and wire mesh sensor output for air/silicone oil flow in a vertical pipe
3rd International Workshop on Process Tomography, 17.-19.04.2009, Tokyo, Japan

Bergner, F.; Heintze, C.; Hernandez-Mayoral, M.
Nanoindentation response and microstructure of irradiated Fe-Cr alloys
IAEA Technical Meeting on Physics of Materials under Neutron and Charged Particle Irradiation, 16.-19.11.2009, Wien, Österreich

Bergner, F.; Heintze, C.; Ulbricht, A.
The microstructure of neutron-irradiated Fe-Cr alloys: A small-angle neutron scattering study
Joint EC-IAEA Topical Meeting on "Development of New Structural Materials for Advanced Fission and Fusion Reactor Systems", 05.-09.10.2009, Barcelona, Spanien

Bergner, F.; Ulbricht, A.; Viehrig, H.-W.
Fluence dependence of SANS and yield stress increase observed for low-Cu RPV steels
15th Workshop of the International Group on Radiation Damage Mechanisms of Pressure Vessel Steels (IGRDM-15), 11.-16.10.2009, Budapest, Ungarn

Beyer, M.; Fischer, F.; Danciu, D. V.; Seidel, T.; Schütz, P.; Pietruske, H.; Lucas, D.; Weiß, F.-P.
Stand der experimentellen Arbeiten im Rahmen des TOPFLOW-II Projektes
CFD im Containment / CFD für Zweiphasenströmungen (Meilstein-Workshop Sommer 2009), 29.07.2009, Dresden, Deutschland

Beyer, M.; Schleicher, E.; Pietruske, H.; Hampel, U.; Weiß, F.-P.
Stand der experimentellen Arbeiten im Rahmen des TOPFLOW-PTS Projektes
Steering Committee Meeting on R&D Cooperation between FZD and AREVA NP GmbH, 07.09.2009, Dresden, Deutschland

Bieberle, M.
Bildrekonstruktion für die ultraschnelle Limited-Angle-Röntgen-Computertomographie von Zweiphasenströmungen
KOMPOST Doktorandenseminar, 10.12.2009, Dresden, FZD, Deutschland

Bieberle, M.
Ultrafast electron-beam x-ray computed tomography for multi-phase flow measurement
FZD Doktorandenseminar, 16.-18.09.2009, Krögis, Deutschland

Bieberle, M.; Hampel, U.; Schleicher, E.; Fischer, F.; Koch, D.; Mayer, H.-G.; Menz, H.-J.
Experimental two-phase flow measurements using two-plane limited-angle electron beam x-ray CT and wire-mesh sensor
3rd International Workshop on Process Tomography (IWPT-3), 15.-17.04.2009, Tokyo, Japan

Bilodid, Y.; Mittag, S.
Spectral-history modeling in DYN3D burnup calculations
Jahrestagung Kerntechnik 2009, 12.-14.05.2009, Dresden, Germany

Birkenheuer, U.; Ulbricht, A.; Bergner, F.; Gokhman, A.
On the formation of mixed vacancy-copper clusters in neutron-irradiated Fe-Cu alloys
XIV International Conference on Small-Angle Scattering, 13.-18.09.2009, Oxford, United Kingdom

Boden, S.; Eckert, S.; Gerbeth, G.; Simonnet, M.; Anderhuber, M.; Gardin, P.
X-ray visualisation of bubble formation and bubble motion in liquid metals
6th International Conference on Electromagnetic Processing of Materials (EPM 2009), 19.-23.10.2009, Dresden, Deutschland

Boden, S.; Willers, B.; Eckert, S.; Gerbeth, G.
X-ray visualisation of solidifying GaIn-alloys in the presence of melt convection
6th International Conference on Electromagnetic Processing of Materials (EPM 2009), 19.-23.10.2009, Dresden, Deutschland

Buchenau, D.; Gerbeth, G.; Priede, J.
Comparison of various contactless flow rate sensors
6th Int. Conf. on Electromagnetic Processing of Materials, 19.-23.10.2009, Dresden, BRD

Cartland Glover, G. M.; Krepper, E.; Weiss, F.-P.; Zacharias, F.; Kratzsch, A.; Alt, S.; Kaestner, W.
Hydrodynamic modeling of mineral wool fiber suspensions in a two-dimensional channel flow
The 13th International Topical Meeting on Nuclear Reactor Thermal Hydraulics (NURETH-13), 27.09.-02.10.2009, Kanazawa, Japan

Cartland Glover, Gregory M.; Grahn, A.; Krepper, E.; Weiss, F.-P.; Alt, S.; Hampel, R.; Kaestner, W.; Kratzsch, A.; Zacharias, F.
Hydrodynamic modeling of mineral wool fiber suspensions in a two-dimensional flow
17th International Conference on Nuclear Engineering, 12.-16.07.2009, Brussels, Belgium

Cheung, Sherman C. P.; Duan, X.; Yeoh, Guan H.; Tu, J.; Krepper, E.; Lucas, D.
Modelling of polydispersed flows using two population balance approaches
6th International Symposium on Multiphase Flow, Heat Mass Transfer and Energy Conversion, 11.-15.07.2009, Xi'an, China

Cramer, A.; Pal, J.; Gundrum, Th.; Gerbeth, G.
MULTIMAG - A MULTIpurpose MAGnetic field system for EPM
Electromagnetic Processing of Materials (EPM), 19.-23.10.2009, Dresden, Deutschland

Cramer, A.; Zhang, X.; Gerbeth, G.
Model experiments on thermo-electromagnetic convection
6th International Conference on Electromagnetic Processing of Materials EPM 2009, 19.-23.10.2009, Dresden, Deutschland

Cramer, A.; Zhang, X.; Gerbeth, G.
Thermoelectromagnetic convection - an alternative stirring technique in metallurgy
International Symposium on Liquid Metal Processing and Casting, 20.-23.09.2009, Santa Fe, New Mexico

Cramer, A.; Zhang, X.; Gerbeth, G.
Thermoelectromagnetic stirring in Metallurgy
54th IWK – Internationales Wissenschaftliches Kolloquium, 07.-11.09.2009, Ilmenau, Deutschland

Da Silva, M. J.
Advanced multiphase flow measurement techniques at FZD
30th Advisory Board Meeting of Tulsa University Separation Tecnology Projects, 12.-13.05.2009, Houston, USA

Da Silva, M. J.; Hampel, U.
Kapazitäts-Gittersensor: Prinzip und Anwendung
XXIII. Messtechnisches Symposium des Arbeitskreises der Hochschullehrer für Messtechnik e.V., 17.-19.09.2009, Bremen, Deutschland

Da Silva, M. J.; Schleicher, E.; Hampel, U.
Advanced wire-mesh sensor technology for fast flow imaging
2009 IEEE International Workshop on Imaging Systems & Techniques, 11.-12.05.2009, Shenzhen, China

Da Silva, M. J.; Thiele, S.; Schleicher, E.; Hampel, U.
Wire-mesh sensors for high-resolution gas-liquid multiphase flow visualization
20th International Congress of Mechanical Engineering, 15.-20.11.2009, Gramado, Brazil

Da Silva, M. J.; Thiele, S.; Schleicher, E.; Hampel, U.
Wire-mesh sensors for fast visualization of multiphase flows
What Where When Multi-dimensional Advances for Industrial Process Monitoring, 23.-24.06.2009, Leeds, United Kingdom

Da Silva, M. J.; Thiele, S.; Schleicher, E.; Hauptmann, T.; Schmid, R.; Hampel, U.
Spezialsensorik für die Prozessindustrie - Technologietransfer aus der Sicherheitsforschung
Informationsveranstaltung bei CHOREN Fuel Freiberg GmbH & Co. KG, 06.02.2009, Freiberg, Deutschland

Da Silva, M. J.; Thiele, S.; Schleicher, E.; Hauptmann, T.; Schmid, R.; Hampel, U.
Spezialsensorik für die Prozessindustrie - Technologietransfer aus der Sicherheitsforschung
Informationsveranstaltung bei EBZ GmbH, 27.01.2009, Dresden, Deutschland

Da Silva, M. J.; Thiele, S.; Schleicher, E.; Hauptmann, T.; Schmid, R.; Hampel, U.
Spezialsensorik für die Prozessindustrie - Technologietransfer aus der Sicherheitsforschung
Informationsveranstaltung für Sick Engineering GmbH, 04.02.2009, Dresden, Deutschland

Da Silva, M. J.; Thiele, S.; Schleicher, E.; Hauptmann, T.; Schmid, R.; Hampel, U.
Spezialsensorik für die Prozessindustrie - Technologietransfer aus der Sicherheitsforschung
Informationsveranstaltung bei der GlaxoSmithKline GmbH & Co. KG, 16.02.2009, Dresden, Deutschland

Da Silva, M. J.; Thiele, S.; Schleicher, E.; Hauptmann, T.; Schmid, R.; Hampel, U.
Spezialsensorik für die Prozessindustrie - Technologietransfer aus der Sicherheitsforschung
Informationsveranstaltung für die Umwelt- und Ingenieurtechnik GmbH Dresden, 17.02.2009, Dresden, Deutschland

Da Silva, M. J.; Thiele, S.; Schleicher, E.; Hauptmann, T.; Schmid, R.; Hampel, U.
Spezialsensorik für die Prozessindustrie - Technologietransfer aus der Sicherheitsforschung
Informationsveranstaltung für Roxar ASA, 23.02.2009, Bergen, Norwegen

Da Silva, M. J.; Thiele, S.; Schleicher, E.; Hauptmann, T.; Schmid, R.; Hampel, U.
Spezialsensorik für die Prozessindustrie - Technologietransfer aus der Sicherheitsforschung
Informationsveranstaltung für Statoil Hydro, 24.02.09, Porsgrunn, Norwegen

Da Silva, M. J.; Thiele, S.; Schleicher, E.; Hauptmann, T.; Schmid, R.; Hampel, U.
Spezialsensorik für die Prozessindustrie - Technologietransfer aus der Sicherheitsforschung
Informationsveranstaltung für die Lechler GmbH, 10.03.2009, Metzingen (Württ), Deutschland

Da Silva, M. J.; Thiele, S.; Schleicher, E.; Hauptmann, T.; Schmid, R.; Hampel, U.
Spezialsensorik für die Prozessindustrie - Technologietransfer aus der Sicherheitsforschung
Informationsveranstaltung für die Riesaer Brennstoffzellentechnik GmbH, 18.02.2009, Riesa, Deutschland

Da Silva, M. J.; Thiele, S.; Schleicher, E.; Hauptmann, T.; Schmid, R.; Hampel, U.
Spezialsensorik für die Prozessindustrie - Technologietransfer aus der Sicherheitsforschung
Informationsveranstaltung für LyondellBasell Industries, 11.03.2009, Ferrara, Italien

Da Silva, M. J.; Thiele, S.; Schleicher, E.; Hauptmann, T.; Schmid, R.; Hampel, U.
Spezialsensorik für die Prozessindustrie - Technologietransfer aus der Sicherheitsforschung
Informationsveranstaltung für Bayer Technology Services GmbH, 13.03.2009, Dresden, Deutschland

Da Silva, M. J.; Thiele, S.; Schleicher, E.; Hauptmann, T.; Schmid, R.; Hampel, U.
Spezialsensorik für die Prozessindustrie - Technologietransfer aus der Sicherheitsforschung
Informationsveranstaltung für die Evonik Oxeno GmbH, 30.03.2009, Marl, Deutschland

Da Silva, M. J.; Thiele, S.; Schleicher, E.; Hauptmann, T.; Schmid, R.; Hampel, U.
Spezialsensorik für die Prozessindustrie - Technologietransfer aus der Sicherheitsforschung
Informationsveranstaltung für das Institut für Leichtbau und Kunststofftechnik (ILK) der TU-Dresden, 26.02.2009, Dresden, Deutschland

Da Silva, M. J.; Thiele, S.; Schleicher, E.; Hauptmann, T.; Schmid, R.; Hampel, U.
Spezialsensorik für die Prozessindustrie - Technologietransfer aus der Sicherheitsforschung
Informationsveranstaltung bei Endress + Hauser - Conducta Gesellschaft für Mess- und Regeltechnik mbH u. Co.KG, 30.03.2009, Waldheim, Deutschland

Da Silva, M. J.; Thiele, S.; Schleicher, E.; Hauptmann, T.; Schmid, R.; Hampel, U.
Spezialsensorik für die Prozessindustrie - Technologietransfer aus der Sicherheitsforschung
Informationsveranstaltung bei der Dow Olefinverbund GmbH, 31.03.2009, Schkopau, Deutschland

Da Silva, M. J.; Thiele, S.; Schleicher, E.; Hauptmann, T.; Schmid, R.; Hampel, U.
Spezialsensorik für die Prozessindustrie - Technologietransfer aus der Sicherheitsforschung
Informationsveranstaltung für das "Institute of Nuclear Safety System" (INSS), 26.05.2009, Dresden, Deutschland

Da Silva, M. J.; Thiele, S.; Schleicher, E.; Hauptmann, T.; Schmid, R.; Hampel, U.
Spezialsensorik für die Prozessindustrie - Technologietransfer aus der Sicherheitsforschung
Informationsveranstaltung für die Firma DuPont (USA), 18.04.2009, Tokyo, USA

Danciu, D. V.; Da Silva, M. J.; Schmidtke, M.; Lucas, D.
Experimental investigations on air entrainment by means of impinging jets
ExHFT-7, 28.06.-03.07.2009, Krakow, Polen

Danciu, D. V.; Da Silva, M. J.; Schmidtke, M.; Lucas, D.; Hampel, U.
Experimental investigation on air entrainment below impinging jets by means of video observations and image processing
Multiphase Flow 2009 Fifth International Conference on Computational and Experimental Methods in Multiphase and Complex Flow, 15.-17.06.2009, New Forest, England

Duan, X.; Cheung, Sherman C. P.; Yeoh, Guan H.; Tu, J.; Krepper, E.; Lucas, D.
An overall assessment of abnd model for large-scale bubbly flows
7th International Conference on CFD in the Minerals and Process Industries CSIRO, 09.-11.12.2009, Melbourne, Australia

Eckert, S.; Buchenau, D.; Gerbeth, G.; Stefani, F.; Weiss, F.-P.
Some recent developments in the field of liquid metal measuring techniques and instrumentation
International Conference on Fast Reactors and Related Fuel Cycles (FR09), 07.-11.12.2009, Kyoto, Japan

Eckert, S.; Buchenau, D.; Gerbeth, G.; Stefani, F.; Weiß, F.-P.; Wondrack, T.
Impact of wetting on velocity measurements in liquid metal flows
3rd International Seminar "Coolants and Innovative Reactor Technologies", 06.-07.07.2009, Aix-en-Provence, France

Eckert, S.; Zhang, C.; Gerbeth, G.
Anwendung von Ultraschallverfahren zur Charakterisierung von Flüssigmetall-Zweiphasenströmungen
Festkolloquium anlässlich des 70. Geburtstags von Prof. Dr. E. Kaiser, 06.11.2009, Dresden, Deutschland

Fischer, F.; Hampel, U.
Ultra fast electron beam X-ray CT scanner for two-phase flow measurement
Jahrestagung Kerntechnik 2009, 12.-14.05.2009, Dresden, Germany

Fischer, F.; Hampel, U.
Ultra fast electron beam x-ray CT scanner for two phase flow measurement
Jahrestagung Kerntechnik 2009, 12.-14.05.2009, Dresden, Deutschland

Franke, S.; Büttner, L.; Czarske, J.; Räbiger, D.; Eckert, S.
Ultrasound Doppler array used for vortex investigations in liquid metals
Sensor 2009, 26.-28.05.2009, Nürnberg, Germany

Franke, S.; Büttner, L.; Czarske, J.; Räbiger, D.; Eckert, S.
Ultrasound Doppler array measurement system for two-dimensional flow investigations in liquid metals
6th International Conference on Electromagnetic Processing of Materials (EPM 2009), 19.-23.10.2009, Dresden, Deutschland

Fridman, E.; Shwageraus, E.
HTGR Fuel Element Depletion Benchmark: Stage One Results
2009 ANS Winter Meeting, 15.-19.11.2009, Washington, DC Omni Shoreham Hotel, USA

Fridman, E.; Volaski, D.; Shwageraus, E.
Thermal design feasibility of Th-233U PWR breeder
GLOBAL 2009, 06.-11.09.2009, Paris, France

Giesecke, A.
Implications of a non-uniform permeability distribution on the generation of magnetic fields in the Von-K\'arm\'an-Sodium dynamo experiment.
Seminar am Laboratoire d'Informatique pour la Mécanique et les Sciences de l'Ingénieur (LIMSI), 05.05.2009, Paris, Frankreich

Giesecke, A.; Stefani, F.; Gerbeth, G.
Application of a grid based hybrid finite volume/boundary element method for simulations of the kinematic induction equation with insulating boundary conditions.
SFB Meeting, 12.11.2009, Dresden, Deutschland

Giesecke, A.; Stefani, F.; Gerbeth, G.
Implications of three dimensional velocity distributions on the generation of magnetic fields in the Von-K\'arm\'an-Sodium dynamo experiment.
Frontiers in Dynamo Theory, 16.-20.03.2009, Paris, France

Giesecke, A.; Stefani, F.; Gerbeth, G.
Kinematic dynamo simulations in cylindrical geometry
Astrophysical Magnetohydrodynamics, 06.-10.04.2009, Nurmijärvi, Finnland

Giesecke, A.; Stefani, F.; Gerbeth, G.
The role of ferromagnetic impellers in the VKS dynamo experiment
Natural Dynamos, 30.08.-05.09.2009, Stará Lesná, Slovakia

Giesecke, A.; Stefani, F.; Gerbeth, G.
The role of the soft-iron impellers in the VKS dynamo experiment
Dynamos d'un point de vue numerique et experimental, 07.-09.12.2009, Marseille, France

Grahn, A.; Krepper, E.; Weiß, F.-P.; Alt, S.; Kästner, W.; Kratzsch, A.; Hampel, R.
Implementation of a pressure drop model for the CFD simulation of clogged containment sump strainers
17th International Conference On Nuclear Engineering ICONE 17, 12.-16.07.2009, Brussels, Belgium

Grants, I.; Klyukin, A.; Gerbeth, G.
Flow stability in magnetically manipulated vertical gradient freeze
6th International Conference on Electromagnetic Processing of Materials (EPM 2009), 19.-23.10.2009, Dresden, Deutschland

Grants, I.; Zhang, C.; Eckert, S.; Gerbeth, G.
Liquid metal tornado
6th International Conference on Electromagnetic Processing of Materials (EPM 2009), 19.-23.10.2009, Dresden, Deutschland

Gundrum, T.; Gerbeth, G.; Stefani, F.; Hollerbach, R.; Priede, J.; Rüdiger, G.; Szklarski, J.
Experiments on the helical magnetorotational instability in a Taylor-Couette flow with reduced Ekman pumping
16th Couette-Taylor Workshop, 09.-11.09.2009, Princeton, USA

Gundrum, T.; Hüller, J.; Stefani, F.; Gerbeth, G.; Herrmannsdörfer, T.; Putzke, C.; Arnold, F.
Alfven wave experiments with liquid rubidium
12. MHD-Tag, 08.-9.12.2009, Potsdam, Germany

Günther, U.
Comments on the holonomy of eigenvector bundles in the vicinity of higher-order exceptional points and on the Lie group structure underlying the embedding of the PTQM brachistochrone into a two-qubit system
Aharonov Bohm Effect and Berry Phase Anniversary 50/25 2009, 14.-15.12.2009, Bristol, United Kingdom

Günther, U.
J-self-adjointness, Krein spaces and related physics
Editorial Board Meeting; Journal of Physics A: Mathematical and Theoretical, 23.-24.04.2009, London, UK

Günther, U.
PT quantum mechanics and some of its underlying mathematics
seminar at the Graduate School of Fundamental Physics; Institute of Physics; Heidelberg University, 04.06.2009, Heidelberg, Deutschland

Günther, U.
The 4D Naimark dilated PT brachistochrone as 2D Hermitian brachistochrone
Analytic and algebraic methods V, 27.-28.05.2009, Prague, Czech Republic

Günther, U.; Samsonov, B.
The Naimark dilated PT-symmetric brachistochrone
QTRF5 - Quantum Theory: Reconsideration of Foundations, 5, 14.-19.06.2009, Vaxjo, Sweden

Günther, U.; Samsonov, B.
Ultra-fast evolution via PT-symmetry and entanglement: extending the BBJM brachistochrone
Arbeitsgruppenseminar "Theoretische Quantenoptik", Institut für Theoretische Physik, TU Dresden, 08.05.2009, Dresden, Deutschland

Günther, U.; Samsonov, B.
Ultra-fast evolution via PT-symmetry and entanglement: extending the BBJM brachistochrone
Quantum Mechanics in the Complex Domain (QMCD09), 27.-28.03.2009, St. Louis, USA

Hádek, J.; Mittag, S.
Validation of DYN3D pin-power calculation against experimental VVER-full-core benchmark
International Conference on Mathematics, Computational Methods & Reactor Physics (M&C 2009), 03.-07.05.2009, Saratoga Springs, New York, USA

Hampel, U.
Gittersensortechnologie und ihr Einsatzpotenzial in der Chemieindustrie
Seminar "Sensoranwendung in der Chemieindustrie" der BASF Ludwigshafen, 14.10.2009, Ludwigshafen, Germany

Hampel, U.
Measurement techniques and experimental investigations for multiphase flows
Multiphase Flows - Simulation, Experiment and Application, 26.-28.05.2009, Dresden, Germany

Hampel, U.
Measurement techniques and experimental investigations for multiphase flows
SIAMUF – Multiphase Flows Meeting, 21.-22.10.2009, Gothenburg, Sweden

Hampel, U.
Wire mesh sensor technology - on the road towards three-phase flow measurement
Multiphase Club, 13.-14.10.2009, London, UK

Hampel, U.; Fischer, F.
Process tomography with electron beams
What, Where, When: Multi-dimensional Advances for Industrial Process Monitoring International Symposium, 23.-24.06.2009, Leeds, UK

Hampel, U.; Fischer, F.
Ultra high speed electron beam tomography for flow measurement and small animal imaging
2009 IEEE International Workshop on Imaging Systems and Techniques (IST 2009), 11.-12.05.2009, Shenzhen, China

Heintze, C.; Bergner, F.; Ulbricht, A.
Characterization of Fe-Cr alloys using SANS, nanoindentation and ultrasound
EUROMAT 2009, 07.-10.09.2009, Glasgow, United Kingdom

Hermann, R.; Behr, G.; Gerbeth, G.; Priede, J.; Guguschev, Ch.; Krauze, A.; Büchner, B.
Single crystal growth of intermetallic compounds by a two-phase RF floating zone method
6th International Conference on Electromagnetic Processing of Materials (EPM 2009), 19.-23.10.2009, Dresden, Deutschland

Höhne, T.
Validation of CFD codes and applications in NRS
3rd Nordic Conference on Fluid Dynamics in the Power Industry, 15.-16.09.2009, Copenhagen, Danmark

Höhne, T.; Rohde, U.; Melideo, D.; Moretti, F.; D'Auria, F.; Shishov, A.; Lisenkov, E.
CFD simulations of GIDROPRESS mixing facility experiments
Working Group C and G of AER, 11.-12.06.2009, Tengelic, Ungarn

Höhne, T.; Rohde, U.; Melideo, D.; Moretti, F.; D'Auria, F.; Shishov, A.; Lisenkov, E.
Experimental and numerical analysis of coolant mixing in VVER-1000 in the framework of TACIS project R2.02/02
Jahrestagung Kerntechnik 2009, 12.-14.05.2009, Dresden, Deutschland

Höhne, T.; Vallee, C.
Experiments and numerical simulations of horizontal two phase flow regimes
Seventh International Conference on CFD in the Minerals and Process Industries, 09.-12.12.2009, Melbourne, Australia

Höhne, T.; Vallee, C.
Modelling of stratified two phase flows using an interfacial area density model
Fifth International Conference on Computational and Experimental Methods in Multiphase and Complex Flow, 15.-17.06.2009, New Forest, Großbritannien

Höhne, T.; Vallee, C.
Numerical prediction of horizontal two phase flow using an interfacial area density model
The 13th International Topical Meeting on Nuclear Reactor Thermal Hydraulics (NURETH-13), 27.09.-02.10.2009, Kanazawa City, Japan

Kirillov, O.; Günther, U.; Stefani, F.
Determining role of Krein signature for 3D Arnold tongues of oscillatory dynamos
Verhandlungen der Deutschen Physikalischen Gesellschaft e.V., 22.-27.03.2009, Dresden, Deutschland

Kirillov, O.; Stefani, F.
On the relation of standard and helical magnetorotational instability
12th MHD Days, 08.-09.12.2009, Potsdam, Germany

Kliem, S.
AER working group D on VVER safety analysis – report of the 2009 meeting
19th Symposium of AER on VVER Reactor Physics and Reactor Safety, 21.-25.09.2009, Varna, Bulgarien

Kliem, S.; Gommlich, A.; Rohde, U.
Integration of DYN3D into the NURESIM platform and coupling with FLICA
NURISP - General Seminar, 30.11.-01.12.2009, Dresden, Germany

Kliem, S.; Höhne, T.; Rohde, U.; Bykov, M.; Lisenkov, E.
Comparative evaluation of coolant mixing experiments at the ROCOM and the Gidropress test facilities
6th International Conference "Safety Assurance of NPP with WWER", 26.-29.05.2009, Podolsk, Russland

Kliem, S.; Langenbuch, S.; Weiß, F.-P.
Uncertainty analyses of coupled thermal hydraulic/neutron kinetic code calculations for transients at NPPs with VVER reactors
OECD Benchmark for Uncertainty Analysis in Best-Estimate Modelling (UAM) for Design, Operation and Safety Analysis of LWRs - Third Workshop, 29.04.-01.05.2009, State College, USA

Kliem, S.; Mittag, S.; Rohde, U.; Weiß, F.-P.
Influence of system and neutron-kinetic parameter variations on an anticipated transient without SCRAM in a PWR
17th International Conference on Nuclear Engineering, 12.-16.07.2009, Brussels, Belgium

Kliem, S.; Mittag, S.; Rohde, U.; Weiß, F.-P.
Influence of the neutron-kinetic feedback parameter variation on an anticipated transient without SCRAM in a PWR
2009 International Conference on Advances in Mathematics, Computational Methods, and Reactor Physics, 03.-07.05.2009, Saratoga Springs, USA

Kliem, S.; Mittag, S.; Rohde, U.; Weiß, F.-P.; Kozmenkov, Y.
The influence of different thermal hydraulic models on the results of a DYN3D boron dilution transient calculation
Jahrestagung Kerntechnik 2009, 12.-14.05.2009, Dresden, Deutschland

Kliem, S.; Rohde, U.; Weiß, F.-P.
Validation of the coupled code system DYN3D/ATHLET on the basis of transients at NPPs with VVER reactors
OECD Benchmark Workshop for Kalinin-3 VVER-1000 Coupled Code Calculations, 27.-28.04.2009, State College, USA

Kotlyar, D.; Fridman, E.; Shwageraus, E.
Coupled neutronic thermo-hydraulic analysis of full PWR core with BGCore system
Jahrestagung Kerntechnik 2009, 12.-14.05.2009, Dresden, Deutschland

Krepper, E.
Capabilities and limits of actual CFD modelling of subcooled boiling
NuFAME-2009 - Nuclear Fuel Assembly Modeling and Experiments, 09.-10.07.2009, Stockholm, Schweden

Krepper, E.
CFD modeling of subcooled boiling–model capabilities for application in nuclear technology and needs for further model development
AER Working Group C and G meeting, 11.-12.06.2009, Tengelic, Ungarn

Krepper, E.; Alt, S.; Renger, S.
Influence of air entrainment on the liquid flow field caused by a plunging jet
Jahrestagung Kerntechnik 2009, 12.-14.05.2009, Dresden, Germany

Krepper, E.; Alt, S.; Renger, S.
Influence of air entrainment on the liquid flow field caused by a plunging jet
Nuclear Energy for New Europe 2009, 14.-17.09.2009, Bled, Slovenia

Krepper, E.; Beyer, M.
Experimental and numerical investigations of temperature stratification phenomena in passive safety systems for decay heat removal
17th International Conference on Nuclear Engineering, ICONE-17, 12.-16.07.2009, Brussels, Belgium

Kryk, H.; Hampel, U.
Visualisierung von Mehrphasenströmungen in der Verfahrenstechnik
ACHEMA 2009, 29. Internationaler Ausstellungskongress für Chemische Technik, Umweltschutz und Biotechnologie, 11.-15.05.2009, Frankfurt, Deutschland

Kryk, H.; Hoffmann, W.; Hessel, G.
Experimentelle Untersuchungen zur Korrosionschemie und zum Anlagerungsverhalten von Korrosionsprodukten
BMWi-Fachkolloquium „Isolationsmaterialbelastete Kühlmittelströmung", 03.-04.03.2009, Dresden, Deutschland

Kryk, H.; Schubert, M.; Schäfer, T.; Da Silva, M. J.; Thiele, S.
Hydrodynamische Untersuchungen in Rieselbettreaktoren mittels kapazitiver Gittersensoren
ProcessNet-Jahrestagung 2009, 08.-10.09.2009, Mannheim, Deutschland

Laczko, G.; Böhlke, S.; Ohlmeyer, H.; Schuster, Ch.; Hurtado, A.
Die Relevanz der Borflüchtigkeit bei Langzeittransienten in einem mit Bor vergifteten Siedewasserreaktor
Jahrestagung Kerntechnik 2009, 12.-14.05.2009, Dresden, Deutschland

Liao, Y.; Lucas, D.
A new model for bubble coalescence and breakup in poly-disperse bubbly flows
The 13th International Topical Meeting on Nuclear Reactor Thermal Hydraulics (NURETH-13), 27.09.-02.10.2009, Kanazawa City, Ishikawa Prefecture, Japan

Liao, Y.; Lucas, D.
Breakup and coalescence models for turbulent air-water mixtures in a vertical pipe
Jahrestagung Kerntechnik 2009, 12.-14.05.2009, Dresden, Germany

Liao, Y.; Lucas, D.
Development and validation of bubble coalescence and breakup models : status of KEK project
German CFD Network 16th Meeting, 07.-08.10.2009, Garching, Germany

Liao, Y.; Lucas, D.
Modeling of the evolution of bubbly flows along a large vertical pipe with new coalescence and breakup model
47th European Two-phase Flow Group Meeting 2009, 1st Joint ETPFG-EFCE Multi-phase Meeting 2009, 03.-06.06.2009, Bled, Slovenia

Liao, Y.; Lucas, D.
The inhomogeneous MUSIG model for upward polydisperse flows with new constitutive models for bubble coalescence and breakup
International Conference Nuclear Energy for New Europe 2009, 14.-17.09.2009, Bled, Slovenia

Lucas, D.; Beyer, M.; Frank, T.; Zwart, P.; Burns, A.
Condensation of Steam Bubbles Injected into Sub-Cooled Water
The 13th International Topical Meeting on Nuclear Reactor Thermal Hydraulics (NURETH-13), 27.09.-02.10.2009, Kanazawa City, Japan

Lucas, D.; Beyer, M.; Szalinski, L.
Experimental investigations on the condensation of steam bubbles injected into sub-cooled water
5th European-Japanese Two-Phase Flow Group Meeting, 20.-25.09.2009, Spoleto, Italien

Lucas, D.; Hampel, U.; Beyer, M.; Weiß, F.-P.
Innovative Experimente an der TOPFLOW Versuchsanlage zur Verfikation und Validierung von CFD Codes
Jahrestagung Kerntechnik 2009, 12.-14.05.2009, Dresden, Deutschland

Maiwald, A.; Timmel, K.; Schwarze, R.; Gerbeth, G.
Comparison of numerical and experimental flow data from a liquid-metal model of a continuous casting mould
6th International Conference on Electromagnetic Processing of Materials (EPM 2009), 19.-23.10.2009, Dresden, Deutschland

Matusiak, B.; Da Silva, M. J.; Grudzien, K.; Hampel, U.
Capacitance wire mesh sensor and electrical capacitance tomography study of trickle-bed reactor hydrodynamics
3rd International Workshop on Process Tomography, 17.-19.04.2009, Tokyo, Japan

Merk, B.
An analytical solution for an external source problem with delayed neutron using the Telegrapher's equation
2009 International Conference on Advances in Mathematics, Computational Methods, and Reactor Physics, 03.-07.05.2009, Saratoga Springs, United States

Merk, B.
On the influence of spatial discretization in LWR-burnup calculations with HELIOS 1.9
2009 International Conference on Advances in Mathematics, Computational Methods, and Reactor Physics, 03.-07.05.2009, Saratoga Springs, United States

Merk, B.
On the influence of spatial discretization on cross-sction preparation during burnup calculations with HELIOS 1.9
Jahrestagung Kerntechnik 2009, 12.-14.05.2009, Dresden, Deutschland

Merk, B.; Glivici, V.; Weiß, F. P.
A three scale expansion solution for the Telegrapher's equation with external source: development and first application
XXI International Conference on Transport Theory, 12.-17.07.2009, Torino, Italy

Meslin, E.; Lambrecht, M.; Hernández-Mayoral, M.; Bergner, F.; Malerba, L.; Pareige, P.; Radiguet, B.; Barbu, A.; Gomez-Briceno, D.; Ulbricht, A.; Almazouzi, A.
Characterization of neutron-irradiated ferritic model alloys and a RPV steel from combined APT, SANS, TEM and PAS analyses
15th Workshop of the International Group on Radiation Damage Mechanisms in Pressure Vessel Steels (IGRDM-15), 11.-16.10.2009, Budapest, Ungarn

Miao, X.; Galindo, V.; Lucas, D.; Gerbeth, G.; Ren, Z.
Numerical Simulation of Two-phase Flow in a Slab Mold by MUSIG Model
6th International Conference on Electromagnetic Processing of Materials (EPM 2009), 19.-23.10.2009, Dresden, Germany

Mittag, S.; Kliem, S.
Burning plutonium and minimizing the radioactive waste in existing PWR
19th AER SYMPOSIUM on VVER Reactor Physics and Reactor Safety, 21.-25.09.2009, St. St. Constantine and Elena resort (Varna), Bulgaria

Mutschke, G.; Schäfer, P.; Weier, T.; Bund, A.; Fröhlich, J.
Numerical and experimental results on Lorentz force driven flows during electrodeposition of copper in homogeneous magnetic fields
6th International Conference on Electromagnetic Processing of Materials, 19.-23.10.2009, Dresden, BRD

Mutschke, G.; Schäfer, P.; Weier, T.; Hess, A.; Bund, A.; Fröhlich, J.
Numerical and experimental results on copper electrolysis in homogeneous and inhomogeneous magnetic fields
216th Meeting of the Electrochemical Society, 04.-09.10.2009, Wien, Österreich

Mutschke, G.; Weier, T.; Schäfer, P.; Hess, A.; Bund, A.; Fröhlich, J.
Numerical and experimental results on copper electrolysis in homogeneous and inhomogeneous magnetic fields
International Conference on Magneto Science, 26.-29.10.2009, Nijmegen, Niederlande

Nikrityuk, Petr A.; Eckert, K.; Eckert, S.
Solidification of a binary metal alloy in a turbulent melt flow driven by AC fields
6th International Symposium on Turbulence, Heat and Mass Transfer, 14.-18.09.2009, Rome, Italy

Pal, J.; Röder, M.; Cramer, A.; Gerbeth, G.
Electromagnetic control of local temperature gradients in a Czochralski crystal growth model
Electromagnetic Processing of Materials (EPM), 19.-23.10.2009, Dresden, Deutschland

Pätzold, O.; Lantzsch, R.; Greif, A.; Galindo, V.; Grants, I.; Gerbeth, G.; Stelter, M.
Melt flow stabilisation in bulk crystal growth by means of external magnetic fields
6th International Conference on Electromagnetic Processing of Materials (EPM 2009), 19.-23.10.2009, Dresden, Germany

Pedchenko, A.; Bojarevics, A.; Priede, J.; Gerbeth, G.; Hermann, R.
Model experiments on the melt flow driven by a two-phase inductor
6th International Conference on Electromagnetic Processing of Materials (EPM 2009), 19.-23.10.2009, Dresden, Deutschland

Post Guillen, D.; Shelley, Jonathan K.; Antal, Steven P.; Tselishcheva, Elena A.; Podowski, Michael Z.; Lucas, D.; Beyer, M.
Optimization of a two-fluid hydrodynamic model of churn turbulent flow
17th International Conference on Nuclear Engineering ICONE 17, 12.-16.07.2009, Brussels, Belgium

Räbiger, D.; Eckert, S.; Gerbeth, G.
Liquid metal flow in a cylinder during the spin-up of a rotating magnetic field
EPM 2009, 6th International Conference on Electromagnetic Processing of Materials, 20.-22.10.2009, Dresden, Germany

Räbiger, D.; Metan, V.; Leonhardt, M.; Eigenfeld, K.; Eckert, S.
Grain refinement in Al-Si Alloys by inoculation and electromagnetic stirring
EPM 2009, 6th International Conference on Electromagnetic Processing of Materials, 20.-22.10.2009, Dresden, Germany

Räbiger, D.; Nikrityuk, P. A.; Leonhardt, M.; Eckert, S.; Eckert, K.
Electromagnetic flow control during solidification of AlSi-alloys using time-modulated AC magnetic fields
EPM 2009, 6th International Conference on Electromagnetic Processing of Materials, 20.-22.10.2009, Dresden, Germany

Rindelhardt, U.
Beispielhafte Wasserkraftnutzung an der Saale: Entwicklung, Stand und Perspektiven
Dresdner Wasserbaukolloquium 2009, 12.-13.03.2009, Dresden, Deutschland

Rindelhardt, U.; Dietrich, A.; Rösner, C.
Tracked megawatt PV plants: Operation results 2008 in Germany and Spain
24th European Photovoltaic Solar Energy Conference and Exhibition, 21.-25.09.2009, Hamburg, Deutschland

Rindelhardt, U.; Schuhknecht, J.; Viehrig, H.-W.
Beltline welding seam and base metal investigations of a WWER-440/230 reactor pressure vessel from the former Greifswald NPP
6th International Scientific and Technical Conference "Safety Assurance of NPP with WWER", 26.-29.05.2009, Podolsk, Russian Federation

Rodriguez, I. H.; Yamaguti, H. K. B.; de Castro, M. S.; Da Silva, M. J.; Rodriguez, O. M. H.
Investigation on drag reduction phenomenon in oil-water dispersed pipe flow via wire-mesh sensor
20th International Congress of Mechanical Engineering, 15.-20.11.2009, Gramado, Brazil

Rohde, U.; Mittag, S.; Grundmann, U.; Petkov, P.; Hadek, J.
Application of a step-wise verification and validation procedure to the 3D neutron kinetics code DYN3D within the European NURESIM project
17th International Conference on Nuclear Engineering ICONE17, 12.-17.07.2009, Brussels, Belgium

Schmidtke, M.; Danciu, D.
Blasenmitriss durch Impinging Jets
Jahrestreffen der Fachausschüsse Mehrphasenströmungen und Wärme- und Stoffübertragung, 03.-05.03.2009, Bad Dürkheim, Deutschland

Schmidtke, M.; Danciu, D.
Empirical and numerical studies on gas entrainment by impinging jets
Jahrestagung Kerntechnik 2009, Beitrag 215, 12.-14.05.2009, Dresden, Deutschland

Schmidtke, Martin; Danciu, D.; Lucas, D.
Air entrainment by impinging jets. Experimental identification of the key phenomena and approaches for their modelling.
17th International Conference on Nuclear Engineering ICONE 17, 12.-16.07.2009, Brussels, Belgium

Schubert, M.
Hydrodynamische Untersuchungen in Festbettreaktoren mit Gittersensoren
Seminar "Sensoranwendung in der Chemieindustrie" der BASF Ludwigshafen, 14.10.2009, Ludwigshafen, Germany

Schubert, M.; Da Silva, M. J.; Kryk, H.
Hydrodynamic studies in trickle bed reactors using wire mesh sensors
Workshop on Multi-Phase Flows: Simulation, Experiment and Application, 26.-28.05.2009, Dresden, Deutschland

Schubert, M.; Hamidipour, M.; Duchesne, C.; Larachi, F.
Hydrodynamic effects of inclination angle on co-current gas-liquid packed beds
9th International Conference on Gas-Liquid, Liquid-Solid, Gas-Liquid-Solid Reactor Engineering, GLS-9, 23.-27.08.2009, Montreal, Canada

Schubert, M.; Schäfer, T.; Da Silva, M. J.; Thiele, S.; Hessel, G.; Kryk, H.; Hampel, U.
Measurement of hydrodynamic non-uniformities and their dynamics in porous particle packings using capacitance wire-mesh sensors
9th International Conference on Gas-Liquid, Liquid-Solid, Gas-Liquid-Solid Reactor Engineering, GLS-9, 23.-27.08.2009, Montreal, Canada

Schuhknecht, J.; Rindelhardt, U.; Viehrig, H.-W.
Investigations of the beltline welding seam and base metal of a WWER-440 first generation reactor pressure vessel from the former Greifswald NPP
Structural Integrity and Life of NPP Equipment: SIL 2009, 20.-22.05.2009, Kiev, Ukraine

Schuhknecht, J.; Viehrig, H.-W.; Rindelhardt, U.
Investigation of the beltline welding seam and base metal of the Greifswald WWER-440 Unit 1 reactor pressure vessel
Proceedings of the 17th International Conference on Nuclear Engineering ICONE17 July 12-16, 2009, Brussels, Belgium, 12.07.2009, Brussels, Belgium

Shatrov, V.; Gerbeth, G.
Marginally turbulent MHD flow in a square duct
6th International Conference on Electromagnetic Processing of Materials (EPM 2009), 19.-23.10.2009, Dresden, Deutschland

Shirai, K.; Voigt, A.; Neumann, M.; Büttner, L.; Czarske, J.; Cierpka, C.; Weier, T.; Gerbeth, G.
Experimental investigation of Lorentz-force controlled flat-plate boundary layer with a laser Doppler velocity profile sensor
6th International Symposium on Turbulence and Shear Flow Phenomena (TSFP6), 22.-24.05.2009, Seoul, Korea

Stefani, F.
Liquid metal experiments on cosmic magnetic fields
Ultra-high Energy Cosmic Rays and Magnetic Fields in the Universe, 11.-14.02.2009, Tegernsee, Germany

Stefani, F.
Liquid metal experiments on dynamo action and magnetic instabilities
Frontiers in Dynamo Theory, 16.-20.03.2009, Paris, France

Stefani, F.
Liquid metal experiments on helical MRI
The Astrophysics of the Magnetorotational Instability and Related Processes, 14.-18.04.2009, Tegernsee, Germany

Stefani, F.
Wie man schwarze Löcher füttert - Theorien und Experimente zur Magnetorotationsinstabilität
Physikalisches Kolloquium, 23.06.2009, Ilmenau, Deutschland

Stefani, F.; Fischer, M.; Gerbeth, G.; Giesecke, A.
Inferring parameters of the geodynamo from temporal reversal characteristics
Natural Dynamos, 30.08.-05.09.2009, Stara Lesna, Slovakia

Stefani, F.; Gerbeth, G.; Gundrum, T.; Hollerbach, R.; Kirillov, O.; Priede, J.; Rüdiger, G.; Szklarski, J.
PROMISEs, fulfillments, and prospects
12th MHD Days, 08.-09.12.2009, Potsdam, Germany

Stefani, F.; Gerbeth, G.; Gundrum, T.; Hollerbach, R.; Priede, J.; Rüdiger, G.; Szklarski, J.
Liquid metal experiments on the magnetorotational instability in a Taylor-Couette flow
Natural dynamos, 30.08.-05.09.2009, Stara Lesna, Slovakia

Szalinski, L.; Da Silva, M. J.; Thiele, S.; Beyer, M.; Lucas, D.; Hampel, U.; Hernandez Perez, V.; Abdulkareem, L. A.; Azzopardi, B. J.
Comparative study of gas-oil and gas-water two-phase flow in a vertical pipe
3rd International Workshop on Process Tomography (IWPT-3), 17.-19.04.2009, Tokyo, Japan

Terzija, N.; Yin, W.; Gerbeth, G.; Stefani, F.; Timmel, K.; Wondrak, T.; Peyton, A.
Electromagnetic inspection of a two-phase GaInSn/Argon flow
6th International Conference on Electromagnetic Processing of Materials (EPM), 19.-23.10.2009, Dresden, Germany

Teschendorff, V.; Glaeser, H.; Kliem, S.
Bedeutung von Experimenten für die Reaktorsicherheit
Jahrestagung Kerntechnik 2009, 12.-14.05.2009, Dresden, Deutschland

Thiele, S.; Schöne, S.; Voigt, F.; Da Silva, M. J.; Hampel, U.
Design of a neutrally buoyant self-powered multi-parameter sensor for data logging in flow applications
IEEE SENSORS 2009 Conference, 25.-28.10.2009, Christchurch, New Zealand

Thiele, S.; Schöne, S.; Voigt, F.; Da Silva, M. J.; Hampel, U.
Entwicklung eines auftriebsneutralen autarken Multi-Parameter-Sensors zur Datenerhebung in Flüssigkeitsströmungen
9. Dresdner Sensor-Symposium, 07.-09.12.2009, Dresden, Deutschland

Timmel, K.; Eckert, S.; Gerbeth, G.; Claussner, J.; Schlenk, R.; Voigtländer, J.
CONCAST: A liquid metal model for continuous steel casting
6th International Conference on Electromagnetic Processing of Materials, 19.-23.10.2009, Dresden, Deutschland

Timmel, K.; Galindo, V.; Miao, X.; Eckert, S.; Gerbeth, G.
CONCAST – a liquid metal experimental facility for modeling the continuous casting process of steel
3rd International Conference on Simulation and Modelling of Metallurgical Processes in Steelmaking, 08.-10.09.2009, Leoben, Austria

Timmel, K.; Galindo, V.; Miao, X.; Eckert, S.; Gerbeth, G.
Flow investigations in an isothermal liquid metal model of the continuous casting process
6th International Conference on Electromagnetic Processing of Materials, 19.-23.10.2009, Dresden, Deutschland

Tselishcheva, E. A.; Antal, Steven P.; Podowski, M. Z.; Post Guillen, D.; Beyer, M.; Lucas, D.
Development and validation of a Multifield Model of churn-turbulent gas/liquid flows
17th International Conference on Nuclear Engineering (ICONE-17), 12.-16.07.2009, Brussels, Belgium

Tusheva, P.; Reinke, N.; Altstadt, E.; Schaefer, F.; Weiss, F.-P.; Hurtado, A.
Analysis of severe accidents in VVER-1000 reactors using the integral code ASTEC
17th International Conference on Nuclear Engineering ICONE17, 12.-16.07.2009, Brussels, Belgium

Tusheva, P.; Schaefer, F.; Reinke, N.; Rohde, U.
Investigation on accident management measures for VVER-1000 Reactors
19th AER SYMPOSIUM on VVER Reactor Physics and Reactor Safety, 21.-25.09.2009, St. St. Constantine and Elena resort, Bulgaria

Ulbricht, A.; Bergner, F.; Heintze, C.
SANS investigation of irradiation-induced phase separation in a binary Fe-Cr alloy
TMS 2009, Symposium Material Characterization: Microstructural Processes in Irradiated Materials, 15.-19.02.2009, San Francisco, USA

Ulbricht, A.; Heintze, C.; Bergner, F.; Eckerlebe, H.
SANS investigation of neutron-irradiated Fe-Cr alloys
XIV International Conference on Small-Angle Scattering, 13.-18.09.2009, Oxford, United Kingdom

Vallee, C.; Seidel, T.; Lucas, D.
TOPFLOW hot leg model experiments: Overview, examples, status of data analysis and future work
15th Meeting of the German CFD Network, 21.-22.01.2009, Garching, Germany

Vallee, C.; Seidel, T.; Lucas, D.; Beyer, M.; Prasser, H.-M.
TOPFLOW experiments on counter-current flow limitation in a model of the hot leg of a PWR
NURISP open General Seminar, 30.11.-01.12.2009, Dresden, Germany

Vallee, C.; Seidel, T.; Lucas, D.; Beyer, M.; Prasser, H.-M.; Pietruske, H.; Schütz, P.; Carl, H.
Comparison of air/water and steam/water flooding experiments in a model of the hot leg of a pressurised water reactor
Jahrestagung Kerntechnik 2009, 12.-14.05.2009, Dresden, Germany

Vallee, C.; Seidel, T.; Lucas, D.; Beyer, M.; Prasser, H.-M.; Pietruske, H.; Schütz, P.; Carl, H.
Influence of the fluid properties on co-current two-phase flows in a horizontal channel connected to a riser
ExHFT-7 - 7th World Conference on Experimental Heat Transfer, Fluid Mechanics and Thermodynamics, 28.06.-03.07.2009, Krakow, Poland

Vallee, C.; Seidel, T.; Lucas, D.; Beyer, M.; Prasser, H.-M.; Pietruske, H.; Schütz, P.; Carl, H.
Counter-current flow limitation experiments in a model of the hot leg of a pressurised water reactor – comparison between high pressure steam/water experiments and low pressure air/water experiments
13th International Topical Meeting on Nuclear Reactor Thermal Hydraulics (NURETH-13), 27.09.-02.10.2009, Kanazawa, Japan

Viehrig, H.-W.; Lucon, E.; Server, William L.
IAEA coordinated research project on Master Curve approach to monitor fracture toughness of RPV steels: effect of loading rate
2009 ASME Pressure Vessels and Piping Division Conference, 26.-30.07.2009, Prague, Czech Republic

Viehrig, H.-W.; Schuhknecht, J.
Fracture mechanics characterisation of the WWER-440 reactor pressure vessel beltline welding seam of Greifswald unit 8
Jahrestagung Kerntechnik 2009, 12.-14.05.2009, Dresden, Deutschland

Viehrig, H.-W.; Schuhknecht, J.
Fracture mechanics characterization of Russian WWER type reactor pressure vessel welding seams
12th International Conference on Fracture, 12.-17.07.2009, Ottawa, Kanada

Weier, T.; Gerbeth, G.
Lorentz force driven rotating flows in electrochemical systems
International Conference on Magneto Science, 26.-29.10.2009, Nijmegen, Niederlande

Wondrak, T.; Galindo, V.; Gerbeth, G.; Gundrum, T.; Stefani, F.; Timmel, K.
Application of contactless inductive flow tomography to the continuous casting process
6th International Conference on Electromagnetic Processing of Materials (EPM), 19.-23.10.2009, Dresden, Germany

Wondrak, T.; Galindo, V.; Gerbeth, G.; Gundrum, T.; Stefani, F.; Timmel, K.
Applying contactless inductive flow tomography to a continuous casting model
12th MHD Days, 08.-9.12.2009, Potsdam, Germany

Wondrak, T.; Stefani, F.; Gundrum, T.; Gerbeth, G.
Recent progress on contactless inductive flow tomography
80th Annual Meeting of the International Association of Applied Mathematics and Mechanics (GAMM), 09.-13.2.2009, Gdansk, Poland

Zhang, C.; Eckert, S.; Gebeth, G.
Investigation of a bubble-driven liquid metal flow under the influence of a travelling magnetic field
6th International Conference on Electromagnetic Processing of Materials (EPM 2009), 19.-23.10.2009, Dresden, Germany

Zurbuchen, C.
Influence of specimen type, crack length and evaluation method on quasi-static and dynamic fracture toughness properties
2009 ASME Pressure Vessels and Piping Division Conference, 26.-30.07.2009, Prag, Czech Republic

Contributions to proceedings and other collected editions

Abdulkareem, L. A.; Hernandez-Perez, V.; Azzopardi, B. J.; Sharaf, S.; Thiele, S.; Da Silva, M. J.
Comparison of different tools to study gas-liquid flow
7th World Conference on Experimental Heat Transfer, Fluid Mechanics and Thermodynamics, 28.06.-03.07.2009, Krakow, Poland
Proceedings of ExHFT-7, Krakow: AGH University of Science and Technology Press, 978-83-7464-235-4, 785-792

Abdulkareem, L. A.; J. Azzopardi, B.; Thiele, S.; Hunt, A.; Da Silva, M. J.
Interrogation of gas/oil flow in a vertical pipe using two tomographic techniques
OMAE 2009, 31.05.-05.06.2009, Honolulu, USA
Proceedings of the ASME 28th International Conference on Ocean, Offshore and Arctic Engineering, 79840

Albrecht, T.; Marlow, F.; Metzkes, H.; Stiller, J.
DNS and LES of separation control using oscillating Lorentz forces
6th International Conference on Electromagnetic Processing of Materials, 19.-23.10.2009, Dresden, Deutschland, pp. 688-691

Azzopardi, B. J.; Abdulkareem, L. A.; Zhao, D.; Thiele, S.; Da Silva, M. J.; Beyer, M.; Hunt, A.
Comparison between electrical capacitance tomography and wire mesh sensor output for air/silicone oil flow in a vertical pipe
3rd International Workshop on Process Tomography, 17.-19.04.2009, Tokyo, Japan
Proceedings of 3rd International Workshop on Process Tomography

Bestion, D.; Lucas, D.; Boucker, M.; Anglart, H.; Tiselj, I.; Bartosiewicz, Y.
Some lessons learned from the use of two-phase CFD for nuclear reactor thermalhydraulics
The 13th International Topical Meeting on Nuclear Reactor Thermal Hydraulics (NURETH-13), 27.09.-02.10.2009, Kanazawa, Japan
Proceedings of the 13th International Topical Meeting on Nuclear Reactor Thermal Hydraulics (NURETH-13), Paper N13P1139

Bieberle, M.; Hampel, U.; Schleicher, E.; Fischer, F.; Koch, D.; Mayer, H.-G.; Menz, H.-J.
Experimental two-phase flow measurements using two-plane limited-angle electron beam x-ray CT and wire-mesh sensor
3rd International Workshop on Process Tomography (IWPT-3), 15.-17.04.2009, Tokyo, Japan, IWPT 3, Nr 77

Bilodid, Y.; Mittag, S.
Spectral-history modeling in DYN3D burnup calculations
Jahrestagung Kerntechnik 2009, 12.-14.05.2009, Dresden, Germany

Boden, S.; Eckert, S.; Gerbeth, G.; Simonnet, M.; Anderhuber, M.; Gardin, P.
X-ray visualisation of bubble formation and bubble motion in liquid metals
6th International Conference on Electromagnetic Processing of Materials (EPM 2009), 19.-23.10.2009, Dresden, Deutschland, 387-390

Boden, S.; Willers, B.; Eckert, S.; Gerbeth, G.
X-ray visualisation of solidifying GaIn-alloys in the presence of melt convection
6th International Conference on Electromagnetic Processing of Materials (EPM 2009), 19.-23.10.2009, Dresden, Deutschland, 261-264

Borodkin, G.; Khrennikov, N.; Konheiser, J.; Noack, K.
Neutron dosimetry study in the region of the support structure of a VVER-1000 type reactor
13th International Symposium on Reactor Dosimetry, 25.-31.05.2008, Alkmaar, Netherlands Reactor Dosimetry State of the Art 2008, New Jersey London Singapore: World Scientific Publishing Co. Pte. Ltd., 13 978-981-4271-10-3, 688-699

Borodkin, P.; Borodkin, G.; Khrennikov, N.; Konheiser, J.; Noack, K.
Neutron dosimetry on the full-core first generation VVER-440 aimed at reactor support structure load evaluation
13th International Symposium on Reactor Dosimetry, 25.-31.05.2008, Alkmaar, Netherlands Reactor Dosimetry State of the Art 2008, New Jersey London Singapore: World Scientific Publishing Co. Pte. Ltd., 13 978-981-4271-10-3, 300-309

Buchenau, D.; Gerbeth, G.; Priede, J.
Comparison of various contactless flow rate sensors
6th Int. Conf. on Electromagnetic Processing of Materials, 19.-23.10.2009, Dresden, BRD, pp. 383-386

Cartland Glover, G. M.; Krepper, E.; Weiss, F.-P.; Zacharias, F.; Kratzsch, A.; Alt, S.; Kaestner, W.
Hydrodynamic modeling of mineral wool fiber suspensions in a two-dimensional channel flow
The 13th International Meeting on Nuclear Reactor Thermal Hydraulics (NURETH-13), 27.09.-02.10.2009, Kanazawa, Japan
Proceedings of 13th International Meeting on Nuclear Reactor Thermal Hydraulics (NURETH-13)

Cartland Glover, Gregory M.; Grahn, A.; Krepper, E.; Weiss, F.-P.; Alt, S.; Hampel, R.; Kaestner, W.; Kratzsch, A.; Zacharias, F.
Hydrodynamic modeling of mineral wool fiber suspensions in a two-dimensional flow
17th International Conference on Nuclear Engineering, 12.-16.07.2009, Brussels, Belgium
Proceedings of ICONE17 17th International Conference on Nuclear Engineering

Cheung, C. P.; Yeoh, G. H.; Tu, J. Y.; Krepper, E.; Lucas, D.
Numerical study on population balance approaches in modeling of isothermal vertical bubbly flows
The 5th International Conference on Computational Fluid Dynamics, ICCFD5, 07.-11.07.2008, Seoul, Korea

Cheung, Sherman C. P.; Duan, X.; Yeoh, Guan H.; Tu, J.; Krepper, E.; Lucas, D.
Modelling of polydispersed flows using two population balance approaches
6th International Symposium on Multiphase Flow, Heat Mass Transfer and Energy Conversion, 11.-15.07.2009, Xi'an, China

Cramer, A.; Pal, J.; Gundrum, Th.; Gerbeth, G.
MULTIMAG - A MULTIpurpose MAGnetic field system for EPM
Electromagnetic Processing of Materials (EPM), 19.-23.10.2009, Dresden, Deutschland
MULTIMAG - A MULTIpurpose MAGnetic field system for EPM, 9783936104653, 826-829

Cramer, A.; Zhang, X.; Gerbeth, G.
Thermoelectromagnetic convection - an alternative stirring technique in metallurgy
International Symposium on Liquid Metal Processing and Casting, 20.-23.09.2009, Santa Fe, New Mexico, 978-0-87339-743-8

Cramer, A.; Zhang, X.; Gerbeth, G.
Model experiments on thermo-electromagnetic convection
6th International Conference on Electromagnetic Processing of Materials EPM 2009, 19.-23.10.2003, Dresden, Deutschland,
wie Konferenztitel, 978-3-936104-65-3, 94-97

Cramer, A.; Zhang, X.; Gerbeth, G.
Thermoelectromagnetic stirring in Metallurgy
54th IWK – Internationales Wissenschaftliches Kolloquium, 07.-11.09.2009, Ilmenau, Germany
"Thermoelectromagnetic Stirring in Metallurgy", Ilmenau: ISLE, 978-3-938843-45-1

Da Silva, M. J.; Hampel, U.
Kapazitäts-Gittersensor: Prinzip und Anwendung
XXIII. Messtechnisches Symposium des Arbeitskreises der Hochschullehrer für Messtechnik e.V., 17.-19.09.2009, Bremen, Deutschland
Tagungsband XXIII. Messtechnisches Symposium des AHMT, Gert Goch (Hrsg.), Aachen: Shaker Verlag, 978-3-8322-8491-6, 139-148

Da Silva, M. J.; Schleicher, E.; Hampel, U.
Advanced wire-mesh sensor technology for fast flow imaging
2009 IEEE International Workshop on Imaging Systems & Techniques, 11.-12.05.2009, Shenzhen, China
Proceedings of IEEE International Workshop on Imaging Systems & Techniques 2009: IEEE, 978-1-4244-3483-1, 253-256

Da Silva, M. J.; Thiele, S.; Schleicher, E.; Hampel, U.
Wire-mesh sensors for fast visualization of multiphase flows
What Where When Multi-dimensional Advances for Industrial Process Monitoring, 23.-24.06.2009, Leeds, United Kingdom
Proceedings of W3MDM 2009, 98-108

Da Silva, M. J.; Thiele, S.; Schleicher, E.; Hampel, U.
Wire-mesh sensors for high-resolution gas-liquid multiphase flow visualization
20th International Congress of Mechanical Engineering, 15.-20.11.2009, Gramado, Brazil
Proceedings of COBEM 2009, Paper No. COB09-2457, 2176-5480

Danciu, D. V.; Da Silva, M. J.; Schmidtke, M.; Lucas, D.
Experimental investigations on air entrainment by means of impinging jets
ExHFT-7, 7th World Conference on Experimental Heat Transfer, Fluid Mechanics and Thermodynamics, 28.06.-03.07.2009, Krakow, Poland
ExHFT-7 7th World Conference on Experimental Heat Transfer, Fluid Mechanics and Thermodynamics 28 June - 03 July 2009, Krakow, Poland Proceedings, ISBN 978-83-7464-235-4, 761-768

Danciu, D. V.; Da Silva, M. J.; Schmidtke, M.; Lucas, D.; Hampel, U.
Experimental investigation on air entrainment below impinging jets by means of video observations and image processing
Multiphase Flow 2009 Fifth International Conference on Computational and Experimental Methods in Multiphase and Complex Flow, 15.-17.06.2009, New Forest, England Computational Methods in Multiphase Flow V: WIT Press, ISSN 1743-3533, 481-491

Duan, X.; Cheung, Sherman C. P.; Yeoh, Guan H.; Tu, J.; Krepper, E.; Lucas, D.
An overall assessment of abnd model for large-scale bubbly flows
7th International Conference on CFD in the Minerals and Process Industries CSIRO, Melbourne, Australia, 09.-11.12.2009, Melbourne, Australia

Fischer, F.; Hampel, U.
Ultra fast electron beam X-ray CT scanner for two-phase flow measurement
Jahrestagung Kerntechnik 2009, 12.-14.05.2009, Dresden, Germany

Franke, S.; Büttner, L.; Czarske, J.; Räbiger, D.; Eckert, S.
Ultrasound Doppler array measurement system for two-dimensional flow investigations in liquid metals
6th International Conference on Electromagnetic Processing of Materials (EPM 2009), 19.-23.10.2009, Dresden, Deutschland, 978-3-936104-65-3, 411-414

Fridman, E.; Shwageraus, E.
HTGR Fuel Element Depletion Benchmark: Stage One Results
2009 ANS Winter Meeting, 15.-19.11.2009, Washington, DC Omni Shoreham Hotel, USA

Fridman, E.; Shwageraus, E.; Volaski, D.
Investigation of fuel assembly design options for high conversion thorium fuel cycle in PWRs
Advances in Nuclear Fuel Management IV, 12.-15.04.2009, Hilton Head Island, South Carolina, USA

Fridman, E.; Volaski, D.; Shwageraus, E.
Thermal design feasibility of Th-233U PWR breeder
GLOBAL 2009, 06.-11.09.2009, Paris, France
Thermal design feasibility of Th-233U PWR breeder

Grahn, A.; Krepper, E.; Weiß, F.-P.; Alt, S.; Kästner, W.; Kratzsch, A.; Hampel, R.
Implementation of a pressure drop model for the CFD simulation of clogged containment sump strainers
17th International Conference On Nuclear Engineering ICONE 17, 12.-16.07.2009, Brussels, Belgium
Implementation of a pressure drop model for the CFD simulation of clogged containment sump strainers

Grants, I.; Klyukin, A.; Gerbeth, G.
Flow stability in magnetically manipulated vertical gradient freeze
6th International Conference on Electromagnetic Processing of Materials (EPM 2009), 19.-23.10.2009, Dresden, Deutschland, pp. 869-872

Grants, I.; Zhang, C.; Eckert, S.; Gerbeth, G.
Liquid metal tornado
6th International Conference on Electromagnetic Processing of Materials (EPM 2009), 19.-23.10.2009, Dresden, Deutschland, 978-3-936104-65-3, 102-105

Hádek, J.; Mittag, S.
Validation of DYN3D pin-power calculation against experimental VVER-full-core benchmark
International Conference on Mathematics, Computational Methods & Reactor Physics (M&C 2009), 03.-07.05.2009, Saratoga Springs, New York, USA
Proceedings on CDROM: paper 200483, La Grange Park, USA: ANS

Hampel, U.; Fischer, F.
Application of CdTe and CZT detectors in ultra fast electron beam X-ray tomography
IEEE - Workshop on X-Ray Micro Imaging of Materials, Devices, and Organisms, 22.-24.10.2008, Dresden, Germany
IEEE NSS/MIC/RTSD Conference Record

Hampel, U.; Fischer, F.
Ultra fast electron beam x-ray tomography and its application to multi phase flow measurement
IEEE Dresden 2008 - Workshop on X-Ray Micro Imaging of Materials, Devices, and Organisms, 22.-24.10.2008, Dresden, Germany
IEEE NSS/MIC/RTSD Conference Record

Hampel, U.; Fischer, F.
Process tomography with electron beams
What, Where, When: Multi-dimensional Advances for Industrial Process Monitoring International Symposium, 23.-24.06.2009, Leeds, UK
Proceedings, Paper #5

Hampel, U.; Fischer, F.
Ultra high speed electron beam tomography for flow measurement and small animal imaging
2009 IEEE International Workshop on Imaging Systems and Techniques (IST 2009), 11.-12.05.2009, Shenzhen, China
Proceedings of IEEE International Workshop on Imaging Systems and Techniques 2009 (IST 2009): IEEE Publishing, 978-1-4244-3483-1, 1-5

Hampel, U.; Fischer, F.; Bergmann, R.
Electron beam CT – a potential tool for small animal imaging ?
2008 Nuclear Science Symposium, Medical Imaging Conference and 16th Room Temperature Semiconductor Detector Workshop, 19.-25.10.2008, Dresden, Germany
IEEE NSS/MIC/RTSD Conference Record

Hampel, U.; Kiessling, N.; Bieberle, A.
Application of GATE to detector optimisation in transmission gamma ray tomography
2008 Nuclear Science Symposium, Medical Imaging Conference and 16th Room Temperature Semiconductor Detector Workshop, 19.-25.10.2008, Dresden, Germany
IEEE NSS/MIC/RTSD Conference Record

Hermann, R.; Behr, G.; Gerbeth, G.; Priede, J.; Guguschev, Ch.; Krauze, A.; Büchner, B.
Single crystal growth of intermetallic compounds by a two-phase RF floating zone method
6th International Conference on Electromagnetic Processing of Materials (EPM 2009), 19.-23.10.2009, Dresden, Deutschland, pp. 849-852

Höhne, T.; Rohde, U.; Melideo, D.; Moretti, F.; D'Auria, F.; Shishov, A.; Lisenkov, E.
Experimental and numerical analysis of coolant mixing in VVER-1000 in the framework of TACIS project R2.02/02
Jahrestagung Kerntechnik 2009, 12.-14.05.2009, Dresden, Deutschland
CD-ROM

Höhne, T.; Vallee, C.
Modelling of stratified two phase flows using an interfacial area density model
Fifth International Conference on Computational and Experimental Methods in Multiphase and Complex Flow, 15.-17.06.2009, New Forest, Großbritannien
CD-ROM

Höhne, T.; Vallee, C.
Numerical prediction of horizontal two phase flow using an interfacial area density model
The 13th International Topical Meeting on Nuclear Reactor Thermal Hydraulics (NURETH-13), 27.09.-02.10.2009, Kanazawa City, Japan
CD-ROM

Höhne, T.; Vallee, C.
Experiments and numerical simulations of horizontal two phase flow regimes
Seventh International Conference on CFD in the Minerals and Process Industries, 09.-12.12.2009, Melbourne, Australia
CD-ROM

Kliem, S.
AER working group D on VVER safety analysis – report of the 2009 meeting
19th Symposium of AER on VVER Reactor Physics and Reactor Safety, 21.-25.09.2009,
Varna, Bulgarien
Proceedings of the 19th Symposium of AER on VVER Reactor Physics and Reactor Safety,
Budapest: KFKI AEKI, 9789633726402, 523-529

Kliem, S.; Höhne, T.; Rohde, U.; Bykov, M.; Lisenkov, E.
Comparative evaluation of coolant mixing experiments at the ROCOM and the
Gidropress test facilities
6th International Conference "Safety Assurance of NPP with WWER", 26.-29.05.2009,
Podolsk, Russland
Proc. of the 6th International Conference "Safety Assurance of NPP with WWER", CDROM,
paper 008, Podolsk: OKB Gidropress Podolsk, 9785948830926

Kliem, S.; Mittag, S.; Rohde, U.; Weiß, F.-P.
Influence of the neutron-kinetic feedback parameter variation on an anticipated
transient without SCRAM in a PWR
2009 International Conference on Advances in Mathematics, Computational Methods, and
Reactor Physics, 03.-07.05.2009, Saratoga Springs, USA
Proceedings of the 2009 International Conference on Advances in Mathematics,
Computational Methods, and Reactor Physics, CDROM paper 201661, La Grange Park:
ANS, 9780894480690

Kliem, S.; Mittag, S.; Rohde, U.; Weiß, F.-P.
Influence of system and neutron-kinetic parameter variations on an anticipated
transient without SCRAM in a PWR
17th International Conference on Nuclear Engineering, 12.-16.07.2009, Brussels, Belgium
Proceedings of the 17th International Conference on Nuclear Engineering, CDROM, paper
75569: ASME

Kliem, S.; Mittag, S.; Rohde, U.; Weiß, F.-P.; Kozmenkov, Y.
The influence of different thermal hydraulic models on the results of a DYN3D boron
dilution transient calculation
Jahrestagung Kerntechnik 2009, 12.-14.05.2009, Dresden, Deutschland
Tagungsband der Jahrestagung Kerntechnik 2009, paper 114, Berlin: INFORUM GmbH

Konheiser, J.; Mittag, S.; Noack, K.; Rindelhardt, U.; Borodkin, G.; Borodkin, P.;
Gleisberg, B.
Retrospective dosimetry study at the RPV of NPP Greifswald unit 1
13th International Symposium on Reactor Dosimetry, 25.-31.05.2008, JRC Petten,
Netherlands
Reactor Dosimetry State of the Art 2008, New Jersey London Singapore: World Scientific
Publishing Co. Pte. Ltd., 13 978-981-4271-10-3, 23-33

Kotlyar, D.; Fridman, E.; Shwageraus, E.
Coupled neutronic thermo-hydraulic analysis of full PWR core with BGCore system
Jahrestagung Kerntechnik 2009, 12.-14.05.2009, Dresden, Deutschland

Krepper, E.
ANNEX XI: SWR 1000
J. Cleveland, J.H. Choi: Passive Safety Systems and Natural Circulation in Water Cooled Nuclear Power Plants, Vienna: IAEA-TECDOC-1624, 2009, 978-92-0-111309-2

Krepper, E.; Alt, S.; Renger, S.
Influence of air entrainment on the liquid flow field caused by a plunging jet
Jahrestagung Kerntechnik 2009, 12.-14.05.2009, Dresden, Germany
Proceedings of the Annual Meeting of Nuclear Technology (CD-ROM), paper No. 220

Krepper, E.; Alt, S.; Renger, S.
Influence of air entrainment on the liquid flow field caused by a plunging jet
Nuclear Energy for New Europe 2009, 14.-17.09.2009, Bled, Slovenia

Krepper, E.; Beyer, M.
Experimental and numerical investigations of temperature stratification phenomena in passive safety systems for decay heat removal
17th International Conference on Nuclear Engineering, ICONE-17, 12.-16.07.2009, Brussels, Belgium

Laczko, G.; Böhlke, S.; Ohlmeyer, H.; Schuster, Ch.; Hurtado, A.
Die Relevanz der Borflüchtigkeit bei Langzeittransienten in einem mit Bor vergifteten Siedewasserreaktor
Jahrestagung Kerntechnik 2009, 12.-14.05.2009, Dresden, Deutschland
Tagungsband der Jahrestagung Kerntechnik 2009, paper 311, Berlin: INFORUM GmbH

Liao, Y.; Lucas, D.
Breakup and coalescence models for turbulent air-water mixtures in a vertical pipe
Jahrestagung Kerntechnik 2009, 12.-14.05.2009, Dresden, Germany

Liao, Y.; Lucas, D.
The inhomogeneous MUSIG model for upward polydisperse flows with new constitutive models for bubble coalescence and breakup
International Conference Nuclear Energy for New Europe 2009, 14.-17.09.2009, Bled, Slovenia

Liao, Y.; Lucas, D.
A new model for bubble coalescence and breakup in poly-disperse bubbly flows
The 13th International Topical Meeting on Nuclear Reactor Thermal Hydraulics (NURETH-13), 27.09.-02.10.2009, Kanazawa City, Ishikawa Prefecture, Japan

Lucas, D.; Beyer, M.; Frank, T.; Zwart, P.; Burns, A.
Condensation of Steam Bubbles Injected into Sub-Cooled Water
The 13th International Topical Meeting on Nuclear Reactor Thermal Hydraulics (NURETH-13), Paper N13P1097, 27.09.-02.10.2009, Kanazawa City, Japan

Lucas, D.; Beyer, M.; Szalinski, L.
Experimental investigations on the condensation of steam bubbles injected into sub-cooled water
5th European-Japanese Two-Phase Flow Group Meeting, 20.-25.09.2009, Spoleto, Italien

Lucas, D.; Hampel, U.; Beyer, M.; Vallée, C.; Weiß, F.-P.
Innovative experiments at the Rossendorf TOPFLOW facility for verification and validation of two-phase flow CFD Codes
Jahrestagung Kerntechnik, 12.-14.05.2009, Dresden, Deutschland

Maiwald, A.; Timmel, K.; Schwarze, R.; Gerbeth, G.
Comparison of numerical and experimental flow data from a liquid-metal model of a continuous casting mould
6th International Conference on Electromagnetic Processing of Materials (EPM 2009), 19.-23.10.2009, Dresden, Deutschland, pp. 239-242

Matusiak, B.; Da Silva, M. J.; Grudzien, K.; Hampel, U.
Capacitance wire mesh sensor and electrical capacitance tomography study of trickle-bed reactor hydrodynamics
3rd International Workshop on Process Tomography, 17.-19.04.2009, Tokyo, Japan
Proceedings of 3rd International Workshop on Process Tomography

Merk, B.
An analytical solution for an external source problem with delayed neutron using the Telegrapher's equation
2009 International Conference on Advances in Mathematics, Computational Methods, and Reactor Physics, 03.-07.05.2009, Saratoga Springs, United States

Merk, B.
On the influence of spatial discretization in LWR-burnup calculations with HELIOS 1.9
2009 International Conference on Advances in Mathematics, Computational Methods, and Reactor Physics, 03.-07.05.2009, Saratoga Springs, United States

Merk, B.
On the influence of spatial discretization on cross-sction preparation during burnup calculations with HELIOS 1.9
Jahrestagung Kerntechnik 2009, 12.-14.05.2009, Dresden, Deutschland

Merk, B.; Glivici, V.; Weiß, F. P.
A three scale expansion solution for the Telegrapher's equation with external source: development and first application
XXI International Conference on Transport Theory, 12.-17.07.2009, Torino, Italy

Merk, B.; Weiß, F. P.
On the effect of spatial discretization in integral transport calculations with HELIOS 1.9
XXI International Conference on Transport Theory, 12.-17.07.2009, Torino, Italy

Miao, X.; Galindo, V.; Lucas, D.; Gerbeth, G.; Ren, Z.
Numerical Simulation of Two-phase Flow in a Slab Mold by MUSIG Model
6th International Conference on Electromagnetic Processing of Materials (EPM 2009), 19.-23.10.2009, Dresden, Germany, 978-3-936104-65-3, 579-582

118

Mittag, S.; Kliem, S.
Burning plutonium and minimizing the radioactive waste in existing PWR
19th AER SYMPOSIUM on VVER Reactor Physics and Reactor Safety, 21.-25.09.2009, St. St. Constantine and Elena resort (Varna), Bulgaria, 363-370

Mutschke, G.; Schäfer, P.; Weier, T.; Bund, A.; Fröhlich, J.
Numerical and experimental results on Lorentz force driven flows during electrodeposition of copper in homogeneous magnetic fields
6th Int. Conf. on Electromagnetic Processing of Materials, 19.-23.10.2009, Dresden, BRD, 461-464

Pal, J.; Röder, M.; Cramer, A.; Gerbeth, G.
Electromagnetic control of local temperature gradients in a Czochralski crystal growth model
Electromagnetic Processing of Materials (EPM), 19.-23.10.2009, Dresden, Deutschland Electromagnetic control of local temperature gradients in a Czochralski crystal growth model, 9783936104653, 591-594

Pätzold, O.; Lantzsch, R.; Greif, A.; Galindo, V.; Grants, I.; Gerbeth, G.; Stelter, M.
Melt flow stabilisation in bulk crystal growth by means of external magnetic fields
6th International Conference on Electromagnetic Processing of Materials (EPM 2009), 19.-23.10.2009, Dresden, Germany, 978-3-936104-65-3, 849-862

Pedchenko, A.; Bojarevics, A.; Priede, J.; Gerbeth, G.; Hermann, R.
Model experiments on the melt flow driven by a two-phase inductor
6th International Conference on Electromagnetic Processing of Materials (EPM 2009), 19.-23.10.2009, Dresden, Deutschland, pp. 131-134

Post Guillen, D.; Shelley, Jonathan K.; Antal, Steven P.; Tselishcheva, Elena A.; Podowski, Michael Z.; Lucas, D.; Beyer, M.
Optimization of a two-fluid hydrodynamic model of churn turbulent flow
17th International Conference on Nuclear Engineering ICONE 17, 12.-16.07.2009, Brussels, Belgium
Optimization of a two-fluid hydrodynamic model of churn turbulent flow

Räbiger, D.; Eckert, S.; Gerbeth, G.
Liquid metal flow in a cylinder during the spin-up of a rotating magnetic field
EPM 2009, 6th International Conference on Electromagnetic Processing of Materials, 20.-22.10.2009, Dresden, Germany, pp. 69-72

Räbiger, D.; Metan, V.; Leonhardt, M.; Eigenfeld, K.; Eckert, S.
Grain refinement in Al-Si Alloys by inoculation and electromagnetic stirring
EPM 2009, 6th International Conference on Electromagnetic Processing of Materials, 20.-22.10.2009, Dresden, Germany, pp. 334-337

Räbiger, D.; Nikrityuk, P. A.; Leonhardt, M.; Eckert, S.; Eckert, K.
Electromagnetic flow control during solidification of AlSi-alloys using time-modulated AC magnetic fields
EPM 2009, 6th International Conference on Electromagnetic Processing of Materials, 20.-22.10.2009, Dresden, Germany, pp. 624-627

Rindelhardt, U.
Beispielhafte Wasserkraftnutzung an der Saale: Entwicklung, Stand und Perspektiven
Dresdner Wasserbaukolloquium 2009, 12.-13.03.2009, Dresden, Deutschland
Dresdner Wasserbauliche Mitteilungen Heft 39: Wasserkraftnutzung im Zeichen des
Klimawandels, Dresden: Selbstverlag TU Dresden, 978-3-86780-101-0, 163-172

Rindelhardt, U.; Dietrich, A.; Rösner, C.
Tracked megawatt PV plants: Operation results 2008 in Germany and Spain
24th European Photovoltaic Solar Energy Conference and Exhibition, 21.-25.09.2009,
Hamburg, Deutschland
Proceedings CD-ROM, contribution 5AO.8.5, 3-936338-25-6

Rindelhardt, U.; Schuhknecht, J.; Viehrig, H.-W.
Beltline welding seam and base metal investigations of a WWER-440/230 reactor
pressure vessel from the former Greifswald NPP
6th International Scientific and Technical Conference "Safety Assurance of NPP with
WWER", 26.-29.05.2009, Podolsk, Russian Federation
Conference CD, Podolsk

Rodriguez, I. H.; Yamaguti, H. K. B.; de Castro, M. S.; Da Silva, M. J.; Rodriguez, O. M. H.
Investigation on drag reduction phenomenon in oil-water dispersed pipe flow via wire-
mesh sensor
20th International Congress of Mechanical Engineering, 15.-20.11.2009, Gramado, Brazil
Proceedings of COBEM 2009, Paper No. COB09-0476

Rohde, U.; Mittag, S.; Grundmann, U.; Petkov, P.; Hadek, J.
Application of a step-wise verification and validation procedure to the 3D neutron
kinetics code DYN3D within the European NURESIM project
17th International Conference on Nuclear Engineering ICONE-17, 12.-16.07.2009, Brussels,
Belgium
CD-ROM paper 75446

Schmidtke, M.; Danciu, D.
Empirical and numerical studies on gas entrainment by impinging jets
Jahrestagung Kerntechnik 2009, 12.-14.05.2009, Dresden, Deutschland
Beitrag 215

Schmidtke, Martin; Danciu, D.; Lucas, D.
Air entrainment by impinging jets. Experimental identification of the key phenomena
and approaches for their modelling.
17th International Conference on Nuclear Engineering ICONE 17, 12.-16.7.2009, Brussels,
Belgium

Schubert, M.; Da Silva, M. J.; Kryk, H.
Hydrodynamic studies in trickle bed reactors using wire mesh sensors
Workshop on Multiphase Flows: Simulation, Experiment and Application, 26.-28.05.2009,
Dresden, Deutschland
Proceedings of "Multiphase Flows: Simulation, Experiment and Application"

Schubert, M.; Hamidipour, M.; Duchesne, C.; Larachi, F.
Hydrodynamic effects of inclination angle on co-current gas-liquid packed beds
9th International Conference on Gas-Liquid, Liquid-Solid, Gas-Liquid-Solid Reactor Engineering, GLS-9, 23.-27.08.2009, Montreal, Canada
Conference Proceedings of the 8th World Congress of Chemical Engineering

Schubert, M.; Schäfer, T.; Da Silva, M. J.; Thiele, S.; Hessel, G.; Kryk, H.; Hampel, U.
Measurement of hydrodynamic non-uniformities and their dynamics in porous particle packings using capacitance wire-mesh sensors
9th International Conference on Gas-Liquid, Liquid-Solid, Gas-Liquid-Solid Reactor Engineering, GLS-9, 23.-27.08.2009, Montreal, Canada
Conference Proceedings of the 8th World Congress of Chemical Engineering

Schuhknecht, J.; Rindelhardt, U.; Viehrig, H.-W.
Investigations of the beltline welding seam and base metal of a WWER-440 first generation reactor pressure vessel from the former Greifswald NPP
Structural Integrity and Life of NPP Equipment: SIL 2009, 20.-22.05.2009, Kiev, Ukraine
Abstracts "SIL-2009", Kiev, 978-966-02-5224-0, 10-11

Schuhknecht, J.; Viehrig, H.-W.; Rindelhardt, U.
Investigation of the beltline welding seam and base metal of the Greifswald WWER-440 Unit 1 reactor pressure vessel
Proceedings of the 17th International Conference on Nuclear Engineering ICONE 17, 12.-16.07.2009, Brussels, Belgium
Proceedings of the 17th International Conference on Nuclear Engineering, CDROM, paper 75063: ASME, 978-0-7918-3852-5

Scibetta, M.; Altstadt, E.; Sang, L. B.; Callejas, R. H.; Miura, N.; Onizawa, K.; Paffumi, E.; Serrano, M.; Tatar, L.; Yin, S.
IAEA coordinated research project on master curve approach to monitor fracture toughness of RPV steels: final results of an analytical round robin exercise to support constraint effects
2009 ASME Pressure Vessels and Piping Conference (PVP2009), 13.-17.07.2009, Prague, Czech Republic
Proceedings of the 2009 ASME Pressure Vessels and Piping Conference

Shatrov, V.; Gerbeth, G.
Marginally turbulent MHD flow in a square duct
6th International Conference on Electromagnetic Processing of Materials (EPM 2009), 19.-23.10.2009, Dresden, Deutschland, pp. 123-126

Shirai, K.; Voigt, A.; Neumann, M.; Büttner, L.; Czarske, J.; Cierpka, C.; Weier, T.; Gerbeth, G.
Experimental investigation of Lorentz-force controlled flat-plate boundary layer with a laser Doppler velocity profile sensor
6th International Symposium on Turbulence and Shear Flow Phenomena (TSFP6), 22.-24.06.2009, Seoul, Südkorea
Turbulence and Shear Flow Phenomena, Vol II, 755-760

Szalinski, L.; Da Silva, M. J.; Thiele, S.; Beyer, M.; Lucas, D.; Hampel, U.; Hernandez Perez, V.; Abdulkareem, L. A.; Azzopardi, B. J.
Comparative study of gas-oil and gas-water two-phase flow in a vertical pipe
3rd International Workshop on Process Tomography, 17.-19.04.2009, Tokyo, Japan
Proceedings of 3rd International Workshop on Process Tomography

Terzija, N.; Yin, W.; Gerbeth, G.; Stefani, F.; Timmel, K.; Wondrak, T.; Peyton, A.
Electromagnetic inspection of a two-phase GaInSn/Argon flow
6th International Conference on Electromagnetic Processing of Materials (EPM), 19.-23.10.2009, Dresden, Germany, 19.-23.10.2009, Dresden, Germany
6th International Conference on Electromagnetic Processing of Materials EPM 2009, Dresden: FZD, 978-3-936104-65-3, 391-394

Teschendorff, V.; Glaeser, H.; Kliem, S.
Bedeutung von Experimenten für die Reaktorsicherheit
Jahrestagung Kerntechnik 2009, 12.-14.05.2009, Dresden, Deutschland
Tagungsband der Jahrestagung Kerntechnik 2009; Fachsitzung: Thermohydraulische Experimente für Reaktoren der Generation II - III, Berlin: INFORUM GmbH

Thiele, S.; Schöne, S.; Voigt, F.; Da Silva, M. J.; Hampel, U.
Design of a neutrally buoyant self-powered multi-parameter sensor for data logging in flow applications
IEEE Sensors 2009 Conference, 25.-28.10.2009, Christchurch, New Zealand
IEEE Sensors 2009 Conference, Sensors 2009, 978-1-4244-5335-1

Thiele, S.; Schöne, S.; Voigt, F.; Da Silva, M. J.; Hampel, U.
Entwicklung eines auftriebsneutralen autarken Multi-Parameter-Sensors zur Datenerhebung in Flüssigkeitsströmungen
9. Dresdner Sensor-Symposium, 07.-09.12.2009, Dresden, Deutschland
9. Dresdner Sensor-Symposium, Dresden: TUDpress, Verlag der Wissenschaften GmbH, 978-3-941298-44-6, 139-142

Timmel, K.; Eckert, S.; Gerbeth, G.; Claussner, J.; Schlenk, R.; Voigtländer, J.
CONCAST: A liquid metal model for continuous steel casting
6th International Conference on Electromagnetic Processing of Materials, 19.-23.10.2009, Dresden, Deutschland, 251-254

Timmel, K.; Galindo, V.; Miao, X.; Eckert, S.; Gerbeth, G.
CONCAST – a liquid metal experimental facility for modeling the continuous casting process of steel
3rd International Conference on Simulation and Modelling of Metallurgical Processes in Steelmaking, 08.-10.09.2009, Leoben, Austria

Timmel, K.; Galindo, V.; Miao, X.; Eckert, S.; Gerbeth, G.
Flow investigations in an isothermal liquid metal model of the continuous casting process
6th International Conference on Electromagnetic Processing of Materials, 19.-23.10.2009, Dresden, Deutschland, 231-234

Tselishcheva, E. A.; Antal, Steven P.; Podowski, M. Z.; Post Guillen, D.; Beyer, M.; Lucas, D.
Development and validation of a Multifield Model of churn-turbulent gas/liquid flows
17th International Conference on Nuclear Engineering (ICONE-17), 12.-16.07.2009, Brussels, Belgium

Tusheva, P.; Reinke, N.; Altstadt, E.; Schaefer, F.; Weiss, F.-P.; Hurtado, A.
Analysis of severe accidents in VVER-1000 reactors using the integral code ASTEC
17th International Conference on Nuclear Engineering ICONE17, 12.-16.07.2009, Brussels, Belgium
Proceedings of the 17th International Conference on Nuclear Engineering ICONE17

Tusheva, P.; Schaefer, F.; Reinke, N.; Rohde, U.
Investigation on accident management measures for VVER-1000 Reactors
19th AER SYMPOSIUM on VVER Reactor Physics and Reactor Safety, 21.-25.09.2009, St. St. Constantine and Elena resort, Bulgaria
Investigation on accident management measures for VVER-1000 Reactors

Vallee, C.; Seidel, T.; Lucas, D.; Beyer, M.; Prasser, H.-M.; Pietruske, H.; Schütz, P.; Carl, H.
Comparison of air/water and steam/water flooding experiments in a model of the hot leg of a pressurised water reactor
Jahrestagung Kerntechnik 2009, 12.-14.05.2009, Dresden, Germany, Berlin: INFORUM Verlags- und Verwaltungsgesellschaft mbH, Compact221

Vallee, C.; Seidel, T.; Lucas, D.; Beyer, M.; Prasser, H.-M.; Pietruske, H.; Schütz, P.; Carl, H.
Influence of the fluid properties on co-current two-phase flows in a horizontal channel connected to a riser
ExHFT-7 - 7th World Conference on Experimental Heat Transfer, Fluid Mechanics and Thermodynamics, 28.06.-03.07.2009, Krakow, Poland, Krakow: AGH University of Science and Technology Press, 978-83-7464-235-4, 443-452

Vallee, C.; Seidel, T.; Lucas, D.; Beyer, M.; Prasser, H.-M.; Pietruske, H.; Schütz, P.; Carl, H.
Counter-current flow limitation experiments in a model of the hot leg of a pressurised water reactor – comparison between high pressure steam/water experiments and low pressure air/water experiments
13th International Topical Meeting on Nuclear Reactor Thermal Hydraulics (NURETH-13), 27.09.-02.10.2009, Kanazawa, Japan, N13P1107

Viehrig, H.-W.; Lucon, E.; Server, William L.
IAEA coordinated research project on Master Curve approach to monitor fracture toughness of RPV steels: effect of loading rate
2009 ASME Pressure Vessels and Piping Division Conference, 26.-30.07.2009, Prague, Czech Republic
Proceedings of the 2009 ASME Pressure Vessels and Piping Division Conference, New York: ASME Technical Publishing Department

Viehrig, H.-W.; Schuhknecht, J.
Fracture mechanics characterization of Russian WWER type reactor pressure vessel welding seams
12th International Conference on Fracture, 12.-17.07.2009, Ottawa, Kanada
Proceedings of the 12th International Conference on Fracture

Viehrig, H.-W.; Schuhknecht, J.
Fracture mechanics characterisation of the WWER-440 reactor pressure vessel beltline welding seam of Greifswald unit 8
Jahrestagung Kerntechnik 2009, 12.-14.05.2008, Dresden, Deutschland
Proceedings Jahrestagung Kerntechnik 2009: INFORUM GmbH

Weier, T.; Cierpka, C.; Gerbeth, G.
Coherent structure eduction from PIV data of an electromagnetically forced separated flow
IUTAM Symposium on Unsteady Separated Flows and Their Control, 18.-22.06.2007, Korfu, Greece
IUTAM Symposium on Unsteady Separated Flows and their Control

Wondrak, T.; Galindo, V.; Gerbeth, G.; Gundrum, T.; Stefani, F.; Timmel, K.
Application of contactless inductive flow tomography to the continuous casting process
6th International Conference on Electromagnetic Processing of Materials (EPM), 19.-23.10.2009, Dresden, Deutschland
Application of contactless inductive flow tomography to the continuous casting process, pp. 395-398

Wondrak, T.; Stefani, F.; Gundrum, T.; Gerbeth, G.
Recent progress on contactless inductive flow tomography
80th Annual Meeting of the International Association of Applied Mathematics and Mechanics (GAMM), 09.-13.2.2009, Gdansk, Poland

Zhang, C.; Eckert, S.; Gerebth, G.
Investigation of a bubble-driven liquid metal flow under the influence of a travelling magnetic field
6th International Conference on Electromagnetic Processing of Materials (EPM 2009), 19.-23.10.2009, Dresden, Germany, 978-3-936104-65-3, 127-130

Zurbuchen, C.
Influence of specimen type, crack length and evaluation method on quasi-static and dynamic fracture toughness properties
2009 ASME Pressure Vessels and Piping Division Conference, 26.-30.07.2009, Prag, Czech Republic
2009 Proceedings of the ASME Pressure Vessels and Piping, West Conshohocken: ASME, 9780791838549

FZD reports and other reports

Anikeev, A. V.; Bagryansky, P. A.; Prikhodko, V. V.; Soldatkina, E. I.; Tsidulko, Yu. A.; Kolesnikov, E. Yu.; Lizunov, A. A.; Noack, K.; Konheiser, J.; Berger, T.
Study of high temperature and high density plasmoids in axially symmetrical magnetic fields
Wissenschaftlich-Technische Berichte / Forschungszentrum Dresden-Rossendorf; FZD-513
2009

Bieberle, A.
Räumlich hochauflösende Computertomografie mit Gammastrahlung zur Untersuchung von Mehrphasenströmungen
Dresden: TUDPress, 2009
122 Seiten

Cierpka, C.
Zeitaufgelöste PIV-Untersuchungen zur Strömungskontrolle mittels elektromagnetischer Kräfte in schwach leitfähigen Fluiden
Wissenschaftlich-Technische Berichte / Forschungszentrum Dresden-Rossendorf; FZD-516
2009

Gerbeth, G.; Eckert, S.; Fautrelle, Y. (Editors)
Proceedings of the 6th International Conference on Electromagnetic Processing of Materials (EPM 2009)
Dresden: Eigenverlag Forschungszentrum Dresden-Rossendorf, 2009
903 Seiten
ISBN: 978-3-936104-65-3

Krepper, E.; Cartland-Glover, G.; Grahn, A.
CFD Modellierung einer partikelbelasteten Kühlmittelströmung im Sumpf und in der Kondensationskammer
Wissenschaftlich-Technische Berichte / Forschungszentrum Dresden-Rossendorf; FZD-521
2009

Weiß, F. P.; Rindelhardt, U. (Editors)
Annual Report 2008 - Institute of Safety Research
Wissenschaftlich-Technische Berichte / Forschungszentrum Dresden-Rossendorf; FZD-524
2009

Granted patents

Bieberle, M.; Hampel, U.; Schleicher, E.
Anordnung zur Röntgen-Computertomographie mit elektromagnetisch abgelenktem Elektronenstrahl
DE 10 2007 040 778 A1 - 2009.03.05

Da Silva, M. J.; Hampel, U.; Schleicher, E.; Prasser, H.-M.
Anordnung zur zweidimensionalen Messung von verschiedenen Komponenten im Querschnitt einer Mehrphasenströmung
DE 10 2006 019 178 B4 - 02 Apr 2009

Eckert, S.; Gerbeth, G.; Gundrum, T.
Verfahren zur Messung von lokalen Strömungsgeschwindigkeiten in flüssigen Schmelzen
DE 10 2007 027 392 B3 - 2009.01.15

Eckert, S.; Gerbeth, G.; Gundrum, T.
Ultraschallsensor zur Messung von lokalen Strömungsgeschwindigkeiten in flüssigen Schmelzen
DE 10 2007 027 391 B3 - 8.1.2009

Eckert, S.; Räbiger, D.; Willers, B.; Gerbeth, G.; Nikrityuk, P. A.; Eckert, K.; Grundmann, R.
Verfahren und Einrichtung zum elektromagnetischen Rühren von elektrisch leitenden Flüssigkeiten
DE 10 2007 037 340 A1 - 19/02/2009

Eckert, S.; Räbiger, D.; Willers, B.; Gerbeth, G.; Nikrityuk, P. A.; Eckert, K.; Grundmann, R.
Verfahren und Einrichtung zum elektromagnetischen Rühren von elektrisch leitenden Flüssigkeiten
WO 2009/018809 A1 - 12/02/09

Eckert, S.; Räbiger, D.; Willers, B.; Gerbeth, G.; Nikrityuk, P. A.; Eckert, K.; Grundmann, R.
Verfahren und Einrichtung zum elektromagnetischen Rühren von elektrisch leitenden Flüssigkeiten
DE 10 2007 038 281 B4 - 18/06/2009

Eckert, S.; Räbiger, D.; Willers, B.; Gerbeth, G.; Nikrityuk, P. A.; Eckert, K.; Grundmann, R.
Verfahren und Einrichtung zum elektromagnetischen Rühren von elektrisch leitenden Flüssigkeiten
DE 10 2007 038 281 A1 - 19/02/2009

Eckert, S.; Räbiger, D.; Willers, B.; Gerbeth, G.; Nikrityuk, P. A.; Eckert, K.; Grundmann, R.
Verfahren und Einrichtung zum elektromagnetischen Rühren von elektrisch leitenden Flüssigkeiten
WO 2009/018810 - 12/02/2009

Grants, I.; Gerbeth, G.
Verfahren zur Reduzierung von Temperaturfluktuationen in Schmelzen
DE 10 2007 036 944 A1 - 05/02/09

Grants, I.; Gerbeth, G.
Verfahren zur Reduzierung von Temperaturfluktuationen in Schmelzen
EP 2090679 A1 - 19/08/09

Hampel, U.
Anordnung zur dreidimensionalen Elektronenstrahltomographie
DE 10 2008 005 718 A1 - 2009/07/30

Priede, J.; Cramer, A.; Gerbeth, G.; Galindo, V.; Andersen, O.; Kostmann, C.; Stephani, G.
Vorrichtung und Verfahren zur Herstellung metallischer Fasern durch Schmelzextraktion
DE 102006005510B4

Schleicher, E.; Sühnel, T.; Boden, D.; Fischer, F.; Futterschneider, H.
Gittersensor
DE 10 2007 019 926 B4 - 9 Apr 2009

PhD and diploma theses

PhD theses

Bieberle, Martina
Bildrekonstruktion für die ultraschnelle Limited-Angle-Röntgen-Computertomographie von Zweiphasenstgrömungen
Technische Universität Dresden

Cierpka, Christian
Zeitaufgelöste PIV Untersuchungen zur Strömungskontrolle mittels periodischer elektromagnetischer Kräfte in schwach leitfähigen Fluiden
Technische Universität Dresden

Fridman, Emil
Fertile Free in LWRs - Core Physics and Cycle Options
Ben-Gurion University of the Negev / Israel

Diploma theses

Bauer, Alexander
Entwicklung einer Small-Punch-Apparatur für bestrahlte Proben in der Heißen Zelle
Hochschule Zittau/Görlitz

Emmerich, Franziska
Untersuchungen der numerischen Lösung des k-ε-Turbulenzmodells für eine polydisperse Zweiphasenströmung
Technische Universität Dresden

Franke, Peter
Herstellung und Charakterisierung von dispersionsverfestigten Fe-Cr-Modelllegierungen für kerntechnische Werkstoffentwicklungen
Technische Universität/Bergakademie Freiberg

Nehring, Harald
Computertomografie mit Gammastrahlung an einem Holzrefiner
Technische Universität Dresden

Voigt, Felix
Elektronische Plattform für einen autonomen multiparametrischen Sensor
Technische Universität Dresden

Christoph Eichler
Simulation des Wärmeeintrages in ein Röntgen-Target durch einen Elektronenstrahl
Hochschule Zittau/Görlitz (FH)

Sebastian Schöne
Aufbau einer Luft-Wasser-Strömungsschleife
Hochschule Zittau/Görlitz (FH)

Awards

Martina Bieberle

Dresdener Barkhausen-Poster Preis 2009 der TU Dresden
Bildrekonstruktion für die ultraschnelle Limited-Angle-Röntgen-Computertomographie von Zweiphasenströmungen
Date of award: January 2010

Christian Cierpka

Doktorandenpreis 2009 des FZD (Anerkennungspreis)
Zeitaufgelöste PIV Untersuchungen zur Strömungskontrolle mittels periodischer elektromagnetischer Kräfte in schwach leitfähigen Fluiden
Date of award: January 2010

Frank Fischer

3. Platz im Kompetenzworkshop der Kerntechnischen Gesellschaft
Ultra fast electron beam X-ray CT scanner for two-phase flow measurement
Jahrestagung Kerntechnik 2009
Date of award: May 2009

Marco da Silva

Arbeitskreis der Hochschullehrer für Messtechnik - Messtechnikpreis 2009
Impedance Sensors for Fast Multiphase Flow Measurement and Imaging
Date of award: May 2009

U. Hampel

1. Preis Future Sax Businessplan-Wettbewerb Phase 1 (ForMaT-Team)
Future Sax Businessplan-Wettbewerb Dresden 2009
Date of award: January 2009

Guests

Betiuk, Jakub
01 April 2009 – 30 September 2009
University Lodz / Poland

Bojarevics, Andris Dr.
15 June 2009 – 18 June 2009
Institute of Physics, Riga / Latvia

Bucenieks, Imants Dr.
15 June 2009 – 18 June 2009
Institute of Physics, Riga / Latvia

Duplii, Stephan Dr.
11 June 2009 – 13 June 2009
University Kharkov / Ukraine

Gokhman, Oleksandr Prof.
01 August 2009 – 31 October 2009
01 November 2009 – 30 November 2009
Southukrainian State University of Education, Odessa / Ukraine

Grants, Ilmars Dr.
18 May 2009 – 29 May 2009
12 October 2009 – 30 October 2009
Institute of Physics, Riga / Latvia

Ieremenko, Maksym
02 December 2009 – 09 December 2009
Scientific-Technical Centre for Nuclear and Radiation Safety Kiew / Ukraine

Kotvytskiy, Albert
18 August 2009 – 20 August 2009
University Kharkov / Ukraine

Kozmenkov, Yaroslav
12 April 2009 – 30 June 2009
Institute of Physics and Power Engeneering Obninsk / Russian Federation

Lakehal, Djamel Dr.
30 April 2009 – 12 May 2009
ETH Zurich / Switzerland

Lopez Mendoza, Jose Manuel
01 March 2009 -30 April 2009
University of Tulsa /USA

Matveev, Yury Dr.
04 September 2009 – 06 November 2009
Institute of Physics and Power Engineering Obninsk / Russian Federation

Matusiak, Bartosz
01 April 2009 – 30 June 2009
University Lodz / Poland

Ovdiienko, Iurii
02 December 2009 – 09 December 2009
Scientific-Technical Centre for Nuclear and Radiation Safety Kiew / Ukraine

Pivovarov, Valeriy Dr.
01 September 2009 – 06 November 2009
Institute of Physics and Power Engineering Obninsk / Russian Federation

Sharaf, Safa
04 July 2009 – 03 October 2009
University of Nottingham / United Kingdom

Thomas, Brain Prof.
18 October 2009 – 22 October 2009
University of Illinois / USA

Iara Hernandez Rodriguez
10. March – 09. Sept. 2009
University of Sao Paulo, Brazil

Jong-Bum Kim
10. October – 31. October 2009
KAERI, South Korea

Meetings and workshops

3rd OECD PKL-II Project Workshop
42 participants
Dresden, 26 – 27 March 2009

ANSYS-FZD-Workshop: Multiphase Flow – Simulation, Experiment and Application
95 participants
Dresden, 26 – 28 May 2009

Nuclear Reactor Integrated Simulation Project (NURISP)
Open General Seminar
80 participants
Dresden, 30 November – 01 December 2009

Klausurtagung SFB-609 "Elektromagnetische Strömungsbeeinflussung in Metallurgie, Kristallzüchtung und Elektrochemie"
50 participants
Dresden, 16-17 December 2009

6th International Conference on Electromagnetic Prosessing of Materials (EPM 2009)
285 participants
Dresden, 19 – 23 December 2009

Seminars of the institute

S. Kliem
Analysen von Störfallszenarien mit unterstelltem Versagen der Reaktorschnellabschaltung mit dem Codesystem DYN3D/ATHLET
15 January 2009

Dr. G. Laczko (VATTENFALL)
Simulation des Boreinspeisesystems und seiner Reaktivitätswirksamkeit in einem Siede-wasserreaktor (SWR)
02 February 2009

Sanjoy Banerjee (Distinguished Professor oc Chemical Engineering, Director, The Energy Institute, The City College of New York)
Numerical Simulation of Two-Phase Flows
13 February 2009

Ch. Valleé, T. Seidel, Dr. D. Lucas
Experimente im Heißstrangmodell der TOPFLOW-Anlage: Überblick und erste Ergebnisse
17 February 2009

P. Sarkadi (TÜV Nord, Hamburg)
Berechnung eines Dampferzeugerheizrohres mit realistischen Anfangs- und Rand-bedingungen; Thermohydraulische Randbedingungen zur Bestimmung des bei einem Kühlmittelverluststörfalls zu erwartenden Brennstabschaden
26 February 2009

M. Bieberle, F. Fischer, E. Schleicher, Dr. U. Hampel
Experimentelle ultraschnelle Röntgentomographie
09 April 2009

Dr. Stefani
Neue Ergebnisse vom MRI-Experiment PROMISE-2
24 April 2009

Y. Bilodid, Dr. S. Mittag
Modeling of History Effects in Burnup Calculations
07 May 2009

Michio Murase
Numerical Calculations on Countercurrent Gas-Liquid Flow in an PWR Hot Leg
29 May 2009

D. Räbiger, S. Eckert, G. Gerbeth
Anwendung zeitmodulierter AC-Magnetfelder zum Rühren metallischer Schmelzen
04 June 2009

Dr. H.-W. Viehrig, J. Schuhknecht
Bruchmechanische Charakterisierung der WWER-440 RDB Schweißnaht des Blockes 8
KKW Greifswald
18 June 2009

Dr. A. Ulbricht
Untersuchung von neutronenbestrahlten Fe-Cr-Legierungen mittels Neutronenkleinwinkel-
streuung
04 September 2009

Dr. S. Mittag
Vermeidung des langlebigen radioaktiven Abfalls in laufenden Kernkraftwerken
11 September 2009

Dr. E. Shwageraus
Review of Recent Studies on Thorium Fuel Cycles for PWRs
14 September 2009

Prof. Rizwan Uddin
CFD and Coupled CFD-System Codes: A Comprehensive Approach for Nuclear Engineering
Applications
24 September 2009

Klaus Timmel
Modellierung des Stahlausgussprozesses mit der Flüssigmetallanlage CONCAST
30 September 2009

Hiroyuki Toyokawa, Ph.D.
Industrial imaging method using high-energy photon beam CT
07 October 2009

Lecture courses

Frank-Peter Weiß
Zuverlässigkeit und Sicherheit technischer Systeme
TU Dresden, Fakultät Maschinenwesen
Summer semester 2009 and winter semester 2009

Matthias Werner
Zuverlässigkeit und Sicherheit technischer Systeme
TU Dresden, Fakultät Maschinenwesen
Summer semester 2009 and winter semester 2009

Udo Rindelhardt
Erneuerbare Energien I und II
Technische Universität Chemnitz, Fakultät für Elektrotechnik/Informationstechnik
Summer semester 2009 and winter semester 2009

Uwe Hampel
Computertomographie in der Medizin und Prozessdiagnostik
TU Dresden, Fakultät Elektro- und Informationstechnik
Summer semester 2009

Departments of the institute

```
          ┌─────────────────────────────────┐
          │          Directorate            │
          │   Prof. Dr. Frank-Peter Weiss    │
          │     Tel.: (0351) 260 3480        │
          └─────────────────────────────────┘
```

Dpt.
Accident Analysis

Dr. U. Rohde
Tel.: (0351)260 2040

Dpt.
Magneto-Hydrodynamics

Dr. G. Gerbeth
Tel.: (0351) 260 3484

Dpt.
Materials and
Components Safety

Dr. E. Altstadt
Tel.: (0351) 260 2276

Dpt.
Experimental Thermal
Fluid Dynamics

Dr. U. Hampel
Tel.: (0351) 260 2772
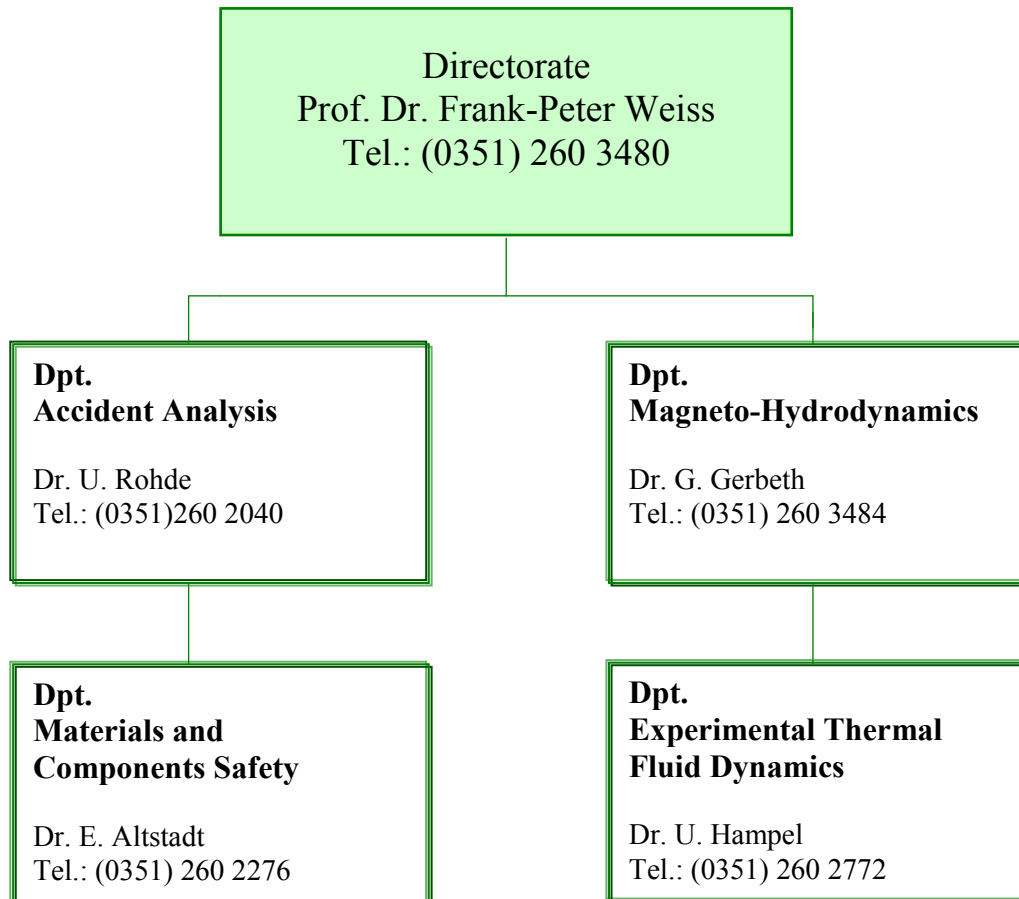
Forschungszentrum Dresden-Rossendorf e.V.
Institut für Sicherheitsforschung
Postfach 51 01 19
D- 01314 Dresden

Personnel

Director: Prof. Dr. Frank-Peter Weiß

Scientific Staff

Albrecht, Thomas
Altstadt, Eberhard Dr.
Apanasevich, Pavel
Arora, Kanwer Shing
Baier, Silvio Dr.
Bergner, Frank Dr.
Beyer, Matthias
Bieberle, André Dr.
Bieberle, Martina Dr.
Birkenheuer, Uwe Dr.
Carl, Helmar Dr.
Cartland-Glover, Gregory Dr.
Cierpka, Christian Dr.
Cramer, Andreas Dr.
Eckert, Sven Dr.
Ferrari, Anna Dr.
Fridman, Emil Dr.
Galindo, Vladimir Dr.
Gerbeth, Gunter Dr.
Giesecke, Andre
Grahn, Alexander Dr.
Gundrum, Thomas
Günter, Uwe Dr.
Hampel, Uwe Dr.
Hauptmann, Tobias
Hoffmann, Wolfgang Dr.
Hoppe, Dietrich Dr.
Höhne, Thomas Dr.
Houska, Mario
Kliem, Sören
Konheiser, Jörg
Kozmenkov, Yroslav Dr.
Krepper, Eckhard Dr.
Kryk, Holger Dr.
Küchler, Roland Dr.
Leonhardt, Monika
Lucas, Dirk Dr.
Merk, Bruno Dr.
Mittag, Siegfried Dr.
Pal, Josef Dr.
Park, Jong-Soo
Rindelhardt, Udo Prof. Dr.

Rohde, Ulrich Dr.
Rzehak, Roland Dr.
Schäfer, Frank Dr.
Schleicher, Eckhard
Schmid, Robert
Schmidtke, Martin Dr.
Schöne, Sebastian
Schubert, Markus Dr.
Schuhknecht, Jan
Shatrov, Viktor Dr.
Silva da, Marco Dr.
Stefani, Frank Dr.
Talati, Minaben Dr.
Ulbricht, Andreas Dr.
Viehrig, Hans-Werner Dr.
Weier, Tom Dr.
Werner, Matthias Dr.
Zurbuchen, Conrad
Zhang, Chaojie
Zhang, Xiugang

PhD Students

Al-Asqalani, Ahmed Tamer
Barth, Thomas
Bärtling, Yves
Bilodid, Yuri
Boden, Stephan
Buchenau, Dominique
Danciu, Dana-Veronica
Dürigen, Susan
Fischer, Frank
Heintze, Cornelia
Glivici-Cotruta, Varvara
Houenouvo, Hermann A.T.
Liao, Yixiang
Miao, Xincheng
Räbiger, Dirk
Seidel, Tobias
Thiele, Sebastian
Timmel, Klaus
Tusheva, Polina
Valleé, Christophe
Wondrak, Thomas

Technical Staff

Berger, Ronny
Berger, Torsten
Bombis, Doris
Borchardt, Steffen
Erlebach, Stephan
Franz, Ronald
Futterschneider, Hein
Gommlich, André
Hessel, Günther
Kunadt, Heiko
Lindner, Klaus
Losinski, Claudia
Mitreuter, Marcel
Müller, Gudrun Dr.
Nowak, Bernd
Paul, Sebastian
Pietzsch, Jens
Pietruske, Heiko
Richter, Annett
Richter, Henry
Roßner, Michaela
Rott, Sonja
Röder, Michael
Rußig, Heiko
Schleßiger, Heike
Schneider, Gisela
Schütz, Peter
Skorupa, Ulrich
Sprewitz, Uwe
Szalinski, Lutz
Tamme, Marko
Thiel, Andre
Tschofen, Martin
Vetter, Petra
Webersinke, Wolfgang
Weichelt, Steffen
Weiß, Rainer
Zimmermann, Wilfried
Zippe, Cornelius Dr.